HHS Public Access

Author manuscript

J Nat Prod. Author manuscript; available in PMC 2023 October 28.

Published in final edited form as:

J Nat Prod. 2022 October 28; 85(10): 2484–2518. doi:10.1021/acs.jnatprod.2c00487.

Total Heterologous Biosynthesis of Fungal Natural Products in *Aspergillus nidulans*

Yi-Ming Chiang,

Department of Pharmacology and Pharmaceutical Sciences, School of Pharmacy, University of Southern California, Los Angeles, California 90089, United States; Department of Pharmacy, Chia Nan University of Pharmacy and Science, Tainan 71710, Taiwan

Tzu-Shyang Lin,

Department of Pharmacology and Pharmaceutical Sciences, School of Pharmacy, University of Southern California, Los Angeles, California 90089, United States

Clay C. C. Wang

Department of Pharmacology and Pharmaceutical Sciences, School of Pharmacy and Department of Chemistry, Dornsife College of Letters, Arts, and Sciences, University of Southern California, Los Angeles, California 90089, United States

Abstract

Fungal natural products comprise a wide range of bioactive compounds including important drugs and agrochemicals. Intriguingly, bioinformatic analyses of fungal genomes have revealed that fungi have the potential to produce significantly more natural products than what have been discovered so far. It has thus become widely accepted that most biosynthesis pathways of fungal natural products are silent or expressed at very low levels under laboratory cultivation conditions. To tap into this vast chemical reservoir, the reconstitution of entire biosynthetic pathways in genetically tractable fungal hosts (total heterologous biosynthesis) has become increasingly employed in recent years. This review summarizes total heterologous biosynthesis of fungal natural products accomplished before 2020 using *Aspergillus nidulans* as heterologous hosts. We review here *Aspergillus* transformation, *A. nidulans* hosts, shuttle vectors for episomal expression, and chromosomal integration expression. These tools, collectively, not only facilitate the discovery of cryptic natural products but can also be used to generate high-yield strains with

Corresponding Authors: Yi-Ming Chiang – Department of Pharmacology and Pharmaceutical Sciences, School of Pharmacy, University of Southern California, Los Angeles, California 90089, United States; Department of Pharmacy, Chia Nan University of Pharmacy and Science, Tainan 71710, Taiwan; Present Address: Hexagon Bio, Inc., Menlo Park, California 94025, United States; ymchiang@mail.cnu.edu.tw, **Clay C. C. Wang** – Department of Pharmacology and Pharmaceutical Sciences, School of Pharmacy and Department of Chemistry, Dornsife College of Letters, Arts, and Sciences, University of Southern California, Los Angeles, California 90089, United States; clayw@usc.edu.

Yi-Ming Chiang - Present Address: Hexagon Bio, Inc., Menlo Park, California 94025, United States

Supporting Information

The Supporting Information is available free of charge at https://pubs.acs.org/doi/10.1021/acs.jnatprod.2c00487.

Vectors used and additional information (PDF)

Complete contact information is available at: https://pubs.acs.org/10.1021/acs.jnatprod.2c00487

The authors declare no competing financial interest.

DEDICATION

This review is dedicated to Professor Yueh-Hsiung Kuo on the occasion of his 80th birthday.

clean metabolite backgrounds. In comparison with total synthesis, total heterologous biosynthesis offers a simplified strategy to construct complex molecules and holds potential for commercial application.

Graphical Abstract

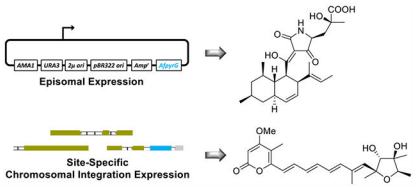

INTRODUCTION

Fungi live in complex ecosystems and are widely distributed in nature. They have evolved to produce bioactive natural products that either benefit their own growth or suppress the growth of their competitors such as bacteria or other fungi.[1] Consequently, fungi have been invaluable sources of new leads for the pharmaceutical and agricultural industries. A number of important drugs and fungicides are produced or derived from fungal natural products.[2]

Typically, the carbon backbone of a fungal natural product is biosynthesized by one or two core enzyme(s) such as polyketide synthases (PKSs),[3,4] nonribosomal peptide synthetases (NRPSs),[5] terpene cyclases (TCs),[6] or prenyltransferases.[7] These core enzymes use primary metabolites such as acyl-CoAs (PKSs), amino acids (NRPSs), or isoprenoids (TCs and prenyltransferases) to generate carbon backbones which define the chemical class of the metabolite. The scaffolds synthesized by core enzymes are further modified by various tailoring enzymes, such as cytochromes P450 monooxygenases, flavin-dependent monooxygenases (FMOs), short-chain dehydrogenase/reductases (SDRs), and methyltransferases (MTs).[8]

Fungal Natural Product Discovery in the Postgenomic Era.

Early studies on the biosynthesis of fungal natural products showed that genes from the same biosynthetic pathway tend to be clustered in the genome.[9] Clustering may facilitate co-regulation or horizontal gene transfer of all genes in a biosynthesis pathway. Later fungal genome projects revealed that biosynthetic gene clusters (BGCs) vastly outnumber known natural products.[1,10] This observation indicated that most BGCs are “cryptic” (completely silent or expressed at a very low level) under laboratory cultivation conditions. Since the signals that trigger their expression are unknown, the chemical diversity of fungi remains largely untapped. Considering that there are millions of fungal species[11] and that certain species contain up to 70 BGCs,[12] there is tremendous potential for fungal natural product discovery.

In addition to the enzymes required for biosynthesis, some BGCs also encode major facilitator superfamily (MFS) transporters,[13] cluster-specific regulators,[14,15] and self-resistant enzymes.[16,17] Most putative transporters have not been functionally characterized, but they are hypothesized to transport substrates, intermediates, or the final products of

a biosynthesis pathway. Cluster-specific regulators modulate the expression of the whole cluster. Therefore, a common strategy for eliciting a silent BGC in a genetically tractable fungus is to induce the positive regulator.[15] However, since not every BGC contains one, it is not a universal strategy to activate cryptic BGCs. Lastly, many BGCs produced toxic natural products that target metabolic enzymes. To prevent self-harm, some BGCs encode a mutated version of the original target that is resistant to the toxic natural product (a resistance enzyme). This feature has greatly facilitated functional assignment or target identification of the toxic natural product.[17]

The field of fungal natural product discovery has dedicated much effort in developing strategies to unlock cryptic natural products. While an in-depth review of the various strategies is out of the scope of this review, readers are referred to articles on this topic.[15,18] Here, we focus on the reconstitution of biosynthetic pathways in genetically tractable hosts (total heterologous biosynthesis). This approach is particularly useful if the producer is uncultivable or has no genetic system for genome editing.[19–23]

Heterologous Expression Hosts.

E. coli and *Saccharomyces cerevisiae* (yeast) are widely used for the expression of fungal genes. They have several advantages such as well-established genetic systems, robust growth, and clean backgrounds due to lack of secondary metabolic pathways.

However, both species also have limitations. *E. coli* is a prokaryote and cannot perform RNA splicing and post-translational modification. As such, most studies using *E. coli* are limited to characterizing individual enzymes rather than full-length BGCs. Yeasts are unicellular eukaryotes and have the machinery for RNA splicing and post-translational modifications. The engineered yeast strain BJ5464-NpgA, with the *npgA* gene from *A. nidulans* integrated into its genome, is widely used for the expression of fungal PKS pathways.[24] *NpgA* encodes for 4′-phosphopantetheine transferase that catalyzes the attachment of a 4′-phosphopantetheine, which converts an inactive *apo* PKS or NRPS to an active *holo* form. Although there are many advantages of using yeasts as heterologous hosts, yeasts lack specialized compartments required to produce certain metabolites.[25] In addition, yeasts cannot splice the mRNA of filamentous fungi correctly, requiring accurate prediction of introns if cDNA cannot be obtained from the producer.[24,26]

In contrast, genetically tractable filamentous fungi have compatible transcription, translation, post-translational modification, and secretion machineries for the expression of foreign fungal genes and therefore are better suited for the heterologous expression of full-length BGCs. Intact BGCs of penicillin,[27] citrinin,[28] fusatins,[29] W493,[29] bikaverin,[30] and flavoglaucin[31] have been transferred and successfully expressed in fungal hosts. Moreover, Bok and Clevenger et al. developed fungal artificial chromosomes to introduce entire BGCs from three *Aspergillus* species into *A. nidulans*, and about 27% of the transferred BGCs produced detectable products.[32,33]

Despite these successful cases, however, most heterologous BGCs do not produce detectable products in filamentous fungal hosts, and even if they do, the titers are often low. The silence could be attributed to the lack of triggering signals, and the poor yield to suboptimal

expression of the foreign genes.[30] While it is possible to increase the titer by overexpression of the positive regulator, as previously discussed, not every fungal BGC harbors one.[28,34,35] Against this background, BGC refactoring with strong promoters offers an alternative route to biosynthesizing compounds in high titers.

EXPRESSION OF HETEROLOGOUS GENES IN ASPERGILLUS

Aspergillus Transformation.

Aspergillus spp. can grow in a wide range of conditions and are widely used as heterologous hosts.[36] Several engineered *Aspergillus* strains are commonly used to express BGCs.[19,20] Since the fungal cell wall is an impenetrable barrier for exogenous DNA, the first step of gene delivery (transformation) is oftentimes enzymatic digestion of the fungal cell wall to generate protoplasts (Figure 1) (for details on the transformation of filamentous fungi, see refs 37 and 38). Once the cell wall has been sufficiently digested, the transforming DNA can be taken up by the cell via polyethylene glycol (PEG)-mediated delivery.

After the transforming DNA reaches the nucleus, it can self-replicate episomally or integrate into the genome. For episomal replication, the autonomous fungal replication element, *AMA1* (autonomous maintenance in *Aspergillus*), has been identified for extrachromosomal replication in *A. nidulans* (see section AMA1-Based Episomal Expression System).[39] For chromosomal integration, either non-homologous integration or homologous recombination (HR) may occur (Figure 1). In the event of non-homologous integration, transforming DNA ligates into spontaneous double-strand breaks (DSBs) via non-homologous end joining (NHEJ), which is the major DNA repair mechanism of DSBs in many eukaryotes. It should be noted that it is not uncommon for multiple copies of the transforming DNA to integrate into different genomic loci with NHEJ. In the event of HR, recombination of the homologous sequences results in the integration of transforming DNA at a specific locus.

Elements in Transforming DNA.

Selection of successful transformants is achieved with the selectable marker in the transforming DNA.[37] Either a dominant (resistance) or auxotrophic (nutritional) selectable marker can be used. Dominant markers (such as *bar* and *hph*) are genes encoding enzymes that confer resistance against toxic chemicals. For example, *bar* encodes phosphinothricin acetyltransferase able to detoxify glufosinate ammonium, and *hph* encodes hygromycin B phosphotransferase able to detoxify the antibiotic hygromycin B. In media containing a specific toxic chemical, only the fungal cells harboring the dominant marker can grow. Auxotrophic markers (such as *pyrG*, *riboB*, and *pyroA*) are based on nutritional genes. Auxotrophy is the inability of an organism to synthesize a specific metabolite required for growth. Growth can be restored with an auxotrophic marker that complements that defect. Therefore, nutritional selection requires an auxotrophic mutant with a specific deficiency in primary metabolism. For example, *pyrG* encodes orotidine 5′-monophosphate decarboxylase, and a *pyrG* mutation with dysfunctional PyrG leads to uridine/uracil auxotrophy, which requires uridine/uracil for the organism to grow (Figure S1A). Transforming DNA with functional *pyrG* can restore growth in media lacking uridine/uracil. Additionally, *pyrG* mutants are resistant to 5-fluoroorotic acid (5-FOA), which can be used

for counter-selection. Strains with functional *pyrG* metabolize 5-FOA to the toxic metabolite 5-fluorouracil. *pyrG* mutants cannot metabolize 5-FOA to 5-fluorouracil and, therefore, can grow in a medium containing uridine/uracil and 5-FOA. Counter-selection enables *pyrG* to be recycled and used for subsequent rounds of transformation. Besides *pyrG*, *riboB* and *pyroA* are two other auxotrophic markers frequently used in *A. nidulans* transformation. RiboB is required for riboflavin biosynthesis, and a *riboB* mutant requires riboflavin to grow (Figure S1B). PyroA is required for pyridoxine biosynthesis, and a *pyroA* mutant requires pyridoxine to grow (Figure S1C).

To express a gene of interest, the transforming DNA also needs to carry an expression cassette. An expression cassette contains the coding region of a gene of interest placed downstream of a promoter and upstream of a terminator to drive expression and ensure the releasing of the synthesized RNA from the transcription machinery, respectively. Either a strong constitutive promoter (such as P*gpdA*) or an inducible promoter (such as P*alcA*, P*amyB*, and P*glaA*) can be used.[40] *gpdA* encodes glyceraldehyde-3-phosphate dehydrogenase, and its expression is independent of transcriptional regulation. *alcA* encodes alcohol dehydrogenase I and can be induced by alcohols, aldehydes, or ketones. *amyB* and *glaA* encode α-amylase and glucoamylase, respectively, and both can be induced by maltose or starch. One advantage of using an inducible expression system is that biomass can be accumulated before induction of the genes of interest, which is especially useful if a reconstituted pathway produces a metabolite toxic to the host.

Aspergillus Hosts.

Today, *A. oryzae* and *A. nidulans* are the most popular fungal hosts for the reconstitution of fungal biosynthesis pathways. *A. oryzae* is identified as a GRAS (generally recognized as safe) organism by the U.S. Food and Drug Administration and has been used by the fermentation industry to produce sake, miso, and soy sauce for centuries.[41] The heterologous expression system was developed based on the fact that *amyB* in *A. oryzae* is highly expressed in media containing maltose.[42] As such, the promoter and terminator from *amyB* can be used to drive the expression of genes of interest. Genetically tractable strains *A. oryzae* M-2–3 (*argB*$^-$)[43] and NSAR1 (*niaD*$^-$, *sC*$^-$, *argB*$^-$, *adeA*$^-$)[44] are widely used for ectopic integration to constitute biosynthesis pathways. *A. oryzae* M-2–3 was used by Heneghan et al. to achieve the first total biosynthesis of the fungal natural product tenellin in 2010.[45] NSAR1 is a quadruple auxotrophic mutant that allows the transformation of at least four expression vectors. Furthermore, the development of multiple expression cassettes in a single vector enabled the expression of multiple genes of interest in one transformation using only one selectable marker.[21,46] Reconstitution of meroterpenoid biosynthesis pathways in *A. oryzae* has recently been reviewed.[47]

In this review, we will focus on total biosynthesis in *A. nidulans*. The most popular *A. nidulans* host strains used are TN02A7 and its derivatives.[48,49] TN02A7 contains the deletion of *nkuA*, a homologue of the human KU70 gene, which is essential for NHEJ. Deletion of *nkuA* greatly impairs NHEJ and, therefore, increases the probability of HR events. TN02A7 also carries three auxotrophic mutations (*pyrG*89, *pyroA*4, and *riboB*2) which can be complemented by homologue genes from *A. fumigatus* or *A. terreus*.

Using homologue genes from other *Aspergillus* species prevents potential HR between the transformation DNA and the mutated gene. TN02A7 has been deposited at Fungal Genetics Stock Center (www.fgsc.net) with FGSC strain number A1145 (Table 1).

TN02A7 (A1145) produces sterigmatocystin and emericellamides in a variety of different culturing conditions. StcA[50] and EasA[51] are the nonreducing (NR)-PKS and NRPS responsible for the biosynthesis of sterigmatocystin and emericellamides, respectively. Using HR facilitated by CRISPR-Cas9[52] to delete *stcA*, *easA*, or both, the Tang group generated A1145ΔST, A1145ΔEM, and A1145ΔSTΔEM strains.[53] Deletion of endogenous BGCs frees up substrates such as malonyl-CoA for the heterologous pathway and simplifies the metabolite background to facilitate detection and purification of new compounds. The Oakley group took the approach one step further and deleted the entire ST BGC *stc* (>50 kb) in A1145 to generate the strain LO4389.[54] While deleting only the core gene *stcA* eliminates ST production, other genes in the *stc* pathway could potentially still interfere with the heterologous pathway. Deletion of the entire BGC eliminates any potential crosstalk. Lastly, the Oakley group created the genetically dereplicated strains LO7890 and LO8030[55] with seven and eight native *A. nidulans* BGCs removed, respectively (Table 1). They were originally created to unearth hidden metabolites buried by the background, but have also been used as hosts in total heterologous biosynthesis.

TOTAL HETEROLOGOUS BIOSYNTHESIS IN *A. NIDULANS*

This review highlights total heterologous biosynthesis work in *A. nidulans* accomplished before 2020 on BGCs with at least four enzymatic steps. A timeline of the highlighted work is depicted in Figure 2. As these works employed either the episomal or site-specific chromosomal integration expression (Table 2), we will examine each system in two separate sections. We recognize that there are numerous manuscripts that describe similar approaches for producing intermediates in biosynthesis pathways that are not covered here. We apologize to the authors whose work we missed in this review. We intended to target audiences with synthetic or natural product chemistry backgrounds and thus have focused this review on biosynthesis. For an overview of fungal heterologous expression systems, readers are directed to relevant literature in refs 19–23.

I. *AMA1*-BASED EPISOMAL EXPRESSION SYSTEM

As mentioned, the *AMA1* replicator supports extrachromosomal vector maintenance in *Aspergillus* spp.,[39] and its utility has been demonstrated in DNA constructs >100 kb in *A. nidulans*.[32] Based on this finding, the Watanabe, Tang, and Chooi groups constructed *E. coli*-yeast-fungal shuttle vectors for episomal expression in *A. nidulans*.

***E. coli*-Yeast-Fungal Shuttle Vectors pKW20088, pYTP, pYTR, and pYTU.—**The Watanabe group created the *E.* coli-yeast-fungal shuttle vector pKW20088[56] from pPTRII[57] (Figure S2A). Besides the *AMA1* replicator, pPTRII also contains pBR322 *ori* and *Amp*^{r} for plasmid maintenance and selection in *E. coli*, respectively. Insertion of *2μ ori* and *URA3*, which allow plasmid maintenance and selection in *S. cerevisiae*, respectively, into pPTRII resulted in pKW19030. *S. cerevisiae* is a powerful molecular tool for the assembly of BGCs because it can assemble DNA fragments with ~30 bp of overlap *in vivo* via HR with

high efficiency and fidelity.[58] The selectable marker from *A. fumigatus*, *AfpyrG*, was then inserted into pKW19030, resulting in pKW20088. The expression cassettes can be inserted between *AMA1* and *AfpyrG*. Since pKW20088 contains elements for maintenance and selection in *E. coli*, yeast, and *Aspergillus*, it can assemble BGCs in yeast, propagate in *E. coli*, and episomally express genes of interest in *Aspergillus*.

Sch 210972 (1).: Based on the shuttle vector pKW20088, the Watanabe group generated pKW10027, pKW10029, and pKW10035 expression vectors (Figure S2B) to reconstitute the biosynthetic pathway of Sch 210972 (**1**) in the A1145 strain.[59] **1** is a tetramic acid-containing metabolite isolated from *Chaetomium globosum* (Figure 3A).[60] It exhibits potent inhibitory activity against chemokine receptor CCR-5, a cell surface receptor that plays an important role in the attachment and entry of HIV-1 into cells.

Four genes, *cghA* (encoding a lipocalin-like enzyme), *cghB* (aldolase), *cghC* (*trans*-acting enoyl reductase (*trans*-ER)), and *chgG* (PKS-NRPS) in the Sch 210972 BGC were identified to be involved in the biosynthesis of **1** (Figure 3A).[59] CghG and the partnering ER (*trans*-ER) CghC were proposed to assemble the backbone of **1**. CghB was proposed to dimerize pyruvic acid via aldol reaction to generate **2**, which then transaminated to **3** (Figure 3B). Interestingly, expression of all four genes resulted in the exclusive production of the endo adduct **1**, while omission of CghA led to a mixture of endo and exo adducts **1** and **4** (Table S1). This suggested that CghA stereoselectively promoted the Diels–Alder reaction, leading to its assignment as a Diels–Alderase.

Using similar methodology to the construction of pKW20088, the Tang group utilized pYTU, pYTP, and pYTR expression vectors carrying *AfpyrG*, *AfpyroA*, and *AfriboB* auxotrophic markers, respectively, to reconstitute fungal biosynthesis pathways. Their total biosynthesis works using *A. nidulans* are summarized and organized according to the class of fungal natural products expressed, i.e., PKS (Figures 4 and 5), NRPS (Figure 6–8), PKS-NRPS hybrid (Figures 9–12), PKS and NRPS (Figures 14–16), and others (Figures 17 and 18).

Pyriculol (5), Sordarial (6), and Trichoxide (7).: Pyriculol (5) is a salicylaldehyde produced by *Magnaporthe oryzae*. It was found to induce lesion formation on rice leaves. A highly reducing (HR)-PKS (*MoPKS19*) was genetically verified to be involved in the biosynthesis of **5** (Figure 4A).[61] It was surprising that an HR-PKS-containing BGC was responsible for the biosynthesis of **5** since nonreducing (NR)-PKSs or partially reducing (PR)-PKSs are well-recognized to synthesize aromatic polyketides.[3] Using a comparative genomic approach, a BGC (*srd*) similar to the pyriculol BGC was identified in *Neurospora crassa* (Figure 4A).[62] Heterologous expression of SrdA–J in the A1145ΔSTΔEM strain produced sordarial (**6**) (Figure 4A). While the detailed biosynthesis of **6** was not elucidated, this study confirmed that fungal salicylaldehydes indeed originated from HR-PKSs.

Using a similar approach, another BGC (*vir*) was identified from *Trichoderma virens* (Figure 4A).[63] Heterologous expression of VirA–L in the A1145 strain led to a new compound, trichoxide (**7**), together with pathway intermediates virensol A (**8**), virensol B (**9**), and 5-deoxyaurocitrin (**10**) (Figure 4B and Table S2). To investigate how the HR-PKS (VirA)

and its associated tailoring enzymes worked together to synthesize salicylaldehyde **10**, different combinations of *vir* genes in A1145 were heterologously expressed.

Expression of VirA produced virensol C (**11**), which existed mostly as a pair of hemiacetals in solution. The production of **11** by VirA alone was surprising since VirA did not contain a reductive releasing (R) domain. When the cupin-domain enzyme VirC was coexpressed with VirA, the yield of **11** increased, suggesting that VirC may be involved in enhancing product turnover. After testing different binary combinations, only coexpression of the SDR VirB with VirA resulted in the disappearance of **11** and emergence of **12**, which also existed as a pair of hemiacetals in solution. Coexpression of another SDR VirD with VirA/B led to the disappearance of **12** and the emergence of **10**, with a trace amount of **9**. Thus, VirB was proposed to dehydrogenate the C-7 alcohol and VirD the C-3 alcohol to generate **13**, which then underwent intramolecular aldol condensation, dehydration, and aromatization to form the salicylaldehyde moiety in **10**. These results demonstrated that two of the three hydroxy groups (C-3 and C-7) in **11** were oxidized back to ketones, which set up the formation of the salicylaldehyde moiety in **10**. The trace amounts of **9** in the VirA/B/D or VirA–D strains likely came from alcohol dehydrogenation of **10** catalyzed by an endogenous enzyme in the host, since when VirG was added to the VirA–D strain exclusive formation of **9** was observed.

When the P450 VirE was introduced to the VirA–D/G strain, the hydroquinone **8** was made. Finally, the VirA–I strain afforded **14**, suggesting the involvement of VirH (cupin domain-containing protein) and VirI (flavin-dependent oxidoreductase) in the oxidation of **8** to quinone and epoxidation to form 14. Since the VirA–L strain produced **7**, the two remaining SDR enzymes (VirK and VirL) were proposed to be responsible for reducing the two ketones in **14**.

Decarestrictine C1 (15).: Decarestrictine C1 (**15**), originally isolated from a *Penicillium* species, contains a 10-membered lactone.[64] A BGC (*dcs*) responsible for the biosynthesis of **15** was identified from the genome of *Beauveria bassiana* ARSEF 2860 (Figure 5A).[65] The *dcs* cluster encoded an HR-PKS (DcsA), a thioesterase (TE, DcsB), a P450 (DcsC), an SDR (DcsD), and an FMO (DcsE). Heterologous expression of the HR-PKS DcsA and TE DcsB in A1145 produced diplodialide B (**16**) (Figure 5B and Table S3), indicating that DcsA and DcsB were sufficient to synthesize the nonanolide. Coexpression of the P450 DcsC with DcsA/B led to the disappearance of **16** and no accumulation of other metabolites. Additional coexpression of the SDR DcsD led to the formation of **15**. It was proposed that DcsC oxidized the allylic C6 position of **16** to form **17**, which was metabolized by the host. DcsE was not found to be required for the biosynthesis of **15**, so its function remained undetermined.

Remarkably, DcsB was shown to have broad substrate promiscuity to form medium-ring lactones. The yields of lactonization for linear substrates of different sizes (7–13 membered) range from 49% to 82%. Compared to a five-membered ring, lactonization of medium-sized rings is synthetically challenging. The characterization of enzymes such as DcsB that perform medium-ring lactonization could facilitate chemoenzymatic preparation of desired lactones.

Herquline A (18).: Herquline A (**18**) is a strained pentacyclic alkaloid isolated from *Penicillium herquei* with weak antiplatelet activity.[66] Forging strained molecules is of great interest to synthetic chemists, and understanding nature's strategy may lead to their biomimetic total syntheses. A six-gene BGC (*hql*) encoding an NRPS (HqlA), a P450 (HqlC), an *N*-MT (HqlE), and three SDRs (HqlB, -D, and -F) was identified in the genome of *P. herquei* (Figure 6A).[67] Activation of all six genes (*hqlA–F*) in A1145 produced **18** and herquline B (**19**) (Figure 6B and Table S4A).

Expression of HqlA and HqlB afforded **20**, which, when fed to an HqlC–F-expressing strain, yielded back **18** and **19** (Table S4A and S4B). Expression of HqlA–C produced **21**, implicating HqlC in the formation of the strained biaryl linkage. A mechanism was proposed involving the aromatization of the dicyclohexadienone intermediate **22** to **21**. However, feeding **21** to a HqlC–F-expressing strain did not give the final product **18**, suggesting that **21** was a shunt product. Indeed, expression of HqlA–C/F generated **20**, **23**, **24**, and **25**, but not **21**. Feeding **23** (3*R*,3′*R*) to a HqlC–F-expressing strain produced its diastereomer **24** (3*S*,3′*S*) along with **18** and **19**, while feeding **24** to the same strain produced no new compounds. This result suggested that **23** was on-pathway, whereas its stereoisomer **24**, which was calculated to be thermodynamically more stable, was not. Conversion of **23** to **19** was catalyzed by the *N*-MT HqlE as validated by recombinant HqlE.

Interestingly, the transformation of **19** to **18** was observed spontaneously, and the exclusion of HqlD, the only unassigned enzyme in the cluster, from the HqlA–F strain had no effect on the production of **18** and **19**. These data suggested that the stereoselective cyclization of **19** to **18** involving the creation of three chiral centers was nonenzymatic. Notably, the 3*R*,3′*R* configuration in **19** appeared to have been locked by methylation, setting the stage for the subsequent steps to **18**. Tautomerization would convert **19** to **26** (1*R*), which was shown to be more stable than its 1*S* stereoisomer by free energy calculations. Michael addition from the α phase of the cyclohexanone would produce **27** (1*R*,2*S*), which then tautomerized to the more stable (1*R*,2*S*,3*R*) configuration in **18**. The nonenzymatic cascade after methylation of the piperazine core in **23** was fascinating and could serve as biomimetic inspiration for total synthesis.

FR901483 (28).: FR901483 (**28**) is a potent immunosuppressant isolated from *Cladobotryum* sp. No. 11231.[68] Its mode of action, which was proposed to be the inhibition of purine nucleotide biosynthesis, is distinct from that of cyclosporine A and FK-506.

Structurally, **28** has a rigid 2-azabicyclo[3,3,1]nonane core, a spiro-fused pyrrolidine, and a phosphate ester at C4′ (Figure 7A). Since **28** contains a phosphate moiety, the phosphotransferase PsiK from the psilocybin biosynthesis pathway was used as a query to search for candidate BGCs of **28** in the genome of *Cladobotryum* sp. No. 11231.[69] The hits were then refined by scanning for a nearby NRPS-encoding gene since **29** and (*S*,*S*)-dityrosyl-piperazine (**30**) (Figure 7B) were proposed to be key intermediates of **28** (see Figure 6 as an example).

The *frz* cluster was identified (Figure 7A), which contained 12 genes including a single-module NRPS (FrzA), two SDRs (FrzB and FrzI), two P450 (FrzC and FrzL), two MT

(FrzE and FrzF), an old-yellow enzyme (OYE) like ene-reductase (FrzD), a nonheme, iron- and α-ketoglutarate (αKG)-dependent oxygenase (FrzG), a phosphotransferase (FrzJ), a hypothetic protein (FrzH), and a phosphoribosylpyrophosphate amidotransferase (PPAT, FrzK). The predicted functions of the encoded protein were consistent with the structure of **28**.

As expected, heterologous expression of FrzA (58% sequence identity to HqlA, Figure 6) and FrzB (64% sequence identity to HqlB, Figure 6) in A1145ΔSTΔEM produced **30** (Figure 7C and Table S5). Coexpression with the P450 FrzC (45% sequence identity to HqlC, Figure 6) delivered **31**, which contained a new N10–C1′ bond. The proposed reaction mechanism is shown in Figure 7C. Based on the structure of the proposed intermediate **29**, the dienone portion of **31** must be reduced to cyclohexanone. The most likely enzyme for this transformation was FrzD, the OYE-like ene-reductase, and coexpression of FrzA–D indeed led to **32**. Additional coexpression with FrzE and FrzF, which were predicted to be *N*-MT and *O*-MT, respectively, produced **33**. The order of the two methylation steps appeared to be interchangeable, as adding either MT alone resulted in monomethylated products. To obtain the aldehyde **29**, the C9–N10′ bond in **33** must be cleaved, likely via the hemiaminal intermediate **34**. There were two enzyme candidates, the P450 FrzL and the αKG FrzG, for the hydroxylation of C9 in **33**. Only coexpression of FrzG with FrzA–F produced a new product, **36**, which was a possible shunt product from the oxidation of the dehydrate imine **35** that existed in equilibrium with **34** and **29**.

For the next aldol reaction, there was no Frz candidate with sequence similarity to known aldolases. Interestingly, the hypothetical protein FrzH showed low sequence identity to ketosteroid isomerase (KSI), which catalyzes olefin isomerization of 3-oxo-Δ^5 ketosteroids to the Δ^4-enone isomers in steroid biosynthesis. The mechanism involves the formation of a dienolate stabilized by the KSI. Coexpression of FrzH with FrzA–G afforded **37**, establishing FrzH to be an aldolase that likely acts through enolate intermediate formation. Additional coexpression of the SDR FrzI in a FrzA–H expressing strain led to the production of 3 mg/L of dephospho-FR901483 (**38**).

Surprisingly, when the phosphotransferase FrzJ was coexpresed with FrzA–I, neither **28** nor **38** was detected. Since **28** was proposed to inhibit purine nucleotide biosynthesis, it is possible that **28** was toxic to the host, which led to either its degradation or transcriptional repression of all or some of *frzA–J*. Interestingly, *frzK* encoded the only copy of PPAT in *Cladobotryum* sp. No 11231. PPAT catalyzes the first step of *de novo* purine biosynthesis in which 5-phosphoribosyl-1-pyrophosphate (PRPP) is converted to 5-phosphoribosyl-1-amine (5-PRA) (Figure 7D). FrzK could be, as aforementioned in the Introduction, a self-resistance enzyme encoded in a BGC to protect the natural producer.[17] If so, PPAT could be the protein target of **28**. If **28** was made by the FrzA–J strain, coexpression with FrzK could protect the host from its toxicity. Indeed, coexpression of FrzK with FrzA–J restored the production of **38** along with the accumulation of **28**. *In vitro* assay using purified FrzJ, ATP, and $MgCl_2$ in the presence of **38** also led to the formation of **28**, confirming the phosphotransferase activity of FrzJ. Coexpression of the second P450 FrzL with FrzA–K did not deliver a new product, so the function of FrzL remained unknown. Although the function of FrzK as a

resistance enzyme awaited biochemical validation, total biosynthesis of **28** was successfully achieved.

Quinolactacin A (39).: Quinolactacin A (**39**) is a quinolone-γ-lactam hybrid fungal natural product isolated from a *Penicillium* sp. It exhibits a broad spectrum of bioactivities, including the inhibition of TNF (tumor necrosis factor) production from stimulated macrophages.[70–72] By analyzing the distribution patterns of ^{13}C atoms in **39** from feeding experiments with ^{13}C-labeled substrates, L-isoleucine and L-kynurenine were proposed to be precursors of **39**.[70] In addition, the *N*-methyl group was found to be derived from methionine, an installation likely catalyzed by a SAM-dependent MT. Guided by this information, Zhao et al. and Liu et al. independently identified the BGC of **39** from *P. citrinum* ATCC 9849 (*qul*) and DSM1997 (*qlt*), respectively (Figure 8A).[71,72] Both BGCs have similar gene organization, including genes encoding two single-module NRPSs (QltA/QulA and QltB/QulB), an FMO (QltD/QulF), an MT(QltE/QulM), and an indoleamine-2,3-dioxygenase (IDO, QltC/QulI).

Heterologous expression of QltA–E in A1145ΔEM produced **39** (Figure 8B and Table S6).[72] While excluding QltA, B, D, or E abolished the production of **39**, excluding QltC, a putative IDO, did not alter the titer. These data suggest that the housekeeping IDO in *A. nidulans* could be complementing the function of QltC in converting tryptophan to kynurenine. Similarly, except for *qulI*, which putatively encodes for an IDO, deletion of each of the individual genes in the *qul* cluster abolished the production of **39**.[71]

The biosynthesis of **39** was established by biochemical studies[71] as well as reconstitution of the pathway *in vitro*, i.e., total enzymatic synthesis[72] (Figure 8B). Incubation of L-kynurenine with all five enzymes (QltA–E) and necessary cofactors did not yield **39**; instead, shunt product **40** was observed. It was then realized that an endogenous amidase (GmdS) was essential to completing the biosynthesis. GmdS hydrolyzed the terminal amide in **41** to an β-keto acid **42**, allowing **42** to be loaded onto the tridomain NRPS QltB. The tetra-domain NRPS QltA activated and loaded L-isoleucine and catalyzed condensation with **42**-*S*-QltB to yield **43**. Finally, intramolecular Dieckmann cyclization and subsequent dehydration resulted in **39**.

Varicidins A (44) and B (45).: An emerging class of fungal Diels–Alderase has sequence homology to lipocalin-like proteins which bind to steroids and other hydrophobic molecules (see the biosynthesis of Sch 210972 in Figure 3).[59,73] Using lipocalin-like fungal Diels–Alderase as a search query, a BGC (*pvh*) from *Penicillium variabile* was identified (Figure 9A).[74] Heterologous expression of PvhA–E in the A1145 strain produced varicidin A (**44**) (Figure 9B and Table S7). Excluding the *N*-MT PvhD resulted in varicidin B (**45**). The *cis*-decalin moieties of **44** and **45** were presumably formed by *exo*-IMDA (intramolecular Diels–Alder) reactions, which were most likely catalyzed by the lipocalin-like Diels–Alderase PvhB. Expression of the PKS-NRPS PvhA and its partnering *trans*-ER PvhC produced **46**, **47**, and **48**. Based on the biosynthesis logic of decalin-containing natural products, the polyketide acyl chain was likely synthesized by the PKS portion of PvhA and the partnering *trans*-ER PvhC. The polyketide chain was then condensed with L-isoleucine and underwent Dieckmann cyclization to yield a released **46**. When **46** was left in a pH =

7.0 buffer, the *trans*-decalin **47** and **48** along with other minor compounds were detected, indicating nonenzymatic *endo*-IMDA formation of **47** and **48** from **46**.

Coexpression of PvhB with PvhA/C did not change the metabolite profile, indicating that **46** was not a substrate of PvhB. Coexpression of the P450 PvhE with PvhA/C produced **49**, confirming the function of PvhE in catalyzing oxidation of the terminal methyl group. Coexpression of PvhD with PvhA/C/E yielded **50**. These results elucidated the biosynthesis of **44** and **45**. Notably, installing the electron-withdrawing carboxylate in **49** (and **50**) significantly suppressed nonenzymatic IMDA reactions. This phenomenon could be explained by the electrostatic repulsion between the two anions in neutral pH solution. In addition, the electron-deficient diene and electron-deficient dienophile increased the reaction barrier, which was overcome by the Diels–Alderase PvhB.

Leporin B (51).: Leporins are 2-pyridone metabolites that exhibit antiinsectan and antifeedant activities from *Aspergillus* species (Figure 10A).[75,76] Based on the structure of leporin B (**51**), Ohashi et al. hypothesized that the leporin BGC *lep* (previously identified and verified in *A. flavus*[76]) encodes for an enzyme that can catalyze the hetero-Diels–Alder (HDA) reaction to construct the heterocycle dihydropyran core of **51**.[77] To identify the HDA-catalyzing enzyme, they heterologously expressed the six *lep* genes in A1145. Similar to the biosynthesis of tenellin,[45] three enzymesa PKS-NRPS LepA, a partnering *trans*-ER LepG, and a ring-expansion P450 LepHwere shown to be sufficient to construct the 2-pyridone core, as evidenced by the emergence of compound **52** (Figure 10B and Table S8). Additional coexpression of the SDR LepF, which was hypothesized to reduce **52** to **53**, led to a mixture of HDA and IMDA products (**54–58**). Among these products, **54** and **55** were proposed to derive from the quinone methide (*E*)-**59**, while **56–58** were from (*Z*)-**59**. There results highlighted the need for enzymatic stereoselectivity for the dehydration of **53** to (*E*)-**59** and the subsequent HDA reaction to the desired compound **54**.

Surprisingly, coexpression of LepI, a predicted *O*-MT with a conserved SAM binding site, in the LepA/F/G/H strain led to the production of **54** exclusively. These data, along with biochemical assays and computational calculations, provided evidence that LepI was responsible for the stereoselective pericyclic transformation of **53** to **54**. Interestingly, SAM was essential for the activity of LepI *in vitro*, indicating the versatility and importance of SAM in metabolism. Lastly, addition of the P450 LepD yielded the final product leporin B (**51**).

Ilicicolin H (60).: Ilicicolin H (**60**) was first isolated from *Cylindrocladium ilicicola* strain MFC-870.[78] It exhibits potent and broad antifungal activities by inhibiting the cytochrome bc1 complex.[79] Based on the 4-hydroxy-2-pyridone moiety in the structure of **60**, a five-gene BGC (*ncc*) in the genome of a producing fungus *Nectria* sp. B-13 was identified (Figure 11A).[80] Searching for the homologues of this five-gene BGC in the NCBI database resulted in 41 different fungal strains minimally containing these five genes. Among them, the cDNA library of *Penicillium variabile* was available to the Tang group; therefore, the BCG *icc* from *P. variabile* was used for the study (Figure 11B and Table S9).

As expected, expression of the PKS-NRPS IccA and partnering *trans*-ER IccB produced **61**. Further coexpression of the ring-expansion P450 IccC afforded **61**, **62**, and trace amounts of 8-*epi*-ilicicolin H (**63**). Adding IccD to the IccA–C strain produced **61** and **63**, confirming that IccD was a Diels–Alderase. The IccA–E expression strain produced **60**, suggesting that IccE was an epimerase. These results indicated that **62** was relatively unreactive under culturing conditions, requiring the Diels–Alderase IccD to produce the *trans*-decalin **63**. IccD selectively catalyzed the inverse-electron-demand Diels–Alder (IEDDA) but not the normal-electron-demand Diels–Alder (NEDDA) reaction to afford **64** (Figure 11B and C). Moreover, unlike LepI in the leporin B biosynthesis pathway (Figure 10), biochemical analysis indicated that IccD-catalyzed IEDDA was SAM-independent. This work expanded the catalytic repertoire of naturally occurring pericyclases.

Harzianopyridone (65) and Atpenin B (66).: Harzianopyridone (**65**) and atpenin A5 (**67**) structurally resemble the electron carrier ubiquinone (coenzyme Q, Figure 12A) and are nanomolar inhibitors of mammalian succinate ubiquinone oxidoreductase (mitochondrial complex II).[81] Isotope labeling studies suggested that **65** was derived from a polyketide-amino acid-containing tetramic acid.[82] This knowledge, together with the fact that dephenylated 2-pyridone is a shunt product of the aspyridone A biosynthesis pathway,[83] allowed researchers to identify a BGC (*har*) encoding several enzymes homologous to those encoded in the aspyridone A BGC from the genome of *Trichoderma harzianum*, a producer of **65** (Figure 12A).[84] This BGC also encoded proteins homologous to those in the *lep* BGC (Figure 10), such as the PKS-NRPS HarA, *trans*-ER HarE, ring expansion P450 HarG, and *N*-hydroxylase HarD. In addition, two FMOs (HarC and HarF) and an *O*-MT (HarB) were also encoded in *har*. The predicted functions of genes in *har* were consistent with the structure of **65**, except for the putative *N*-hydroxylase (HarD).

Heterologous expression of the seven genes *harA–G* in the A1145ΔEM strain yielded **65** along with **68** and two *N*-methoxylated compounds, **69** and **70** (Figure 12B and Table S10). The presence of an *N*-methoxy in **69** and **70** was surprising, as **65** did not contain this moiety, although this finding agreed with the function of HarD. To elucidate the biosynthesis of **65**, different combinations of *har* genes were expressed. The HarA/E expression strain produced **71**, consistent with the assigned function of the two enzymes. The HarA/E/G strain produced **68**, **71**, and **72**, indicating HarG was responsible for both ring expansion and phenyl cleavage. Feeding **68** to the HarG expression strain did not lead to the cleavage of the phenyl moiety, suggesting that **68** was a shunt product. A possible reaction mechanism from **71** to **72** via radical intermediates was proposed (Figure 12C). After ring expansion, dehydration of the 6-hydroxy-dihydro-pyridone (**73**) led to **68**. If the P450 heme-iron could be reduced prior to dehydration, HarG could further catalyze oxidation of the phenyl, which could lead to the loss of the quinone and give **72**.

To determine the functions of the remaining enzymes, HarB, -C, and -D were individually coexpressed with HarA/E/G. Only coexpression of HarD with HarA/E/G led to the production of a new product, *N*-hydroxy pyridone **74**. Further coexpression of HarB led to the emergence of **69** and **70**. While methylation of **74** to **69** fitted with the predicted function of HarB, methoxylation of **69** to **70** was not expected. **65** was produced when HarC

was coexpressed with HarA/B/D/E/G strain, demonstrating HarF was not essential for the biosynthesis of **65**.

To further clarify the *har* biosynthetic pathway, the authors conducted feeding experiments. Feeding **69**, **70**, or **74** to yeast expressing HarB/C led to the formation of **65**, indicating **69**, **70**, and **74** were *bona fide* biosynthetic intermediates. However, **72** was not consumed by the HarB/C expression yeast strain. Therefore, *N*-methoxylation was required for the formation of **65**. Moreover, feeding **74** to yeast expressing HarB only produced **69**, indicating that emergence of **70** in *A. nidulans* expressing HarA/B/D/E/G was likely due to crosstalk with endogenous monooxygenases. These results also demonstrated that HarB was responsible for all methylation reactions and HarC was required for C-5 and C-6 hydroxylation.

Guided by the *har* BGC, a homologous cluster (*apn*) in *Penicillium oxalicum*, an atpenin A5 (**67**) producer, was identified (Figure 12A). Heterologous expression of ApnA–E/G in *A. nidulans* led to the production of atpenin B (**66**) at 0.3 mg/L. The *apn* BGC contained additional genes possibly involved in the chlorination steps.

Citridone B/B′ (75/75′).: Citridones are a family of pyridone-containing fungal natural products that can potentiate the activity of miconazole against *Candida albicans*.[85] The pyridone moiety in citridones suggested a PKS-NRPS origin. By using PKS-NRPS and ring expansion P450 sequences as queries, the citridone BGC (*pfp*) was identified from the genome of the natural producer *Penicillium* FKI-1938 (Figure 13A).[86] Besides the PKS-NRPS PfpA and ring expansion P450 PfpB, *pfp* also encoded a SDR PfpC and the two additional P450s PfpD and PfpE. The absence of a *trans*-ER enzyme indicated a possible polyene product from PfpA.

Heterologous expression of PfpA in A1145 produced **76** (Figure 13B and Table S11). Coexpression of PfpA with PfpB was expected to form the ring expansion product **77**, but instead the major metabolite detected was (±)-citridone E (**78**), a Michael addition product of **77**. The formation of **78** was attributed to the two methyl substitutions at C-8 and C-10, which caused a nonplanar conformation of the diene due to steric repulsion. Disruption of the conjugation facilitated the Michael addition. Coexpression of PfpA–C produced (±)-citridone A (**79**) and (±)-tersone D (**80**). PfpC belonged to the SDR superfamily, and its homologues in other 2-pyridone pathways reduce the C-7 ketone to alcohol, which can dehydrate spontaneously to form *E* or *Z ortho*-quinone methide (see LepF in Figure 10 as an example). Therefore, PfpC was proposed to catalyze the reduction of **77** to **81**, which then dehydrated to (*E*)-**82** and (*Z*)-**82**. (*E*)-**82** and (*Z*)-**82** could undergo electrocyclization to produce C4-*O*-pyranopyridone **80** or C2-*O*-pyranopyridone **84**, respectively. *E*–*Z* isomerization of (*E*)-**82** to **83** set up a nonenzymatic cycloisomerization to give **79**. The production of **79** and **80** but not **84** in the PfpA–C strain suggested that **79** and **80** are the thermodynamically favored products.

To produce the C2-*O*-furopyridine moiety in **75/75′**, enzymatic reaction on the thermodynamically unfavored intermediate **84** was necessary to push the pathway forward. Considering the appearance of a quaternary carbon (C-8) connected to the pyridine ring in **75/75′**, a rearrangement involving the formation of an epoxide at the C-7–C-8 olefin was

proposed (Figure 13C). Coexpression of PfpA–D produced CJ-15696 (**85**) and CJ-16173 (**86**), along with decreased levels of previously observed metabolites. Although the absolute configurations at C-8 and C-9 were not determined, both **85** and **86** were enantiomerically pure. Since the putative substrate **84** was a racemate, PfpD must stereospecifically epoxidize the 9*S*-**84** isomer so that after carbon–carbon rearrangement **85** could be formed (Figure 13C). Hydroxylation of C-14 in **85** by PfpD or an endogenous oxidase, followed by hemiacetal formation, yielded **86**. Lastly, coexpression of all five enzymes PfpA–E produced **75/75′**, isolated as a mixture. Feeding **85** to the PfpE expression strain also produced **75/75′**. Therefore, PfpE was proposed to stereospecifically epoxidize **85**. After water-mediated epoxide opening, **75/75′** were formed.

Fusaric Acid (87).: Fusaric acid (**87**) is a mycotoxin isolated from *Fusarium* species that exhibits strong phytotoxicity and causes wilt symptoms.[87] The BGC of **87** has been identified in several *Fusarium* species, and gene knockout studies indicated that five genes (*fub1*, *fub4*, and *fub6*–8) were essential for its biosynthesis (Figure 14A).[88] To characterize the biosynthesis of **87**, all five essential genes were reconstituted in the A1145ΔEM strain.[89] However, instead of **87**, an unstable compound with m/z = 184 ($[M + H]^+$, proposed structure **88**) was detected (Figure 14B and Table S12). To support the proposed structure of **88**, the crude **88** was reduced by sodium cyanoborohydride, which led to the identification of (2*S*,5*S*)-and (2*S*,5*R*)-5-butyl-L-pipeoclic acid (**89** and **90**). This result implied that **88** was epimerized at C-5, presumably through tautomerization. The production of **88** from heterologous expression of the five essential genes indicated that the enzyme responsible for the last oxidation step was missing. An FMN-dependent oxidase encoded in the *fub* BGC, Fub9, seemed like a plausible candidate, and, indeed, its coexpression with Fub1/4/6/7/8 led to the accumulation of **87**. This discrepancy with the gene inactivation studies suggested that an endogenous pathway in *Fusarium* compensated for the activity of Fub9.

The functions of Fub6-9 were biochemically characterized. Recombinant Fub8, a predicted NRPS-like carboxylic acid reductase, reduced *trans*-2-hexenoic acid (**91**) to *trans*-2hexenal (**92**) in the presence of ATP, NADPH, and $MgCl_2$. Incubation of Fub6, a putative medium-chain dehydrogenase/reductase, with **92** and NADPH afforded *n*-hexanal (**93**), indicating that it was an ene-reductase. Incubation of Fub7, a predicted PLP-dependent enzyme, with **93** and *O*-acetyl-L-homoserine (OAH) afforded **88**, showing that Fub7 catalyzed C–C bond formation. As expected, its activity was abolished when Fub7 was pretreated with hydroxylamine, an inhibitor for PLP-dependent enzymes. Lastly, including Fub9 in the Fub7 reaction mixture using **93** and OAH as substrates produced **87**. Biochemical characterization of Fub6-9 allowed total enzymatic synthesis of **87** in one pot from **91** and OAH in the presence of Fub6-9 and the necessary cofactors.

Thermolides A–E (94–98).: Thermolides A–E (**94–98**) (Figure 15A) are 13-membered macrolactones discovered from the extreme thermophilic fungi *Talaromyces thermophilus* YM 3–4.[90] Thermolides A (**94**) and B (**95**) exhibit potent toxicity toward nematodes with LC_{50} value of 0.5–1 μg/mL. Genome sequenced strain *T. thermophilus* NRRL 2155 was found to produce **94–98**, providing the opportunity to identify the BGC of Thermolides.[91] Based on the structures of **94–98**, a seven-gene BGC (*thm*) encoding an HR-PKS (ThmA),

a single-module NRPS (ThmB), an SDR (ThmC), a flavin-dependent oxidase (ThmD), an acetyltransferase (ThmE), a glycosylhydrolase (ThmF), and a glycotransferase (ThmG) was identified (Figure 15A).[92]

Heterologous expression of ThmA–G in A1145 produced **94**, **96**, **99**, and **100** (Figure 15B and Table S13). To investigate the functions of the Thm enzymes, different combinations were expressed. Heterologous expression of the HR-PKS ThmA and NRPS ThmB produced **101** and **102**, indicating that ThmA and -B were sufficient to synthesize the backbone. Coexpression of ThmC with ThmA/B produced **97** and **98**, while coexpression of ThmE with ThmA/B produced **103–106**, indicating that both **101** and **102** can be the substrate of the SDR ThmC and the acetyltransferase ThmE. Conversion of **103** to **105** and **104** to **106** were likely spontaneous since **106** could be formed within 12 h in a pH = 7.5 Tris buffer containing **104**. The ThmA–C/E strain produced **94**, **96**, **99**, and **100**, demonstrating that only four genes were required to complete the total biosynthesis.

Beauveriolides I (107) and III (108).: *Cordyceps militaris* is an entomopathogenic fungus that has been widely used in traditional Chinese medicine for centuries.[93] Genome mining of *C. militaris* CM01 led to the identification of the *cm3* BGC encoding an NRPS (Cm3A), an HR-PKS (Cm3B), an acyltransferase (Cm3C), and an acyl-CoA synthetase (Cm3D)[94] (Figure 16A). Heterologous expression of Am3A–D in the A1145 strain produced beauveriolides I (**107**) and III (**108**) (Table S14). Beauveriolides have been identified from *Beauveria* species and were found to inhibit acyl-CoA:cholesterol acyltransferases.[95] The biosynthesis pathway of **107** was proposed as shown in Figure 16B. The HR-PKS Cm3B iteratively catalyzes the formation of the linear polyketide, which is then transferred to the first T domain of the NRPS Cm3A facilitated by Cm3D and Cm3C. Cm3A then activates and incorporates L-phenylalanine, L-alanine, and L-leucine into the growing peptide chain followed by intramolecular cyclization to produce **107**. The intramolecular cyclization is catalyzed by the ester-bond-forming C domain in the C terminal of Cm3A.[96] However, considering that the leucine and *allo*-leucine residues in **107** and **108**, respectively, are both D form and the fact that epimerization (E) domains show sequence and structure homology to C domains,[96] the domain architecture of the last module of Cm3A is likely A-T-E-C rather than A-T-C-C as originally proposed.

Mycophenolic Acid (109).: Mycophenolic acid (109) isolated from *Penicillium brevicompactum* is an active component of immunosuppressants used in organ transplantations. It is a potent inhibitor of inosine-5′-monophosphate dehydrogenase (IMPDH), a rate-limiting enzyme in guanosine monophosphate (GMP) biosynthesis.[97] The *mpa* BGC responsible for producing **109** had been identified from *P. brevicompactum* (Figure 17A).[98] The *mpa* BGC encoded an NR-PKS (MpaC), a prenyltransferase (MpaA), a globin-like enzyme (MpaB) with unknown function, a P450 (MpaD), a hydrolase (MpaE), an IMPDH (MpaF, a putative self-resistance enzyme), an *O*-MT (MpaG), and a putative protein (MpaH) containing an α/β-hydrolase fold. *mpaD* and *mpaE* were later demonstrated to be transcribed as a single gene that encoded a single polypeptide MpaDE, and coexpression of MpaC and MpaDE in *A. nidulans* produced 5,7-dihydroxy-4-methylphthalide (**110**) (Figure 17B).[99]

The *mpa* BGC was also identified from *P. griseofulvum*, a high producer of mycophenolic acid.[100] The *mpa* clusters from the two strains showed high similarity/identity (Figure 17A). Reconstitution of PgMpaA/C/DE in A1145 produced **110** and demethylmycophenolic acid (**111**) (Figure 17B and Table S15). Feeding **112** to A1145 produced **111**, indicating that the oxidative cleavage step from **112** to **111** in A1145 was an *mpa* cluster-independent process. PgMpaA was a membrane-bound prenyltransferase. Incubation of **110**, FPP, Mg^{2+}, and PgMpaA prepared from the microsome fraction of the PgMpaA-expressing yeast strain produced **112**, which confirmed that MpaA catalyzed the regioselective farnesylation. When **112** was incubated with the cell-free lysate containing PgMpaB, **113–115** were detected. **114** and **115** were likely derived from **113** in the presence of cell-free lysate. Therefore, **113** was proposed to be the real product from **112** catalyzed by PgMpaB. Feeding **113** to the *P. griseofulvum mpaC*Δ mutant restored the biosynthesis of **109**, confirming **113** to be an intermediate in the *mpa* pathway. Lastly, coexpression of PgMpaA–C/DE/G produced **109**, **110**, and a trace amount of **112**, which completed the total biosynthesis of **109**.

Flavunoidine (116).: Among the known fungal NPs, the hybrid TC/NRPS core is underrepresented as suggested by the prevalence of TC/NRPS BGCs in sequenced fungal genomes.[101] Yee et al. investigated one such uncharacterized nine-gene BGC (*flv*) from *Aspergillus flavus* (Figure 18A). This BGC was conserved in several fungal species and encoded two TCs (FlvE and FlvF) and one NRPS (FlvI). Heterologous expression of FlvA–I in A1145 led to the identification of the novel compound flavunoidine (**116**) (Figure 18B and Table S16A). The omission of FlvI resulted in the disappearance of **116** but the emergence of its component precursors 5,5-dimethyl-L-pipecolic acid (**117**) and **118**. Feeding **117** and **118** to A1145-expressing FlvI yielded back **116** (Figure 18B and Table S16B), revealing that FlvI catalyzed their esterification.

The biosynthesis of pipecolic acid has been shown to involve a PLP-dependent enzyme and a reductase.[102] FlvA was a didomain enzyme: the N-terminal domain was predicted to be a PLP-dependent lyase, while the C-terminal domain was predicted to be an α-ketoglutarate-dependent oxygenase. Thus, FlvA and FlvB (a predicted SDR) were proposed to be involved in the biosynthesis of **117**. This hypothesis was validated when the FlvA/B expression strain produced only **117**, the FlvC–H strain produced only **118**, and the FlvA/B/I strain produced **116** from the feeding of **118** (Table S16A and S16B). The PLP-dependent lyase and oxygenase domains of FlvA were proposed to catalyze the γ-replacement and decarboxylation reactions, respectively (Figure 18B).

To examine the functions of the two TCs (FlvE and FlvF), each gene was removed from the *flvC–H* strain separately. The removal of *flvE* abolished the related metabolites, suggesting that FlvE was involved in the formation of the terpene core. The function of FlvE was confirmed by heterologous expression of the enzyme in *S. cerevisiae*, which afforded (1*R*,4*R*,5*S*)-(+)-acoradiene (**119**). On the other hand, the removal of *flvF* led to accumulation of **120a** and **120b**, which indicated that FlvF was involved in making the C–N bond in **118**. To determine if oxidative modifications of **119** could generate the terpene core in **118**, FlvC and FlvD were coexpressed with FlvE. While the FlvC/D/E strain produced **120a** and **120b**, the FlvD/E strain produced **121a** and **121b**. Moreover, the FlvD–

H strain produced **122**. Collectively, these results indicated that FlvD was responsible for the oxidative conversion of **119** into the tetracyclic terpene core and FlvC was responsible for the hydroxylation of the C-10.

Feeding **119** to the FlvD/F/G/H strain generated **122**, while feeding **121a**/**121b** to the same strain did not (Table S16B), confirming that **119** was a precursor and **121a**/**121b** were shunt products. Endogenous ethanolamine might have entered the active site of FlvD and quenched the carbocation intermediate **123** to form **121a**/**121b**. When FlvF was expressed, the quenching was suppressed and dimethyl cadaverine (**124**) could stereoselectively quench **123** to afford **122**. To test the function of FlvF, **124** was fed to the FlvD/E and FlvD–F strains, and only the latter produced **122**. The two remaining enzymes in the pathway, FlvH and FlvG, were verified to synthesize **124** from L-lysine. Removing FlvH from the FlvC–H strain, trace amounts of **118** were formed. The titer of **118** was restored upon feeding of *Nε*,*Nε*-dimethyl-L-lysine (**125**). When **125** was fed to the FlvC–F strain, **118** was not detected and only **120a/120b** were observed. Feeding of **124** restored **118**. These results indicated that FlvH methylated L-lysine to give **125**, which was then decarboxylated by FlvG to afford **124**. Therefore, in the *flv* pathway, the TC FlvE and the P450 FlvD constructed the tetracyclic core, while the second TC FlvF attached the C-13 axial dimethyl cadaverine (**124**). The NRPS FlvI acylated the terpenoid core with dimethylpipecolate (**117**).

***E. coli*–Yeast–Fungal Shuttle Vectors pYFAC-CH2, pYFAC-CH3, and pYFAC-CH4.—**The Chooi group renamed pKW20088 to pYFAC-*pyrG* (Figure S2A; YFAC stands for yeast fungal artificial chromosome).[103] Insertion of different alcohol-inducible promoters into pYFAC-*pyrG* yielded pYFAC-CH2 (Figure S2C).[34] The pYFAC-CH2 vector contains an *alcA* promoter, a bidirectional *alcS/M* promoter,[104] and an *aldA* promoter[105] along with terminators in between. Replacing *AfpyrG* with *AfriboB* and *AfpyroA* generated pYFAC-CH3 and pYFAC-CH4, respectively. Since each vector contains four expression cassettes, this system is capable of expressing up to 12 genes in a *pyrG*89, *pyroA*4, and *riboB*2 mutant strain.

Elsinochrome A (126).: Perylenequinones are a group of reactive oxygen species (ROS)-generating photosensitizers that function as phytotoxins and have potential application in photodynamic cancer therapy.[106] Using the YFAC-CH system, the biosynthesis of the *elc* pathway in the wheat pathogen *Parastagonospora nodorum* was elucidated (Figure 19).[34] Heterologous expression of the NR-PKS ElcA in the genetically dereplicated strain LO7890[55] (Table 1) yielded *nor*-toralactone (**127**) (Figure 19B and Table S17).[107] The product template (PT) domain of ElcA was proposed to catalyze C4–C9 and C2–C11 cyclization, while the thioesterase (TE) domain to catalyze pyrone formation.[108] ElcB was a didomain enzyme containing an N-terminal *O*-MT and a C-terminal FMO domain.[34,109] Coexpression of ElcA with the truncated ElcB containing only the *O*-MT domain produced toralactone (**128**) (Figure 19C). Coexpression of ElcA with the full-length ElcB yielded **129**, **130**, and unstable intermediate **131**. **129** and **130** were likely derived from **132** via the glutathione *S*-transferase detoxification pathway in the host. Coexpression of the *O*-MT ElcD with ElcA/B produced the major compound **133** with a mass almost three times that

of the putative product **134**. The chemical structure of **133** was proposed as shown in Figure 19B but has not been confirmed.

Coexpression of ElcA/B/D/E had little change to the metabolic profile compared to ElcA/B/D. Only the ElcA/B/D/E/F/G strain made (*P*)-**135** (hypocrellin A) and (*P*)-**136**. The (*P*) helicity of **135** and **136** was confirmed by electronic circular dichroism (ECD) spectra. Intriguingly, some ElcA/B/D/E/G transformants produced less amounts of (*P*)-**135** and (*P*)-**136**, while others produced no (*P*)-**135** and (*P*)-**136** at all.

Therefore, ElcE and ElcG were proposed to be involved in the dimerization of **134**, leading to the formation of the pentacyclic perylenequinone core in **137** (Figure 19D). In addition, a putative FMO gene, *elcH*, located ~8 kb upstream of the *elc* cluster was found to be co-upregulated with the *elc* genes. Expression of ElcH in a strain producing (*P*)-**135** and (*P*)-**136** resulted in the formation of elsinochrome A (**126**), confirming the involvement of ElcH in the biosynthesis of **126**. Interestingly, **126** had (*M*) helicity, while the isolated **135** and **136** had (*P*) helicity. These data suggested that **137** was first converted to (*M*)-**135** and (*M*)-**136** via transannular *syn* aldol reactions followed by spontaneous atropisomerization to afford (*P*)-**135** and (*P*)-**136**.

(M)-Viriditoxin ((M)-138).: (*M*)-Viriditoxin ((*M*)-**138**) is a biaryl mycotoxin first isolated from *A. viridinutans*.[110] (*M*)-**138** and its derivatives possess antibacterial and cytotoxic activities.[111] A BLASTp search using the NR-PKS ElcA from the elsinochrome pathway (see Figure 19) as a query led to the identification of a candidate BGC of (*M*)-**138**, *vdt*, from the producer *Paecilomyces variotii* CBS101075 (Figure 20A).[112] Heterologous expression of the NR-PKS VdtA in LO7890 produced the naphtho-α-pyrone **139**, the predicted core of (*M*)-**138** (Figure 20B and Table S18). Coexpression of the *O*-MT VdtC with VdtA yielded **140**. Coexpression of the SDR VdtF with VdtA/C resulted in **141**. Next, coexpression of the Baeyer–Villiger monooxygenase (BVMO) VdtE with VdtA/C produced **142** and **143**, while coexpression of VdtE with VdtA/C/F produced **144** and **145**. These results confirmed that VdtE functioned as a BVMO. However, BVMOs have never been reported to possess hydrolyzing activity.

To characterize the function of VdtE, recombinant VdtE was assayed, and it was found to fully convert **140** to **142** and **141** to **144** in the presence of flavin adenine dinucleotide (FAD) and NADPH. The result indicated that VdtE was a methyl ester-forming BVMO, which had not been reported before. The formation of **143** and **145** was likely due to the activity of an endogenous hydrolase in the host. The Baeyer–Villiger reaction catalyzed by VdtE was intriguing, as the formation of a methyl ester required the migration of the less electron-rich methyl group, against migratory aptitude.

Since VdtD was a predicted hydrolase, the authors initially proposed that coexpression of VdtD with VdtA/C/E would produce more carboxylic acid derivative **143**. Interestingly, the VdtA/C/D/E strain produced more **142** and the VdtA/C/D/E/F strain produced exclusively **144**. These results suggested that instead of functioning as a hydrolase, VdtD possessed the opposite role. Analysis of the VdtD protein sequence identified a mutation in the catalytic Ser-(Glu/Asp)-His triad, in which the Ser was mutated to Asp. Therefore,

VdtD might be able to bind to the methyl esters **142** and **144** and protect them from hydrolyzation by endogenous hydrolases. Addition of the multicopper oxidase (MCO) VdtB to the VdtA–F strain produced (*M*)-**138** and its atropisomer (*P*)-viriditoxin ((*P*)-**138**) at a 20:1 ratio. Interestingly, without VdtD, the VdtA/B/C/E/F strain generated a mixture of bisnaphthopyrones along with trace (*M*)-**138** and (*P*)-**138**. Among them, the major metabolites isolated were (*M*)-**146**, (*P*)-**146**, **147**, and **148** (Figure 20B). The ratio of (*M*)-**138**:(*P*)-**138** and (*M*)-**146**: (*P*)-146 produced by the VdtA/B/C/E/F strain was 1:2 (Table S18). It appeared that in the absence of VdtD, VdtB lost the stereoselectivity and substrate fidelity for the oxidative coupling reaction.

To corroborate the functions of VdtB and VdtD, cell-free lysates containing VdtB and VdtD were prepared separately from *A. nidulans*. When **144** was used as a substrate, cell-free extracts containing VdtB alone converted **144** to (*M*)-**138** and (*P*)-**138** at a 1:2 ratio, while VdtB and VdtD converted **144** to (*M*)-**138** predominantly. The *in vitro* data demonstrated VdtB as a regioselective coupling MCO and that VdtD controlled the stereoselectivity in the formation of (*M*)-**138**. Therefore, VdtD was a noncatalytic hydrolase with a function analogous to the dirigent protein, which could orient phenoxy radicals to direct stereospecific formation of biaryl products.[113] Lastly, coexpression of the HR-PKS ORF1 with VdtA–F did not change the metabolic profile, indicating ORF1 was not involved in the biosynthesis of (*M*)-**138**.

Stemphyloxin II (149).: The *sth* BGC from the wheat pathogen *Parastagonospora nodorum* was found to be highly expressed during plant infection (Figure 21A).[114] It had high homology to the previously identified *bet* cluster responsible for betaenones B (**150**) and C (**151**) biosynthesis,[115] hinting that *sth* might produce betaenone-like molecules (Figure 21B). Indeed, overexpression of the putative regulator *sthR* in *P. nodorum* led to the accumulation of the phytotoxin stemphyloxin II (**149**), which was originally isolated from *Stemphylium botryosum* along with stemphyloxin I (**152**).[116] In order to elucidate the biosynthesis of the unique tricyclo[6.2.2.0^{2,7}] system in **149**, *sth* was reconstituted in LO7890 using the YFAC-CH vectors (Table S19).

Coexpression of the HR-PKS SthA and its partner *trans*-ER SthE produced dehydroprobetaenone I (**153**). Coexpression of the SDR SthC with SthA/E yielded probetaenone I (**154**), indicating the aldehyde reductase activity of SthC. Coexpression of the P450 SthF with SthA/E produced **153**, small amounts of **150** and **151**, and epoxybetaenone (**155**). The production of **155** led to the hypothesis that SthF catalyzed the transformation of **153** to **151** by successive epoxidation, oxidative epoxide opening, and hydroxylation. The small amount of **150** likely came from the reduction of **151** by an endogenous reductase. Coexpression of SthA/C/E/F resulted in the exclusive accumulation of **150**.

Sequence analysis of SthB revealed that SthB comprised a FAD-binding domain and a berberine bridge enzyme (BBE) domain. Coexpression of SthB with SthA/E/F gave a new compound, **156**, which contained the tricyclo[6.2.2.0^{2,7}] system in **149**. Incubation of **151** with the cell-free lysate of *A. nidulans* containing SthB also yielded **156**, indicating that SthB was responsible for the intramolecular aldol reaction that generated the bridged

tricyclic system. Lastly, coexpression of the second P450 SthD with SthA/B/E/F generated **149**, confirming that SthD hydroxylated the C-15 methyl group. Surprisingly, when SthA/E/F/D were coexpressed, instead of stemphyloxin I (**152**), dihydrostemphyloxin I (**157**) was obtained. Formation of **157** from **152** was likely due to an endogenous reductase.

The discovery of SthB as an aldolase in the *sth* pathway represented the first example of a dedicated aldolase in the biosynthesis of a fungal secondary metabolite. However, the function of the FAD-binding domain in SthB remained unknown, awaiting further biochemical characterization.

Nanangelenin A (158).: Nanangelenin A (**158**) was isolated from *A. nanangensis*, a rare *Aspergillus* species from Australia.[117] It exhibited moderate cytotoxicity and no significant antifungal, antibacterial, or antiparasitic activity. Notably, it contained a rare 1-benzazepine scaffold. Retrobiosynthesis analysis suggested that **158** was derived from anthranilic acid and L-kynurenine. L-Kynurenine is an intermediate in the metabolism of L-tryptophan. Conversion of L-tryptophan to L-kynurenine is first catalyzed by tryptophan-2,3-dioxygenase (TDO) or IDO, as aforementioned in the quinolactacin A (**39**) biosynthesis pathway (Figure 8), to generate *N*-formyl-L-kynurenine, which is then hydrolyzed spontaneously[118] or by kynurenine formamidase to form L-kynurenine.

Genomic and retrobiosynthetic analyses led to the identification of a BGC (*nan*) encoding an IDO (NanC), an NRPS (NanA), a prenyltransferase (NanD), an *N*-MT (NanE), an FAD oxidoreductase (NanF), and an acetyltransferase (NanB) in the genome of *Aspergillus nanangensis* (Figure 22A).[117] Heterologous expression of the NRPS NanA in LO7890 did not produce any new metabolite, which was likely due to the absence of the substrate L-kynurenine. Gratifyingly, coexpression of the IDO NanC with NanA yielded nanangelenin B (**159**) (Figure 22B and Table S20). These data, together with the fact that feeding L-kynurenine to the NanA expression strain yielded **159**, indicated that NanC converted L-tryptophan to *N*-formyl-L-kynurenine, which then hydrolyzed spontaneously to L-kynurenine. NanA then activated and condensed anthranilic acid and L-kynurenine to generate **159**. Coexpression of the prenyltransferase NanD with NanA/C yielded nanangelenin C (**160**), while coexpression of the *N*-MT NanE with NanA/C led to partial conversion of **159** to nanangelenin D (**161**). When NanA/C/D/E were expressed together, a new product, nanangelenin E (**162**), was formed.

To assess the function of the FAD oxidoreductase NanF (proposed to be an *N*-hydroxylase) and the acetyltransferase NanB, NanA/C/F- and NanA/B/C/F-expressing strains were constructed. However, both strains still produced **159**, suggesting that *N*-hydroxylation and acetylation could not occur before prenylation. Indeed, the NanA/C/D/F and NanA/C/D/E/F strains produced putative MS peaks corresponding to the *N*-hydroxylated intermediates **163** and **164**, respectively. However, due to low yield and instability, purification of both compounds for structural characterization was unsuccessful. Lastly, the NanA–D/F- and NanA–F-expressing strains delivered nanangelenin F (**165**) and **158**, respectively.

To characterize the C-terminal C_T-T_3 didomain of NanA, point mutations were introduced. Coexpression of NanC with NanA-H2106A (containing a point mutation of the catalytic

histidine in the C_T domain) lost the ability to synthesize **159**, and coexpression of NanC with NanA-S2401A (containing a point mutation of the active site serine in the T_3 domain) greatly reduced the yield of **159**. These results indicated that the C_T domain was required for cyclization release to give **159** and that the T_3 domain enhanced the catalytic efficiency of C_T. In addition, incubation of the *N*-acetylcysteamine thioester **166** with recombinant Nan-C_T produced **159**, while incubation of **166** with boiled Nan-C_T produced **167**, which was thought to be formed spontaneously (Figure 22C). These results indicated that Nan-C_T catalyzed the regioselective cyclization of **166** to afford **159**.

Burnettramic Acid A (168).: Burnettramic acids A (**168**) and B (**169**), together with their aglycones (**170** and **171**), were isolated from *A. burnettii* (Figure 23A).[119] **168** and **169** are unusual bolaamphiphilic pyrrolizidinediones with antibiotic activities. Genome sequencing and comparative genomic analysis led to the identification of a BGC (*bua*) that encoded a proline hydroxylase (BuaE), a PKS-NRPS (BuaA), a *trans*-ER (BuaC), two P450s (BuaD and BuaG), and a glycosyltransferase (BuaB). To verify that *bua* encoded for the biosynthesis of **168**, strains expressing BuaA/C, BuaA/C/E, BuaA–C/E/F/G, and BuaA–G were constructed from LO7890 (Table S21). While the BuaA/C and BuaA/C/E strains did not produce new metabolites, the BuaA–C/E/F/G and BuaA–G strains yielded **168**, **170**, and **171**. **168** converted to **169**, **170**, and **171** in acidic condition, raising the prospect that the minor epimers **169** and **171** were artifacts from the isolation process. Based on these results, a tentative biosynthesis pathway of **168** was proposed (Figure 23B). First, BuaE hydroxylated proline to form 4-hydroxyproline, which was then activated and transferred to the PKS-NRPS/*trans*-ER BuaA/BuaC to produce the intermediate **172**. Multiple hydroxylations of **172** by the P450 BuaG yielded the aglycone **170**, which was then mannosylated by the glycosyltransferase BuaB to produce **168**. The reason that the BuaA/C/E strain did not accumulate a detectable amount of **172** remained unclear.

II. SITE-SPECIFIC CHROMOSOMAL INTEGRATION EXPRESSION SYSTEM

In contrast to the heterologous expression systems that use ectopic integration and extrachromosomal replication described above, the Oakley group and our group used homologous recombination to integrate genes of interest into specific sites in the chromosome. The high-efficiency gene targeting system in *A. nidulans nkuA*Δ strains[48,49] allows heterologous genes to be inserted scarlessly (i.e., without restriction site) into a defined locus. There are at least two advantages to this approach. First, a defined integration site circumvents positional effects and allows further strain engineering to be designed more rationally. Second, and most importantly, chromosomal integration provides intrinsic genetic stability, which is crucial for large-scale and long-term bioproduction.[120] The *wA* and *yA* loci were chosen as the sites of integration because both genes are involved in the biosynthesis of green conidial pigment. wA, an NR-PKS, synthesizes a yellow-colored polyketide, which is converted to green pigment by yA, a conidial laccase. Therefore, *wA* and *yA* mutants produce white and yellow spores, respectively, allowing correct transformants to be quickly identified visually.

Reiterative Recombination.

In our workflow, transforming fragments are generated by PCR, bypassing cloning and yeast assembly. Because PKS and NRPS genes are large and sometimes difficult to amplify, we often generate two smaller transforming fragments that are fused by HR *in vivo* to yield the full-length coding sequence (gene A) under the control of P*alcA* (Figure 24A).[54] Each fragment carries a selection marker, and transformants carrying both markers (markers 1 and 2) are selected and verified by diagnostic PCR. To integrate another gene (gene B), we apply an iterative recombination strategy (Figure 24B).[121] Insertion of gene B simultaneously removes marker 2; thus transformants carrying markers 1 and 3 are selected. Since a selection marker is recycled with each transformation, in principle, an unlimited number of heterologous genes can be sequentially integrated.

Asperfuranone (173).—The utility of this system was demonstrated in the reconstitution of the *Ateafo* biosynthesis pathway from *A. terreus* in LO4389 (Figure 25A).[54] A homologous BGC (*afo*) existed in *A. nidulans*, which we have previously activated by placing the positive regulator *afoA* under the control of P*alcA* and identified the encoded metabolite, asperfuranone (**173**).[122] We first deleted *afo* from the host strain to eliminate possible crosstalk between the homologous pathways. The *Ateafo* genes were then introduced sequentially into the *wA* locus using the reiterative recombination strategy.

While expression of the NR-PKS AteAfoE alone yielded no product, coexpression with the HR-PKS AteAfoG produced asperbenaldehyde (**174**) (Figure 25B and Table S22). This data confirmed our previous hypothesis that the HR-PKS synthesized a highly reduced polyketide side chain, which was transferred to the SAT domain of the NR-PKS for extension, aldol condensation, aromatization, and reductive release to generate **174**.[122] Coexpression of the FAD-dependent oxygenase AteAfoF with AteAfoE/G did not result in a new product, indicating that AteafoF did not modify **174**. On the other hand, coexpression of the monooxygenase AteAfoD with AteAfoE/G resulted in preasperpyranone (**175**) and asperpyranone (**176**), both of which contained a hydroxy group at C-4, suggesting that AteAfoD dearomatized **174** to generate intermediate **A**. This reaction has also been demonstrated by Davison et al.[123] and Zabala et al.[124]

Interestingly, coexpression of AteAfoC greatly increased the yield of **174** and its two hemiacetal derivatives **177** and **178**. AteAfoC and its homologue CtnB were initially misassigned as oxidoreductases,[28,122] but Zabala et al. revised their function to be esterases/lipases.[124] To investigate whether AteAfoC could release the polyketide side chain **179** from AteafoG, we created an AteAfoG/C coexpression strain. Even though **179** was produced, it was at a very low level (~1 mg/L). Alternatively, AteAfoC could be responsible for transferring **179** from AteAfoG to AteAfoE, considering the high yield of 174 (~300 mg/L) in the AteAfoG/E/C strain. Coexpression of AteAfoC/D/E/G resulted in increased yields of **175** and **176** compared to AteAfoD/E/G. Adding another copy of *AteafoC* further increased the yield about 1.5-fold, and we were able to isolate minor shunt products proasperfuranone A (**180**) and B (**181**) from this strain. Lastly, coexpression of the FAD-dependent oxygenase AteAfoF with AteAfoC/D/E/G produced **173**, completing the total biosynthesis of asperfuranone (**173**). Based on these data, we proposed that AteAfoF

oxidized C-8 to generate **182**, which abolished enol formation and six-membered ring cyclization (Figure 25B and C). Fivemembered ring cyclization and dehydration of **182** yielded **183**, which was then reduced to **173**. The fact that no **183** had been identified indicated that the conversion of **183** to **173** was catalyzed by an endogenous reductase. The *afo* and *Ateafo* clusters did contain a dehydrogenase (*orf 2*), but its deletion did not alter the yield of **173**.[122] If *orf 2* was involved in the transformation of **183** to **173**, its function was likely compensated by an unknown endogenous reductase.

We created three strains with different orders of *AteafoC*, *AteafoD*, and *AteafoF* (Table S22). All three strains had nearly identical metabolite profiles, suggesting that positional effects were minimal or nonexistent. Coexpression of the putative efflux pump AteAfoB with AteAfoC–G did not change the metabolite profile, so its function remained unknown.

Citreoviridin (184).—Citreoviridin (**184**) is a mycotoxin that binds the β-subunit of F1-ATPase.[125] It is an uncompetitive inhibitor of ATP hydrolysis and a noncompetitive inhibitor of ATP synthesis catalyzed by membrane-bound F_1-ATPase.[126] The *A. terreus* var. *aureus* CBS503.65 strain was a known citreoviridin producer, but its genome was not publicly available at the time of the study. Searching instead the published genome of *A. terreus* NIH2624, we identified a candidate BGC of **184**.[127] However, **184** was undetectable in *A. terreus* NIH2624 in various culturing conditions, and heterologous expression of the putative HR-PKS gene did not lead to the production of the polyene precursor. Thus, we cloned the BGC of **184** from the CBS503.65 strain (*ctv*, Figure 26A) using primers designed from the sequence of the NIH2624 strain.

Five genes were successfully amplified, and they were found to share >85% DNA sequence identities and >84% amino acid identities with their homologues in the NIH2624 strain. Heterologous expression of the PKS CtvA in the *yA* locus in LO8030 produced **185** (Figure 26B and Table S23). While coexpression of the FMO CtvC with CtvA did not produce a new product, coexpression of the *O*-MT CtvB with CtvA yielded citreomontanin (**186**). This indicated that methylation of **185** preceded epoxidation. Coexpression of CtvA–C led to the emergence of many peaks on the HPLC including **184**. Since epoxide is a reactive functional group, spontaneous hydrolysis might be responsible for these peaks. When the hydrolase CtvD was coexpressed with CtvA–C, only **184** was produced, indicating that CtvD regioselectively hydrolyzed the epoxide of 186. Interestingly, *ctvE* encoded an ATP synthase β-chain, which was likely a resistance enzyme; however, its function awaits validation.

Cluster Refactoring with the *afo* Regulon.

While the heterologous expression systems described so far employ promoters from housekeeping or primary metabolic genes, several groups have instead used promoters of high-titer secondary metabolites.[128] the rationale is that placing genes of a target BGC under the control of promoters of a high-yield secondary metabolite would similarly result in abundant production of the target molecule. This idea was proposed in a pioneer review paper, where Lubertozzi and Keasling propounded heterologous expression by swapping the coding regions of a native BGC with the coding regions from a target BGC.[36]

In line with this concept, we developed a cluster refactoring strategy to assemble heterologous biosynthesis pathways using the *afo* transcriptional regulatory elements (regulon).[129] As mentioned above, induction of the positive regulator *afoA* activated the *afo* genes and resulted in good yield of asperfuranone (**173**) (Figure 25). By swapping the *afo* genes with genes of interest from a target BGC, we aimed to obtain a good yield of the encoded molecule by induction of *afoA*. Accordingly, we constructed the chassis strain YM87 (derived from LO4389) (Figure 27A), in which the promoter of *afoA* was replaced by P*alcA* and the sequences from *afoC* to *afoG* by *AfriboB*.

The transforming DNA fragments were generated by (1) amplifying the intergenic regions of *afo* (the *afo* regulon) and the genes of interest by PCR, (2) purifying the amplified fragments by gel extraction, (3) assembling those purified fragments by Gibson assembly, and (4) amplifying large transforming fragments by PCR using templates from step 3. Gibson assembly can isothermally assemble multiple DNA fragments in 1 h, and therefore, transforming fragments can be obtained within 1 day. The transforming fragments were then assembled *in vivo* via HR with high efficiency in the *nKuA*Δ strains, allowing the simultaneous introduction of multiple genes of interest in one transformation.

We first refactored the *ctv* genes with the *afo* regulon and successfully obtained citreoviridin (**184**) with high yield (~600 mg/L) and high purity (>95%) after a liquid–liquid partition of the culture broth (Figure 27A and B). Notably, we were able to introduce all four *ctv* genes (18.7 kb) in just one transformation, in contrast to the reiterative recombination strategy that would have required four transformations. Using the same strategy, we also refactored the seven-gene pleuromutilin biosynthesis pathway (*pl*) from the Basidiomycete *Clitopilus passeckerianus*[130] (Figure 27C). Pleuromutilin derivatives are a new class of antibiotics used against topical infections, and their total biosynthesis has been achieved from *A. oryzae*.[131] Gratifyingly, pleuromutilin (**187**) was produced with good yield (~150 mg/L) and obtained with high purity (>95%) after liquid–liquid partition.

The *afo* refactoring system thus is a robust and efficient fungal platform for total heterologous biosynthesis. The genes of interest are refactored into a defined genomic locus, minimizing positional effects caused by differential integration sites and facilitating further rational design of strain engineering. Moreover, the ability to introduce multiple genes of interest in a single step using transforming fragments generated by Gibson assembly and PCR allows us to quickly generate producing strains. With our platform, we aim to engineer “microbial factory” strains that produce high-value fungal natural products with high yield and purity. This “one-strain one-compound” approach would greatly simplify the downstream purification processes and lower the cost of production. It remains elusive why the refactored strains only produced the final metabolite without the accumulation of intermediates or shunt products. One possibility is that the downstream enzymes were catalytically more efficient and readily converted intermediates to the final metabolite. Another possibility is that the pathway enzymes formed a complex through protein–protein interactions to keep the intermediates protected as they were passed between the catalytic pockets until ejection in the final step.

CONCLUDING REMARKS

Total synthesis of structurally complex fungal natural products faces challenges in steps that require stereo- or chemoselective transformations, such as the construction of stereocenters and site-specific functionalization.[132] Biosynthesis, on the other hand, employs pathway-specific enzymes with remarkable efficiency and selectivity to generate enantiomerically pure molecules. Yet the low yields and complex metabolite backgrounds of natural producers often render the costs for obtaining sufficient material for downstream development prohibitively high.

In recent years, reconstitution of biosynthetic pathways in genetically tractable hosts has emerged as a feasible alternative to accessing complex natural products apart from total synthesis or natural producers.[20–22,133] Total heterologous biosynthesis leverages the selectivity of pathway enzymes while benefiting from a dereplicated host and from high-yielding regulatory elements. Moreover, it holds the promise of unlocking cryptic corners of the vast fungal BGC universe. The platforms and tools developed in *A. nidulans* described in this review represent significant advancements toward the efficient exploration of that space; the challenge is now prioritizing the most valuable biosynthesis dark matter for investigation.[134] With continued advancements in high-throughput genome sequencing, bioinformatics, genetics, molecular biology, and strain engineering, the potential for total heterologous biosynthesis to transform pharmaceutical and agrochemical lead discovery and production awaits to be realized.

Supplementary Material

Refer to Web version on PubMed Central for supplementary material.

ACKNOWLEDGMENTS

This work was supported by the National Institute of Allergy and Infectious Diseases (Grant R21AI127640).

REFERENCES

(1). Brakhage AA Nat. Rev. Microbiol 2013, 11 (1), 21–32. [PubMed: 23178386] Keller NP Nat. Rev. Microbiol 2019, 17 (3), 167–180. [PubMed: 30531948]

(2). Bills GF; Gloer JB Microbiol Spectr 2016, 4 (6). DOI: 10.1128/microbiolspec.FUNK-0009-2016Newman DJ; Cragg GM J. Nat. Prod 2020, 83 (3), 770–803. [PubMed: 32162523] Sparks TC; Hahn DR; Garizi NV Pest Manag Sci 2017, 73 (4), 700–715. [PubMed: 27739147]

(3). Chooi YH; Tang YJ Org. Chem 2012, 77 (22), 9933–9953.

(4). Herbst DA; Townsend CA; Maier T Nat. Prod Rep 2018, 35 (10), 1046–1069. [PubMed: 30137093]

(5). Hur GH; Vickery CR; Burkart MD Nat. Prod Rep 2012, 29 (10), 1074–1098. [PubMed: 22802156]

(6). Quin MB; Flynn CM; Schmidt-Dannert C Nat. Prod Rep 2014, 31 (10), 1449–1473. [PubMed: 25171145] Christianson DW Chem. Rev 2017, 117 (17), 11570–11648. [PubMed: 28841019]

(7). Chang HY; Cheng TH; Wang AH IUBMB Life 2021, 73 (1), 40–63. [PubMed: 33246356]

(8). Hoffmeister D; Keller NP Nat. Prod Rep 2007, 24 (2), 393–416. [PubMed: 17390002] Wang X; Jarmusch SA; Frisvad JC; Larsen TO Nat. Prod. Rep 2022, DOI: 10.1039/D1NP00074H.

(9). Keller NP; Hohn TM Fungal Genet Biol 1997, 21 (1), 17–29.

(10). Keller NP; Turner G; Bennett JW Nat. Rev. Microbiol 2005, 3 (12), 937–947. [PubMed: 16322742]

(11). Blackwell M Am. J. Bot 2011, 98 (3), 426–438. [PubMed: 21613136]

(12). Inglis DO; Binkley J; Skrzypek MS; Arnaud MB; Cerqueira GC; Shah P; Wymore F; Wortman JR; Sherlock G BMC Microbiol 2013, 13, 91. [PubMed: 23617571] Robey MT; Caesar LK; Drott MT; Keller NP; Kelleher NL Proc. Natl. Acad. Sci. U. S. A 2021, 118 (19). DOI: 10.1073/pnas.2020230118

(13). Mousa JJ; Bruner SD Nat. Prod Rep 2016, 33 (11), 1255–1267. [PubMed: 27472662]

(14). Bergmann S; Schü J; Scherlach K; Lange C; Brakhage AA; Hertweck C Nat. Chem. Biol 2007, 3 (4), 213–217. [PubMed: 17369821]

(15). Lyu HN; Liu HW; Keller NP; Yin WB Nat. Prod Rep 2020, 37 (1), 6–16. [PubMed: 31033969]

(16). Yeh HH; Ahuja M; Chiang YM; Oakley CE; Moore S; Yoon O; Hajovsky H; Bok JW; Keller NP; Wang CC; et al. ACS Chem. Biol 2016, 11 (8), 2275–2284. [PubMed: 27294372]

(17). Yan Y; Liu N; Tang Y Nat. Prod Rep 2020, 37 (7), 879–892. [PubMed: 31912842]

(18). Wiemann P; Keller NPJ Ind. Microbiol Biotechnol 2014, 41 (2), 301–313.Scherlach K; Hertweck C Nat. Commun 2021, 12 (1), 3864. [PubMed: 34162873] Brakhage AA; Schroeckh V Fungal Genet Biol 2011, 48 (1), 15–22. [PubMed: 20433937]

(19). Anyaogu DC; Mortensen UH Front Microbiol 2015, 6, 77. [PubMed: 25713568] Meng X; Fang Y; Ding M; Zhang Y; Jia K; Li Z; Collemare J; Liu W Biotechnology Advances 2022, 54, 107866. [PubMed: 34780934]

(20). He Y; Wang B; Chen W; Cox RJ; He J; Chen F Biotechnol Adv 2018, 36 (3), 739–783. [PubMed: 29421302]

(21). Lazarus CM; Williams K; Bailey AM Nat. Prod Rep 2014, 31 (10), 1339–1347. [PubMed: 25140842]

(22). Qiao Y-M; Yu R-L; Zhu P RSC Adv 2019, 9 (60), 35124–35134. [PubMed: 35530690]

(23). Greco C; Keller NP; Rokas A Curr. Opin Microbiol 2019, 51, 22–29. [PubMed: 31071615]

(24). Bond C; Tang Y; Li L Fungal Genet Biol 2016, 89, 52–61. [PubMed: 26850128]

(25). Kistler HC; Broz K Front Microbiol 2015, 6, 68. [PubMed: 25709603] Roze LV; Chanda A; Linz JE Fungal Genet Biol 2011, 48 (1), 35–48. [PubMed: 20519149]

(26). Tsunematsu Y; Ishiuchi K; Hotta K; Watanabe K Nat. Prod Rep 2013, 30 (8), 1139–1149. [PubMed: 23824111]

(27). Smith DJ; Burnham MK; Edwards J; Earl AJ; Turner G Biotechnology (N Y) 1990, 8 (1), 39–41. [PubMed: 1368505]

(28). Sakai K; Kinoshita H; Shimizu T; Nihira TJ Biosci Bioeng 2008, 106 (5), 466–472.

(29). Nielsen MR; Wollenberg RD; Westphal KR; Sondergaard TE; Wimmer R; Gardiner DM; rensen JL Fungal Genet Biol 2019, 132, 103248. [PubMed: 31279974]

(30). de Reus E; Nielsen MR; Frandsen RJ N. Mol. Microbiol 2019, 112 (6), 1684–1700.

(31). Nies J; Ran H; Wohlgemuth V; Yin WB; Li SM Org. Lett 2020, 22 (6), 2256–2260. [PubMed: 32134669]

(32). Bok JW; Ye R; Clevenger KD; Mead D; Wagner M; Krerowicz A; Albright JC; Goering AW; Thomas PM; Kelleher NL; et al. BMC Genomics 2015, 16, 343. [PubMed: 25925221]

(33). Clevenger KD; Bok JW; Ye R; Miley GP; Verdan MH; Velk T; Chen C; Yang K; Robey MT; Gao P; et al. Nat. Chem. Biol 2017, 13 (8), 895–901. [PubMed: 28604695]

(34). Hu J; Sarrami F; Li H; Zhang G; Stubbs KA; Lacey E; Stewart SG; Karton A; Piggott AM; Chooi YH Chem. Sci 2019, 10 (5), 1457–1465. [PubMed: 30809363]

(35). Nielsen MT; Nielsen JB; Anyaogu DC; Holm DK; Nielsen KF; Larsen TO; Mortensen UH PLoS One 2013, 8 (8), e72871. [PubMed: 24009710] Yin WB; Chooi YH; Smith AR; Cacho RA; Hu Y; White TC; Tang Y ACS Synth. Biol 2013, 2 (11), 629–634. [PubMed: 23758576] Zhang P; Wang X; Fan A; Zheng Y; Liu X; Wang S; Zou H; Oakley BR; Keller NP; Yin WB Mol. Microbiol 2017, 105 (3), 469–483. [PubMed: 28517364] Ma Z; Li W; Zhang P; Lyu H; Hu Y; Yin WB Appl. Microbiol. Biotechnol 2018, 102 (1), 297–304. [PubMed: 29098413]

(36). Lubertozzi D; Keasling JD Biotechnol Adv 2009, 27 (1), 53–75. [PubMed: 18840517]

(37). Lichius A; Ruiz DM; Zeilinger S Genetic transformation of filamentous fungi: achievements and challenges. In Grand Challenges in Fungal Biotechnology; Nevalainen H, Ed.; Springer International Publishing, 2020; pp 123–164.

(38). Li D; Tang Y; Lin J; Cai W Microb Cell Fact 2017, 16 (1), 168. [PubMed: 28974205]

(39). Aleksenko A; Clutterbuck AJ Fungal Genet Biol 1997, 21 (3), 373–387. [PubMed: 9290250]

(40). Fleissner A; Dersch P Appl. Microbiol. Biotechnol 2010, 87 (4), 1255–1270. [PubMed: 20532762]

(41). Barbesgaard P; Heldt-Hansen HP; Diderichsen B Appl. Microbiol. Biotechnol 1992, 36 (5), 569–572. [PubMed: 1368061]

(42). Tada S; Gomi K; Kitamoto K; Takahashi K; Tamura G; Hara S Mol. Gen Genet 1991, 229 (2), 301–306. [PubMed: 1921978] Tada S; Gomi K; Kitamoto K; Kumagai C; Tamura G; Hara S Agric. Biol. Chem 1991, 55 (7), 1939–1941. [PubMed: 1368722]

(43). Gomi K; Iimura Y; Hara S Agric. Biol. Chem 1987, 51 (9), 2549–2555.

(44). Jin FJ; Maruyama J; Juvvadi PR; Arioka M; Kitamoto K FEMS Microbiol Lett 2004, 239 (1), 79–85. [PubMed: 15451104]

(45). Heneghan MN; Yakasai AA; Halo LM; Song Z; Bailey AM; Simpson TJ; Cox RJ; Lazarus CM Chembiochem 2010, 11 (11), 1508–1512. [PubMed: 20575135]

(46). Pahirulzaman KA; Williams K; Lazarus CM Methods Enzymol 2012, 517, 241–260. [PubMed: 23084942]

(47). Awakawa T; Abe I; et al. J. Fungi (Basel) 2021, 7 (6), 468–486. [PubMed: 34200666]

(48). Nayak T; Szewczyk E; Oakley CE; Osmani A; Ukil L; Murray SL; Hynes MJ; Osmani SA; Oakley BR Genetics 2006, 172 (3), 1557–1566. [PubMed: 16387870]

(49). Szewczyk E; Nayak T; Oakley CE; Edgerton H; Xiong Y; Taheri-Talesh N; Osmani SA; Oakley BR; Oakley B Nat. Protoc 2006, 1 (6), 3111–3120. [PubMed: 17406574]

(50). Brown DW; Yu JH; Kelkar HS; Fernandes M; Nesbitt TC; Keller NP; Adams TH; Leonard TJ Proc. Natl. Acad. Sci. U. S. A 1996, 93 (4), 1418–1422. [PubMed: 8643646]

(51). Chiang YM; Szewczyk E; Nayak T; Davidson AD; Sanchez JF; Lo HC; Ho WY; Simityan H; Kuo E; Praseuth A; et al. Chem. Biol 2008, 15 (6), 527–532. [PubMed: 18559263]

(52). Nø CS; Nielsen JB; Kogle ME; Mortensen UH PLoS One 2015, 10 (7), No. e0133085. [PubMed: 26177455]

(53). Liu N; Hung YS; Gao SS; Hang L; Zou Y; Chooi YH; Tang Y Org. Lett 2017, 19 (13), 3560–3563. [PubMed: 28605916]

(54). Chiang YM; Oakley CE; Ahuja M; Entwistle R; Schultz A; Chang SL; Sung CT; Wang CC; Oakley BR J. Am. Chem. Soc 2013, 135 (20), 7720–7731. [PubMed: 23621425]

(55). Chiang YM; Ahuja M; Oakley CE; Entwistle R; Asokan A; Zutz C; Wang CC; Oakley BR Angew. Chem., Int. Ed. Engl 2016, 55 (5), 1662–1665. [PubMed: 26563584]

(56). Tsunematsu Y; Ishikawa N; Wakana D; Goda Y; Noguchi H; Moriya H; Hotta K; Watanabe K Nat. Chem. Biol 2013, 9 (12), 818–825. [PubMed: 24121553]

(57). Kubodera T; Yamashita N; Nishimura A Biosci Biotechnol Biochem 2002, 66 (2), 404–406. [PubMed: 11999416]

(58). Hua SB; Qiu M; Chan E; Zhu L; Luo Y Plasmid 1997, 38 (2), 91–96. [PubMed: 9339466] Oldenburg KR; Vo KT; Michaelis S; Paddon C Nucleic Acids Res 1997, 25 (2), 451–452. [PubMed: 9016579]

(59). Sato M; Yagishita F; Mino T; Uchiyama N; Patel A; Chooi YH; Goda Y; Xu W; Noguchi H; Yamamoto T; et al. Chembiochem 2015, 16 (16), 2294–2298. [PubMed: 26360642]

(60). Yang SW; Mierzwa R; Terracciano J; Patel M; Gullo V; Wagner N; Baroudy B; Puar M; Chan TM; McPhail AT; et al. J. Nat. Prod 2006, 69 (7), 1025–1028. [PubMed: 16872138]

(61). Jacob S; Grötsch T; Foster AJ; Schü A; Rieger PH; Sandjo LP; Liermann JC; Opatz T; Thines E Microbiology 2017, 163 (4), 541–553. [PubMed: 27902426]

(62). Zhao Z; Ying Y; Hung YS; Tang YJ Nat. Prod 2019, 82 (4), 1029–1033.

(63). Liu L; Tang MC; Tang YJ Am. Chem. Soc 2019, 141 (50), 19538–19541.

(64). Grabley S; Granzer E; Hütter K; Ludwig D; Mayer M; Thiericke R; Till G; Wink J; Philipps S; Zeeck AJ Antibiot (Tokyo) 1992, 45 (1), 56–65.Göhrt A; Zeeck A; Hütter K; Kirsch R; Kluge H; Thiericke R J. Antibiot (Tokyo) 1992, 45 (1), 66–73. [PubMed: 1548191]

(65). Gao DW; Jamieson CS; Wang G; Yan Y; Zhou J; Houk KN; Tang YJ Am. Chem. Soc 2021, 143 (1), 80–84.

(66). Omura S; Hirano A; Iwai Y; Masuma RJ Antibiot (Tokyo) 1979, 32 (8), 786–790.

(67). Yu X; Liu F; Zou Y; Tang MC; Hang L; Houk KN; Tang YJ Am. Chem. Soc 2016, 138 (41), 13529–13532.

(68). Sakamoto K; Tsujii E; Abe F; Nakanishi T; Yamashita M; Shigematsu N; Izumi S; Okuhara MJ Antibiot (Tokyo) 1996, 49 (1), 37–44.

(69). Zhang Z; Tamura Y; Tang M; Qiao T; Sato M; Otsu Y; Sasamura S; Taniguchi M; Watanabe K; Tang YJ Am. Chem. Soc 2021, 143 (1), 132–136.

(70). Sasaki T; Takahashi S; Uchida K; Funayama S; Kainosho M; Nakagawa AJ Antibiot (Tokyo) 2006, 59 (7), 418–427.

(71). Zhao F; Liu Z; Yang S; Ding N; Gao X Angew. Chem., Int. Ed. Engl 2020, 59 (43), 19108–19114. [PubMed: 32663343]

(72). Liu M; Ohashi M; Tang Y Org. Lett 2020, 22 (16), 6637–6641. [PubMed: 32806159]

(73). Flower DR; North AC; Sansom CE Biochim. Biophys. Acta 2000, 1482 (1–2), 9–24. [PubMed: 11058743]

(74). Tan D; Jamieson CS; Ohashi M; Tang MC; Houk KN; Tang YJ Am. Chem. Soc 2019, 141 (2), 769–773.

(75). Tepaske M; Gloer J; Wicklow D; Dowd P Tetrahedron Lett 1991, 32 (41), 5687–5690.

(76). Cary JW; Uka V; Han Z; Buyst D; Harris-Coward PY; Ehrlich KC; Wei Q; Bhatnagar D; Dowd PF; Martens SL; et al. Fungal Genet Biol 2015, 81, 88–97. [PubMed: 26051490]

(77). Ohashi M; Liu F; Hai Y; Chen M; Tang MC; Yang Z; Sato M; Watanabe K; Houk KN; Tang Y Nature 2017, 549 (7673), 502–506. [PubMed: 28902839]

(78). Hayakawa S; Minato H; Katagiri KJ Antibiot (Tokyo) 1971, 24 (9), 653–654.

(79). Gutierrez-Cirlos EB; Merbitz-Zahradnik T; Trumpower BL J. Biol. Chem 2004, 279 (10), 8708–8714. [PubMed: 14670947]

(80). Zhang Z; Jamieson CS; Zhao YL; Li D; Ohashi M; Houk KN; Tang YJ Am. Chem. Soc 2019, 141 (14), 5659–5663.

(81). Miyadera H; Shiomi K; Ui H; Yamaguchi Y; Masuma R; Tomoda H; Miyoshi H; Osanai A; Kita K; Omura S Proc. Natl. Acad. Sci. U. S. A 2003, 100 (2), 473–477. [PubMed: 12515859]

(82). Dickinson J; Hanson J; Hitchcock P; Claydon N Journal of the Chemical Society-Perkin Transactions 1 1989, No. 11, 1885–1887.

(83). Wasil Z; Pahirulzaman K; Butts C; Simpson T; Lazarus C; Cox R Chemical Science 2013, 4 (10), 3845–3856.

(84). Bat-Erdene U; Kanayama D; Tan D; Turner WC; Houk KN; Ohashi M; Tang YJ Am. Chem. Soc 2020, 142 (19), 8550–8554.

(85). Fukuda T; Yamaguchi Y; Masuma R; Tomoda H; Omura SJ Antibiot (Tokyo) 2005, 58 (5), 309–314.Fukuda T; Tomoda H; Omura SJ Antibiot (Tokyo) 2005, 58 (5), 315–321.

(86). Zhang Z; Qiao T; Watanabe K; Tang Y Angew. Chem., Int. Ed. Engl 2020, 59 (45), 19889–19893. [PubMed: 32779306]

(87). Bacon CW; Porter JK; Norred WP; Leslie JF Appl. Environ. Microbiol 1996, 62 (11), 4039–4043. [PubMed: 8899996] Bani M; Rispail N; Evidente A; Rubiales D; Cimmino AJ Agric. Food Chem 2014, 62 (12), 2574–2580.Singh VK; Singh HB; Upadhyay RS Plant Physiol Biochem 2017, 118, 320–332. [PubMed: 28683401]

(88). Brown DW; Butchko RA; Busman M; Proctor RH Fungal Genet Biol 2012, 49 (7), 521–532. [PubMed: 22652150] Niehaus EM; von Bargen KW; Espino JJ; Pfannmü A; Humpf HU; Tudzynski B Appl. Microbiol. Biotechnol 2014, 98 (4), 1749–1762. [PubMed: 24389666] Brown DW; Lee SH; Kim LH; Ryu JG; Lee S; Seo Y; Kim YH; Busman M; Yun SH; Proctor RH; et al. Mol. Plant-Microbe Interact 2015, 28 (3), 319–332. [PubMed: 25372119] Studt L; Janevska S;

Niehaus EM; Burkhardt I; Arndt B; Sieber CM; Humpf HU; Dickschat JS; Tudzynski B Environ. Microbiol 2016, 18 (3), 936–956. [PubMed: 26662839]

(89). Hai Y; Chen M; Huang A; Tang YJ Am. Chem. Soc 2020, 142 (46), 19668–19677.

(90). Guo JP; Zhu CY; Zhang CP; Chu YS; Wang YL; Zhang JX; Wu DK; Zhang KQ; Niu XM J. Am. Chem. Soc 2012, 134 (50), 20306–20309. [PubMed: 23210772]

(91). Niu X; Chen L; Yue Q; Wang B; Zhang J; Zhu C; Zhang K; Bills GF; An Z Org. Lett 2014, 16 (14), 3744–3747. [PubMed: 24999817]

(92). Zhang JM; Wang HH; Liu X; Hu CH; Zou YJ Am. Chem. Soc 2020, 142 (4), 1957–1965.

(93). Yue K; Ye M; Zhou Z; Sun W; Lin XJ Pharm. Pharmacol 2013, 65 (4), 474–493.

(94). Wang X; Gao YL; Zhang ML; Zhang HD; Huang JZ; Li LJ Biotechnol 2020, 309, 85–91.

(95). Namatame I; Tomoda H; Ishibashi S; Omura S Proc. Natl. Acad. Sci. U. S. A 2004, 101 (3), 737–742. [PubMed: 14718664]

(96). Bloudoff K; Schmeing TM Biochim Biophys Acta Proteins Proteom 2017, 1865 (11), 1587–1604. [PubMed: 28526268]

(97). Bentley R Chem. Rev 2000, 100 (10), 3801–3826. [PubMed: 11749328]

(98). Regueira TB; Kildegaard KR; Hansen BG; Mortensen UH; Hertweck C; Nielsen J Appl. Environ. Microbiol 2011, 77 (9), 3035–3043. [PubMed: 21398490]

(99). Hansen BG; Mnich E; Nielsen KF; Nielsen JB; Nielsen MT; Mortensen UH; Larsen TO; Patil KR Appl. Environ. Microbiol 2012, 78 (14), 4908–4913. [PubMed: 22544261]

(100). Chen X; Wang L; Zhang J; Jiang T; Hu C; Li D; Zou Y Acta Pharm. Sin B 2019, 9 (6), 1253–1258. [PubMed: 31867170]

(101). Yee DA; Kakule TB; Cheng W; Chen M; Chong CTY; Hai Y; Hang LF; Hung YS; Liu N; Ohashi M; et al. J. Am. Chem. Soc 2020, 142 (2), 710–714. [PubMed: 31885262]

(102). Hartmann M; Kim D; Bernsdorff F; Ajami-Rashidi Z; Scholten N; Schreiber S; Zeier T; Schuck S; Reichel-Deland V; Zeier J Plant Physiol 2017, 174 (1), 124–153. [PubMed: 28330936]

(103). Li H; Hu J; Wei H; Solomon PS; Vuong D; Lacey E; Stubbs KA; Piggott AM; Chooi YH Org. Lett 2018, 20 (19), 6148–6152. [PubMed: 30226784]

(104). Fillinger S; Felenbok B Mol. Microbiol 1996, 20 (3), 475–488. [PubMed: 8736527]

(105). Flipphi M; Mathieu M; Cirpus I; Panozzo C; Felenbok BJ Biol. Chem 2001, 276 (10), 6950–6958.

(106). Olivo M; Chin WJ Environ. Pathol Toxicol Oncol 2006, 25 (1–2), 223–237.Daub ME; Herrero S; Chung KR Antioxid Redox Signal 2013, 19 (9), 970–989. [PubMed: 23259634]

(107). Chooi YH; Zhang G; Hu J; Muria-Gonzalez MJ; Tran PN; Pettitt A; Maier AG; Barrow RA; Solomon PS Environ. Microbiol 2017, 19 (5), 1975–1986. [PubMed: 28251756]

(108). Newman AG; Vagstad AL; Belecki K; Scheerer JR; Townsend CA Chem. Commun. (Camb) 2012, 48 (96), 11772–11774. [PubMed: 23108075]

(109). Newman AG; Townsend CA J. Am. Chem. Soc 2016, 138 (12), 4219–4228. [PubMed: 26938470]

(110). Weisleder D; Lillehoj E Tetrahedron Lett 1971, 12 (48), 4705–4706.Suzuki K; Nozawa K; Nakajima S; Kawai K Chem. Pharm. Bull 1990, 38 (11), 3180–3181.

(111). Wang J; Galgoci A; Kodali S; Herath KB; Jayasuriya H; Dorso K; Vicente F; González A; Cully D; Bramhill D; et al. J. Biol. Chem 2003, 278 (45), 44424–44428. [PubMed: 12952956] Liu Y; Kurtán T; Yun Wang C; Han Lin W; Orfali R; ller WE; Daletos G; Proksch PJ Antibiot (Tokyo) 2016, 69 (9), 702–706.Kundu S; Kim TH; Yoon JH; Shin HS; Lee J; Jung JH; Kim HS Int. J. Oncol 2014, 45 (6), 2331–2340. [PubMed: 25231051]

(112). Hu J; Li H; Chooi YH J. Am. Chem. Soc 2019, 141 (20), 8068–8072. [PubMed: 31045362]

(113). Davin LB; Wang HB; Crowell AL; Bedgar DL; Martin DM; Sarkanen S; Lewis NG Science 1997, 275 (5298), 362–366. [PubMed: 8994027]

(114). Li H; Hu J; Wei H; Solomon PS; Stubbs KA; Chooi YH Chemistry 2019, 25 (66), 15062–15066. [PubMed: 31553484]

(115). Ugai T; Minami A; Fujii R; Tanaka M; Oguri H; Gomi K; Oikawa H Chem. Commun. (Camb) 2015, 51 (10), 1878–1881. [PubMed: 25530455]

(116). Manulis S; Kashman Y; Netzer D; Barash I Phytochemistry 1984, 23 (10), 2193–2198.

(117). Li H; Gilchrist CLM; Phan CS; Lacey HJ; Vuong D; Moggach SA; Lacey E; Piggott AM; Chooi YH J. Am. Chem. Soc 2020, 142 (15), 7145–7152. [PubMed: 32182055]

(118). Kurnasov O; Jablonski L; Polanuyer B; Dorrestein P; Begley T; Osterman A FEMS Microbiol Lett 2003, 227 (2), 219–227. [PubMed: 14592712]

(119). Li H; Gilchrist CLM; Lacey HJ; Crombie A; Vuong D; Pitt JI; Lacey E; Chooi YH; Piggott AM Org. Lett 2019, 21 (5), 1287–1291. [PubMed: 30735051]

(120). Li L; Liu X; Wei K; Lu Y; Jiang W Biotechnol Adv 2019, 37 (5), 730–745. [PubMed: 30951810]

(121). Wingler LM; Cornish VW Proc. Natl. Acad. Sci. U. S. A 2011, 108 (37), 15135–15140. [PubMed: 21876185]

(122). Chiang YM; Szewczyk E; Davidson AD; Keller N; Oakley BR; Wang CC J. Am. Chem. Soc 2009, 131 (8), 2965–2970. [PubMed: 19199437]

(123). Davison J; al Fahad A; Cai M; Song Z; Yehia SY; Lazarus CM; Bailey AM; Simpson TJ; Cox RJ Proc. Natl. Acad. Sci. U. S. A 2012, 109 (20), 7642–7647. [PubMed: 22508998]

(124). Zabala AO; Xu W; Chooi YH; Tang Y Chem. Biol 2012, 19 (8), 1049–1059. [PubMed: 22921072]

(125). Gause EM; Buck MA; Douglas MG J. Biol. Chem 1981, 256 (2), 557–559. [PubMed: 6450205]

(126). Sayood SF; Suh H; Wilcox CS; Schuster SM Arch. Biochem. Biophys 1989, 270 (2), 714–721. [PubMed: 2523213]

(127). Lin TS; Chiang YM; Wang CC Org. Lett 2016, 18 (6), 1366–1369. [PubMed: 26954888]

(128). Kakule TB; Jadulco RC; Koch M; Janso JE; Barrows LR; Schmidt EW ACS Synth. Biol 2015, 4 (5), 625–633. [PubMed: 25226362] Gressler M; Hortschansky P; Geib E; Brock M Front Microbiol 2015, 6, 184. [PubMed: 25852654] Wiemann P; Soukup AA; Folz JS; Wang PM; Noack A; Keller NP Fungal Biol. Biotechnol 2018, 5, 6. [PubMed: 29564145]

(129). Chiang YM; Lin TS; Chang SL; Ahn G; Wang CC C. ACS Synth. Biol 2021, 10 (1), 173–182.

(130). Bailey AM; Alberti F; Kilaru S; Collins CM; de MattosShipley K; Hartley AJ; Hayes P; Griffin A; Lazarus CM; Cox RJ; et al. Sci. Rep 2016, 6, 25202. [PubMed: 27143514]

(131). Alberti F; Khairudin K; Venegas ER; Davies JA; Hayes PM; Willis CL; Bailey AM; Foster GD Nat. Commun 2017, 8 (1), 1831. [PubMed: 29184068]

(132). Roberts AA; Ryan KS; Moore BS; Gulder T Top Curr. Chem 2010, 297, 149–203. [PubMed: 21495259]

(133). Alberti F; Foster GD; Bailey AM Appl. Microbiol. Biotechnol 2017, 101 (2), 493–500. [PubMed: 27966047]

(134). Gilchrist CLM; Li H; Chooi YH Org. Biomol Chem 2018, 16 (10), 1620–1626. [PubMed: 29393329] Tran PN; Yen MR; Chiang CY; Lin HC; Chen PY Appl. Microbiol. Biotechnol 2019, 103 (8), 3277–3287. [PubMed: 30859257]

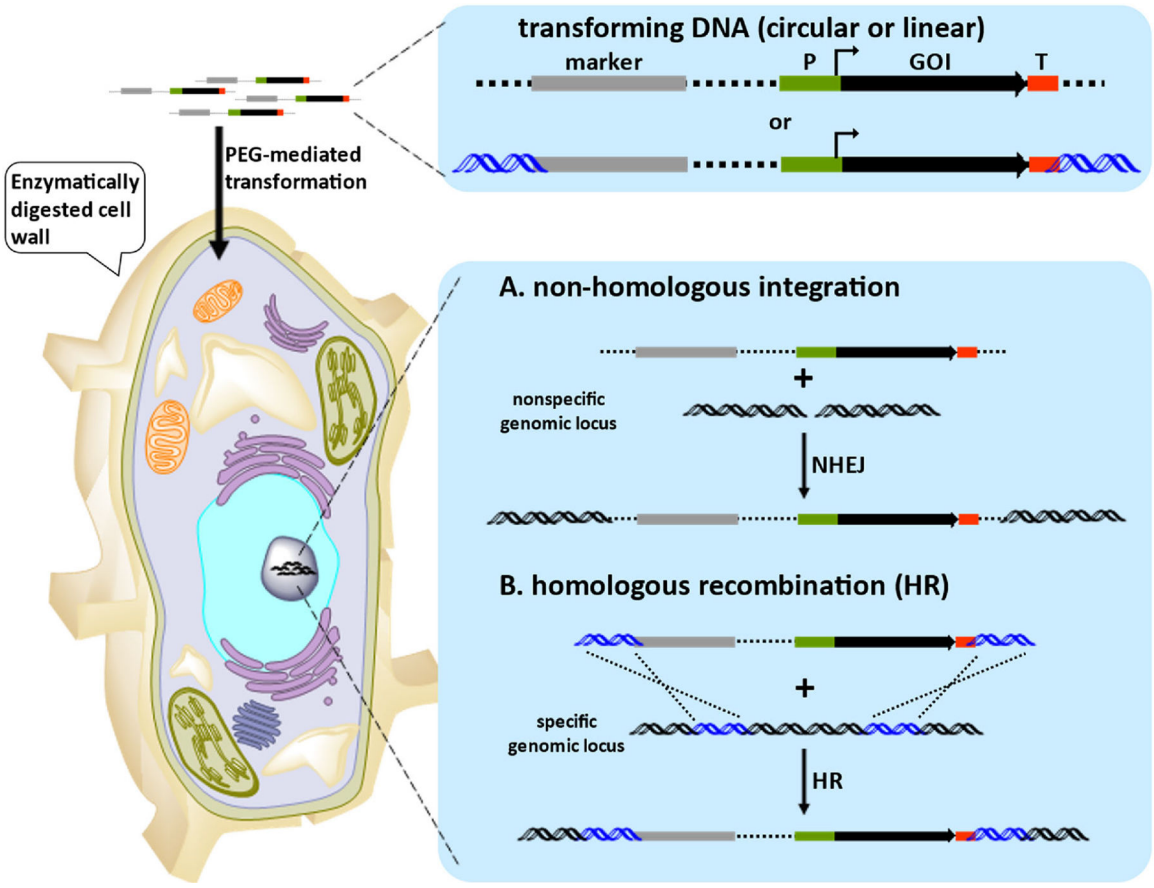

Figure 1.

Overview of chromosomal integration expression. Enzymatic digestion of the fungal cell results in a protoplast, which allows transforming DNA to be delivered into the nucleus via PEG-mediated transformation. Transforming DNA contains a selectable marker and at least one expression cassette. Expression of a gene of interest (GOI) is driven by a constitutive or inducible promoter (P). The 3′ untranslated region (3′-UTR) of a GOI functions as a terminator (T), which ensures the releasing of the transcribed mRNA, so that the "GOI + T" fragment can be amplified from the gnomic DNA (gDNA) of the native producer. Once the transforming DNA reaches the nucleus, it can integrate into the host's chromosome via (A) non-homologous end joining (NHEJ) or (B) homologous recombination (HR). NHEJ results in the integration of the transforming DNA into a nonspecific genomic locus, while recombination of homologous sequences (blue) results in the integration at a specific genomic locus.

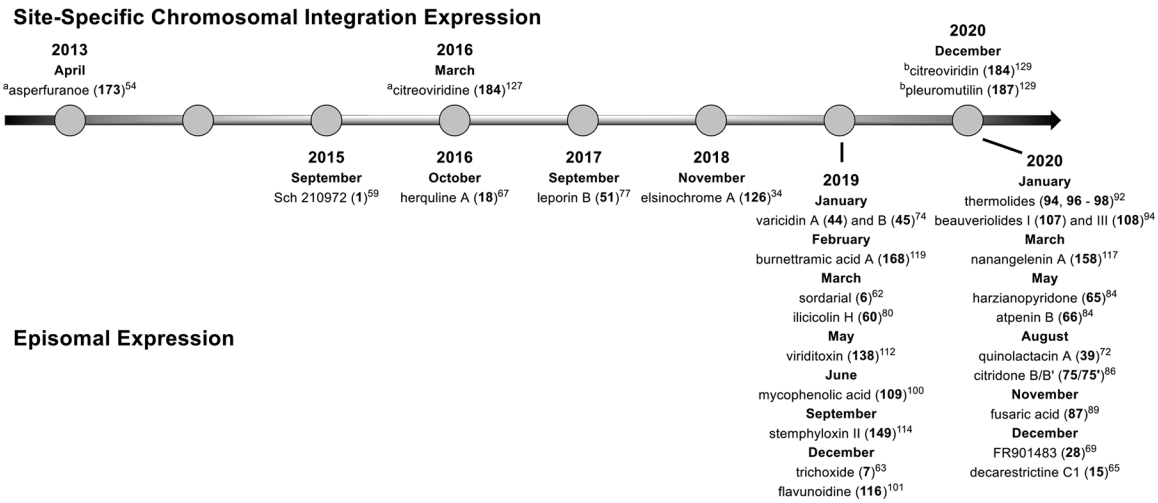

Figure 2.

Timeline of total heterologous biosynthesis in *A. nidulans* by publication date. [a]Reiterative recombination. [b]Cluster refactoring in the *afo* regulon.

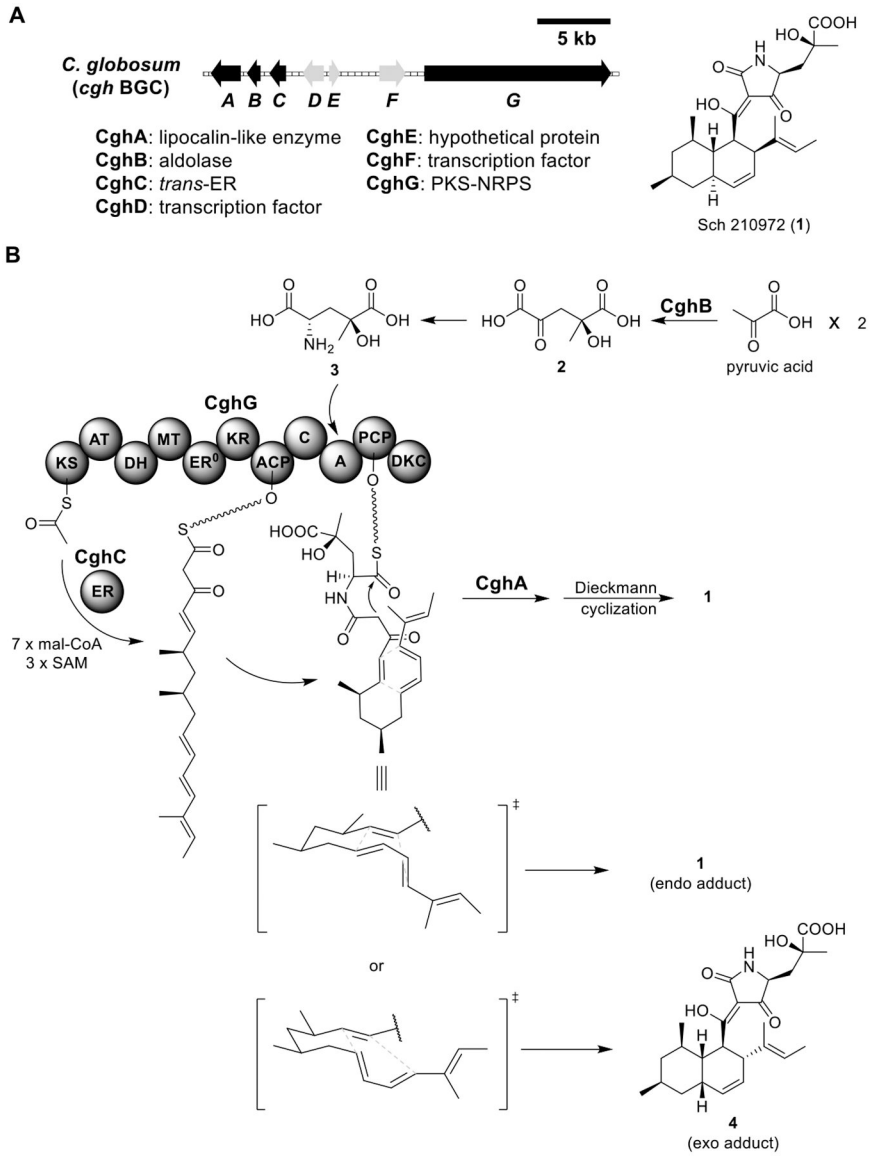

Figure 3.

Total biosynthesis of Sch 210972 (**1**). (A) Organization and predicted gene functions of the *cgh* BGC. Black ORFs encode for enzymes involved in the biosynthesis of **1**. (B) Proposed biosynthesis of **1**.

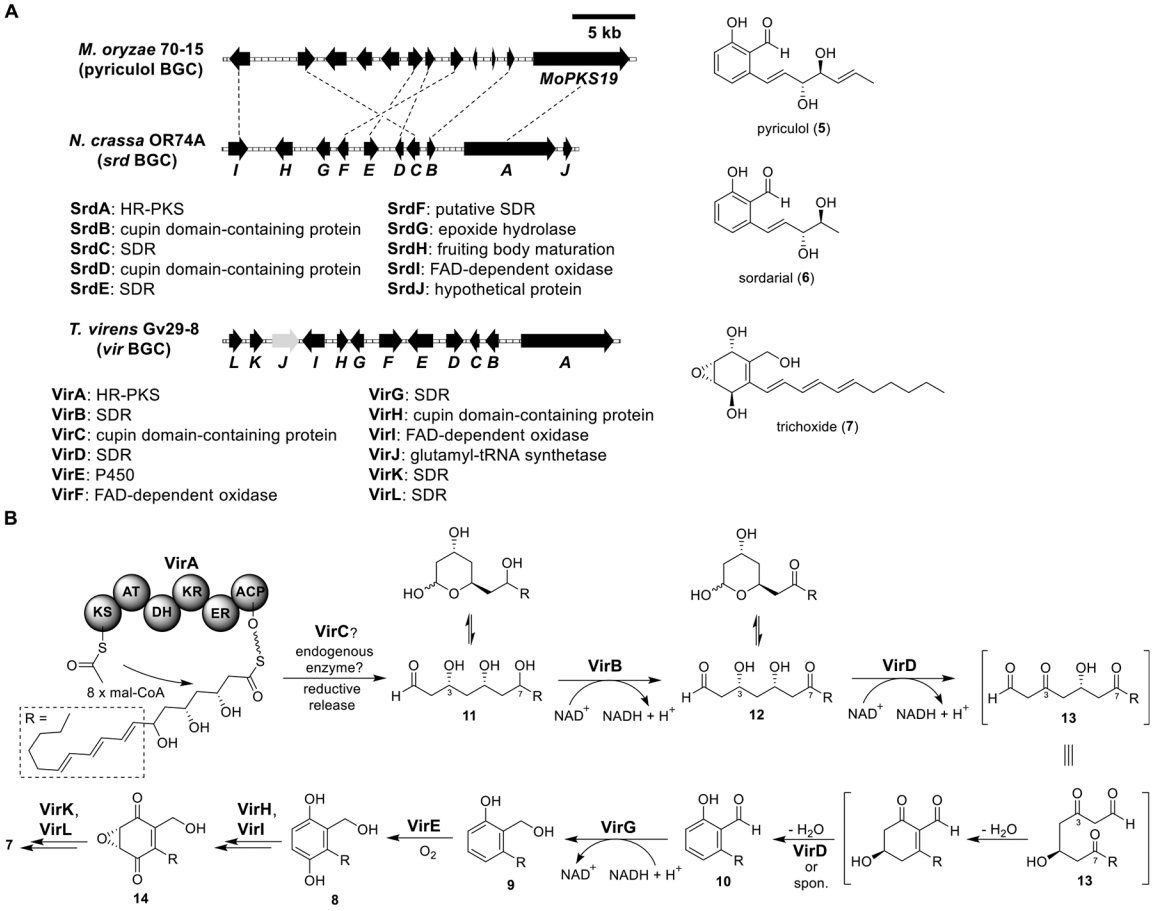

Figure 4.

Total biosynthesis of trichoxide (**7**). (A) Organization and predicted gene functions of the pyriculol, *srd*, and *vir* BGCs. Black ORFs encode for enzymes involved in the biosynthesis of pyriculol (**5**), sordarial (**6**), and **7**. (B) Proposed biosynthesis of **7**.

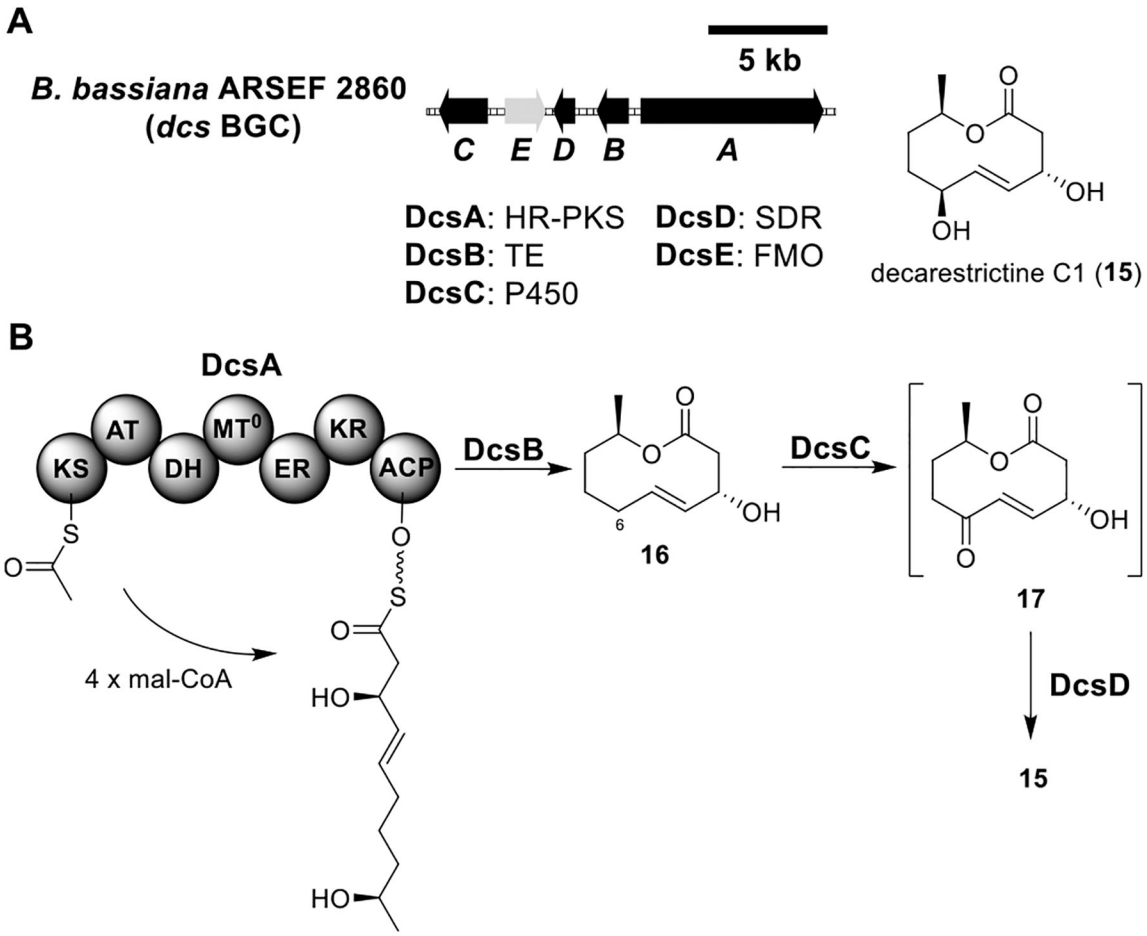

Figure 5.

Total biosynthesis of decarestrictine C1 (**15**). (A) Organization and predicted gene functions of the *dcs* BGC. Black ORFs encode for enzymes involved in the biosynthesis of **15**. (B) Proposed biosynthesis of **15**.

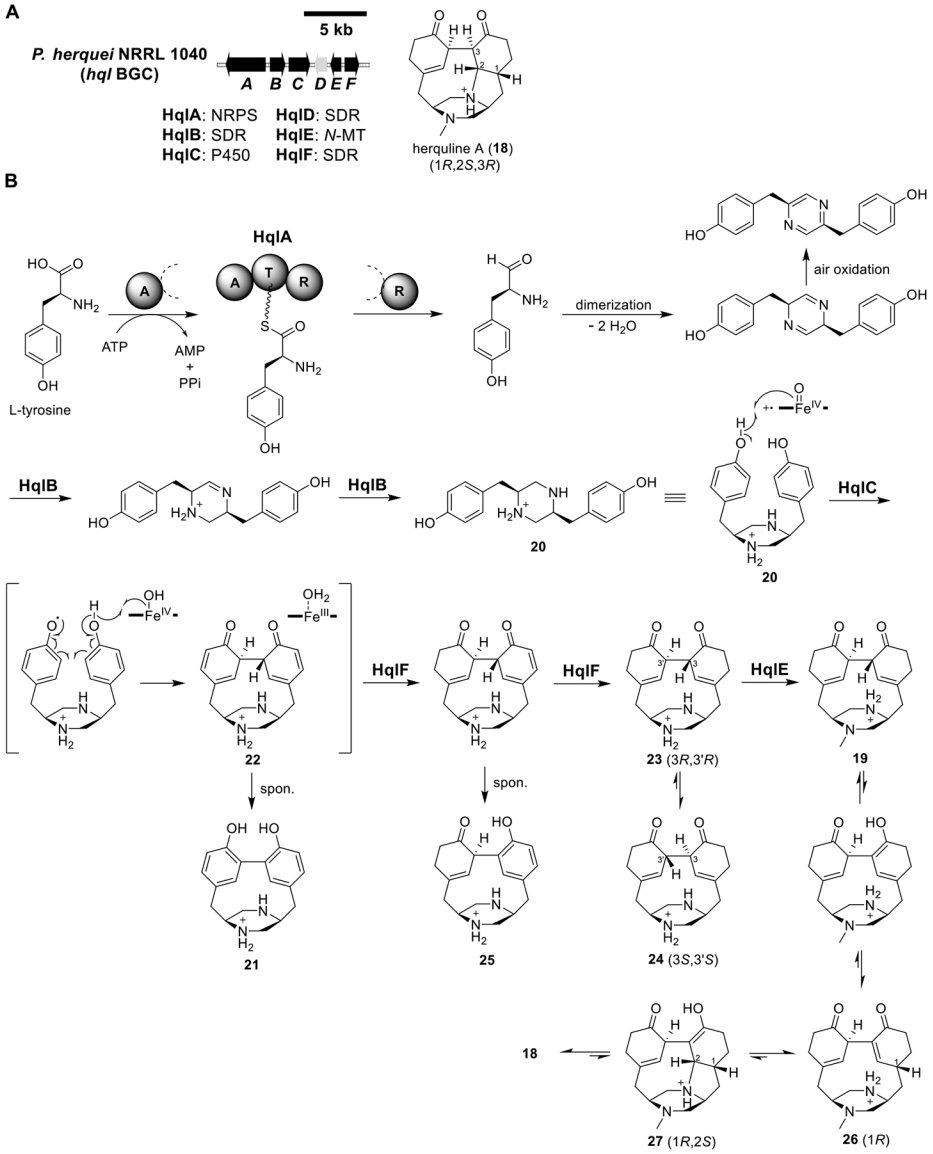

Figure 6.

Total biosynthesis of herquline A (**18**). (A) Organization and predicted gene functions of the *hql* BGC. Black ORFs encode for enzymes involved in the biosynthesis of **18**. (B) Proposed biosynthesis of **18**.

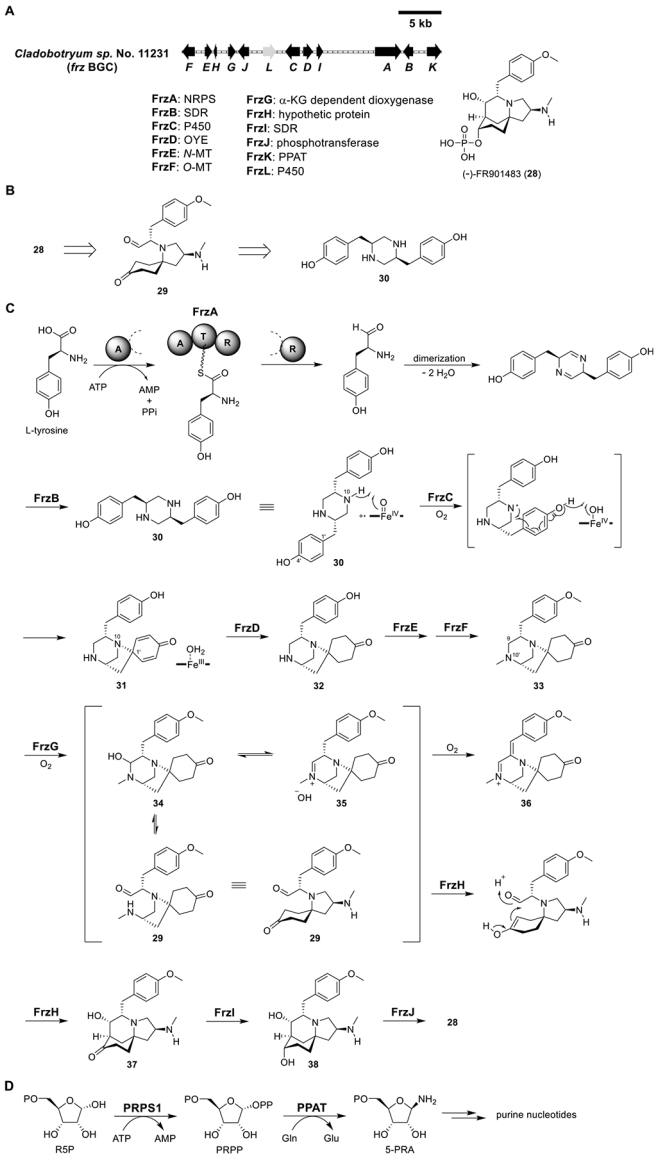

Figure 7.

Total biosynthesis of FR901483 (**28**). (A) Organization and predicted gene functions of the *frz* BGC. Black ORFs encode for enzymes involved in the biosynthesis of **28**. (B) Retrosynthetic analysis of **28**. (C) Proposed biosynthesis of **28**. (D) *De novo* purine biosynthesis.

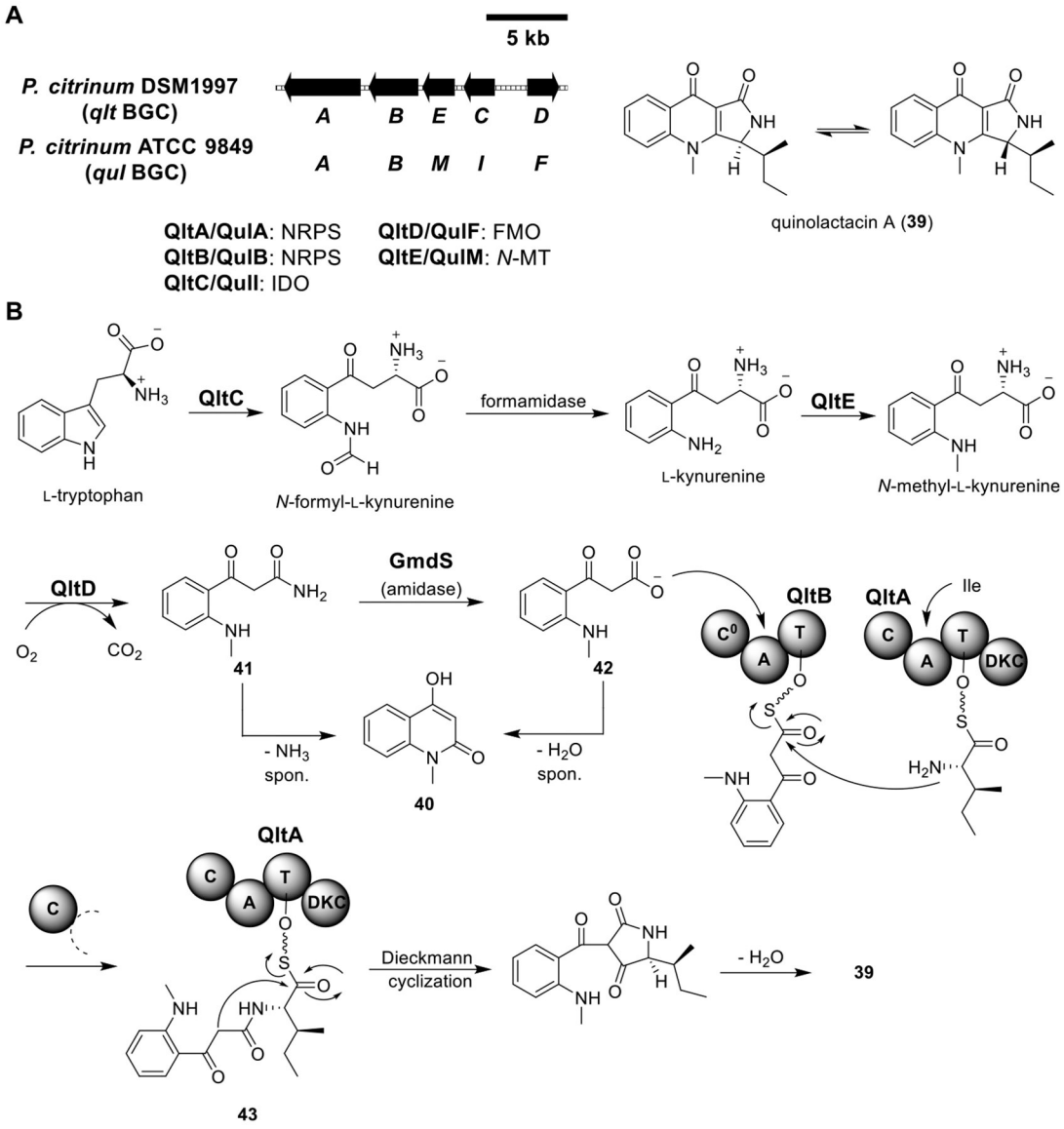

Figure 8.

Total biosynthesis of quinolactacin A (**39**). (A) Organization and predicted gene functions of the *qlt* and *qul* BGCs. Black ORFs encode for enzymes involved in the biosynthesis of **39**. (B) Proposed biosynthesis of **39**.

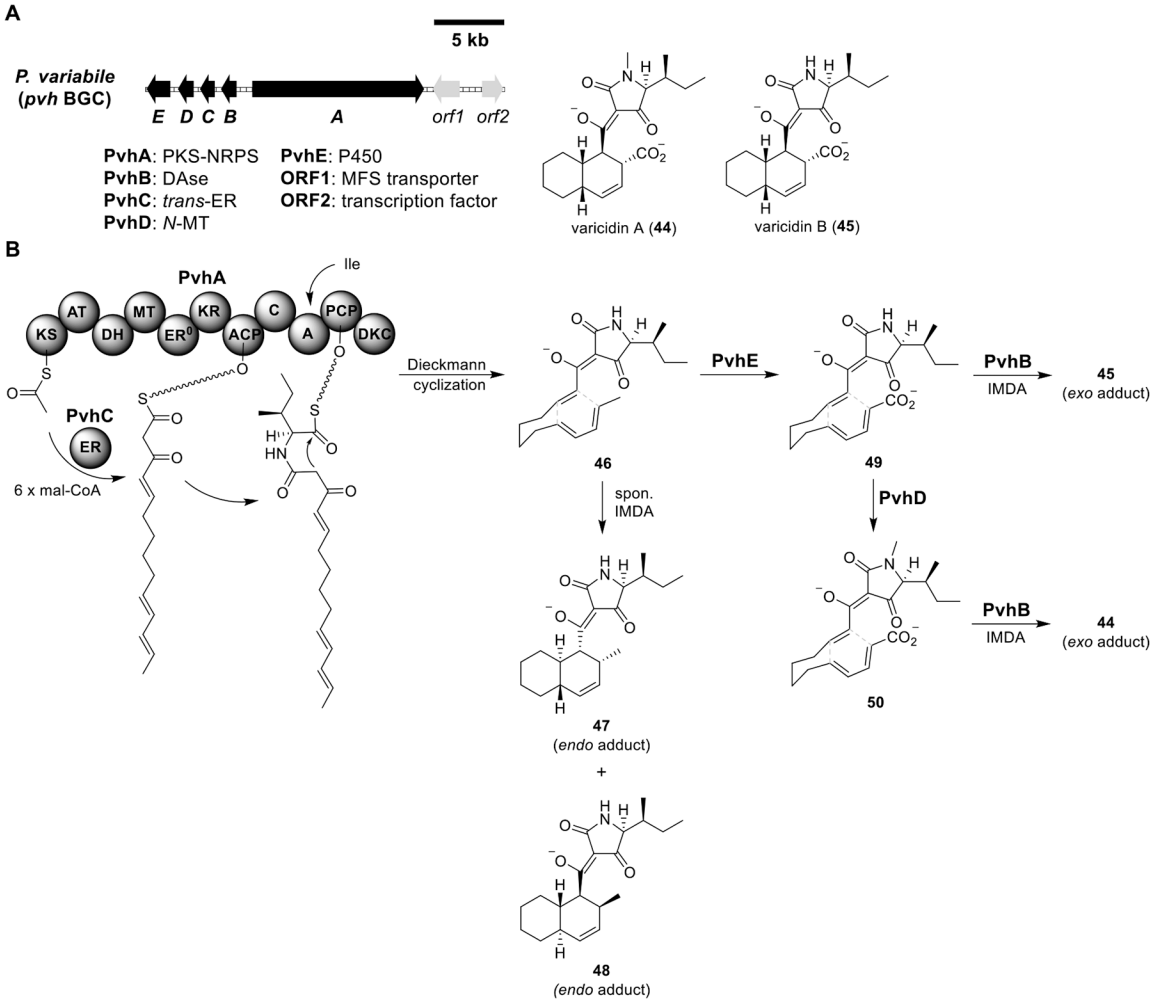

Figure 9.

Total biosynthesis of varicidins A (**44**) and B (**45**). (A) Organization and predicted gene functions of the *pvh* BGC. Black ORFs encode for enzymes involved in the biosynthesis of **44** and **45**. (B) Proposed biosynthesis of **44** and **45**.

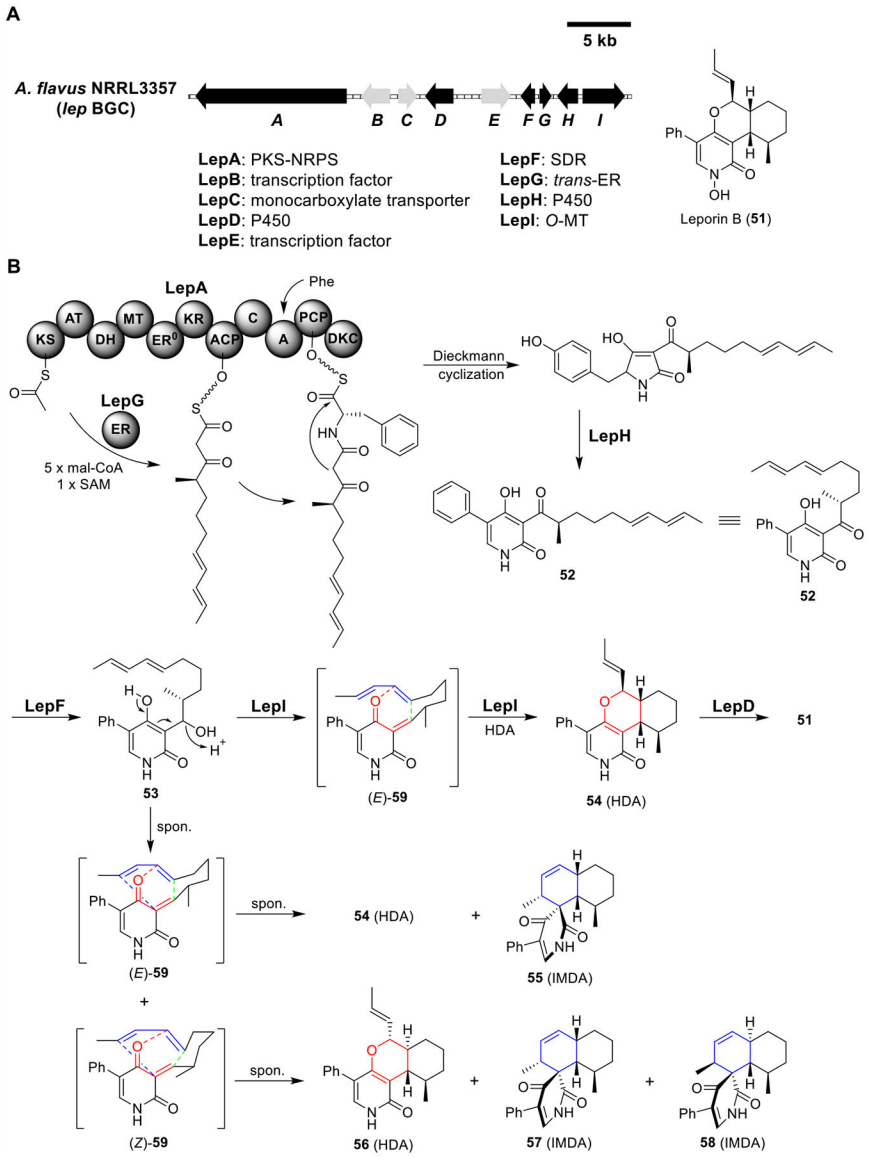

Figure 10.

Total biosynthesis of leporin B (**51**). (A) Organization and predicted gene functions of the *lep* BGC. Black ORFs encode for enzymes involved in the biosynthesis of **51**. (B) Proposed biosynthesis of **51**.

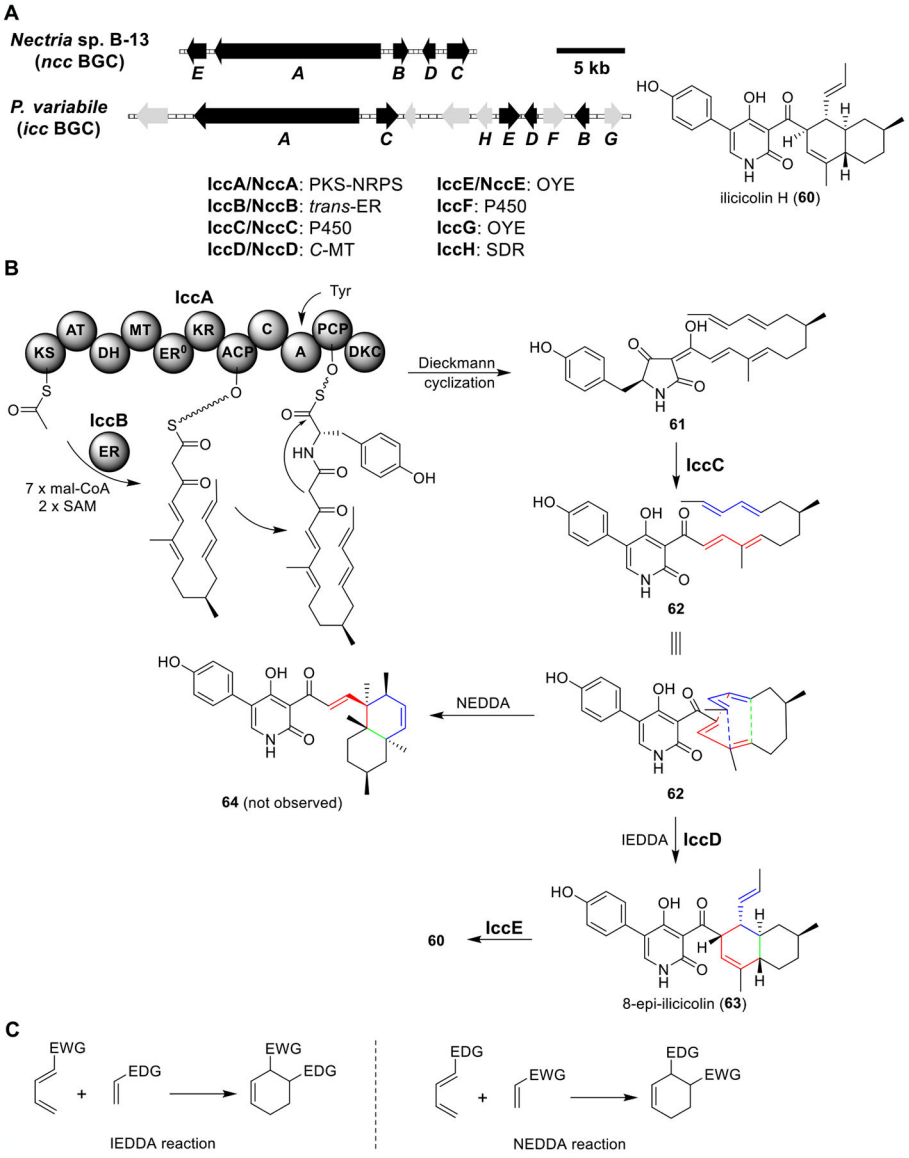

Figure 11.

Total biosynthesis of ilicicolin H (**60**). (A) Organization and predicted gene functions of the *ncc* and *icc* BGCs. Black ORFs encode for enzymes involved in the biosynthesis of **60**. (B) Proposed biosynthesis of **60**. (D) Inverse-electron-demand Diels–Alder (IEDDA) and normal-electron-demand Diels–Alder (NEDDA) reactions. EWG: electron-withdrawing group. EDG: electron-donating group.

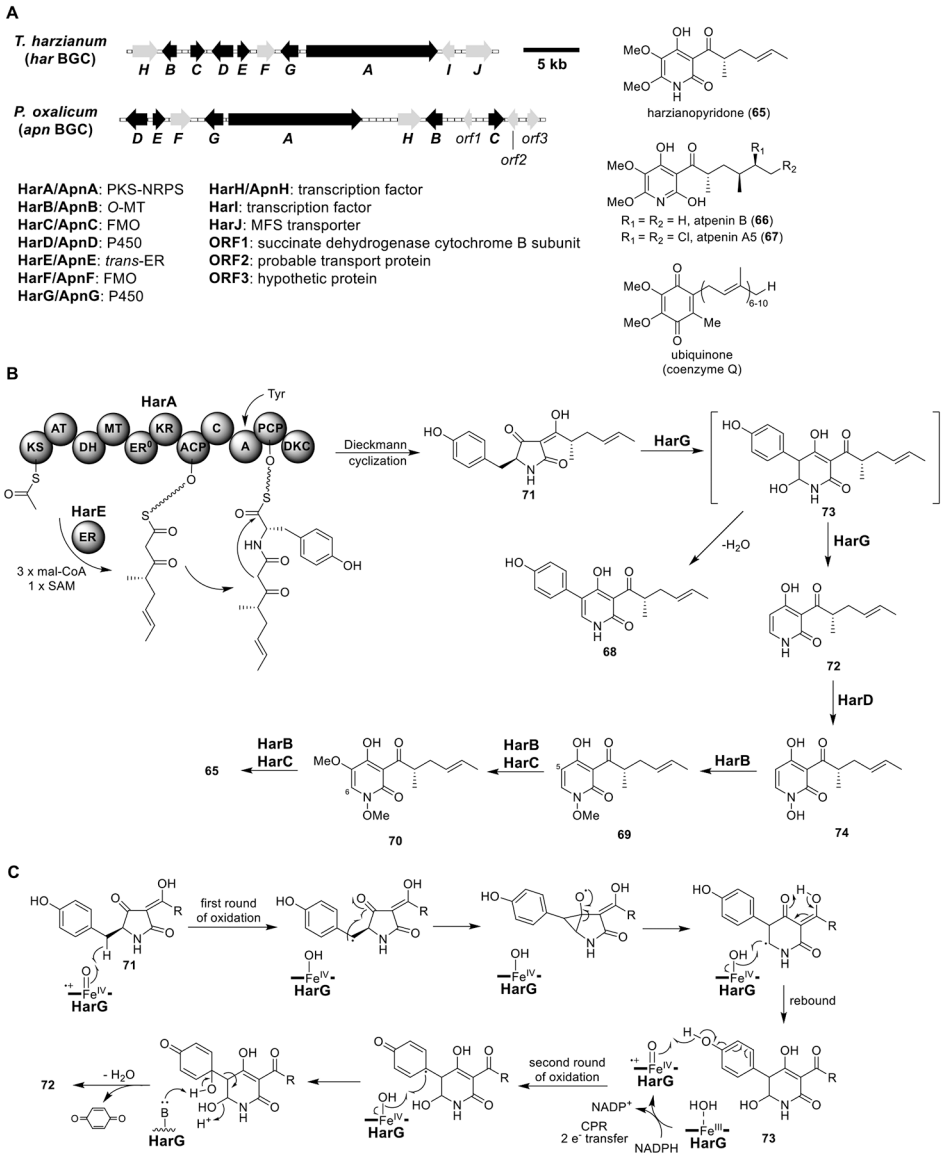

Figure 12.

Total biosynthesis of harzianopyridone (**65**) and atpenin B (**66**). (A) Organization and predicted gene functions of the *har* and *apn* BGCs. Black ORFs encode for enzymes involved in the biosynthesis of **65** and **66** in the *har* and *apn* BGCs, respectively. (B) Proposed biosynthesis of **65**. (C) Proposed mechanism of ring expansion and phenyl cleavage for the formation of **72** via radical intermediates.

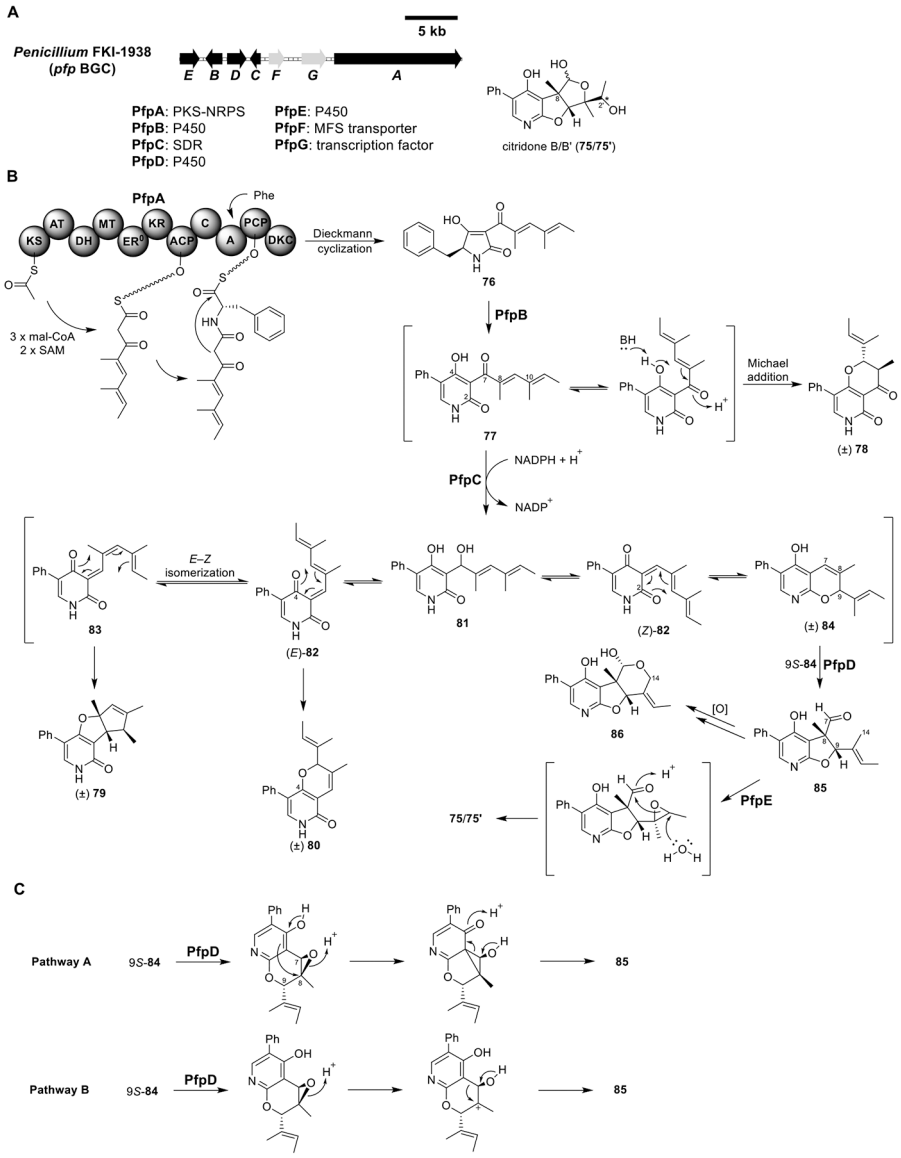

Figure 13.

Total biosynthesis of citridone B/B (**75/75′**). (A) Organization and predicted gene functions of the *pfp* BGCs. Black ORFs encode for enzymes involved in the biosynthesis of **75/75′**. (B) Proposed biosynthesis of **75/75′**. (C) Proposed mechanisms for the formation of **85** via 9*S*-**84**. *The relative configuration of C-2′ in **75/75′** was not determined.

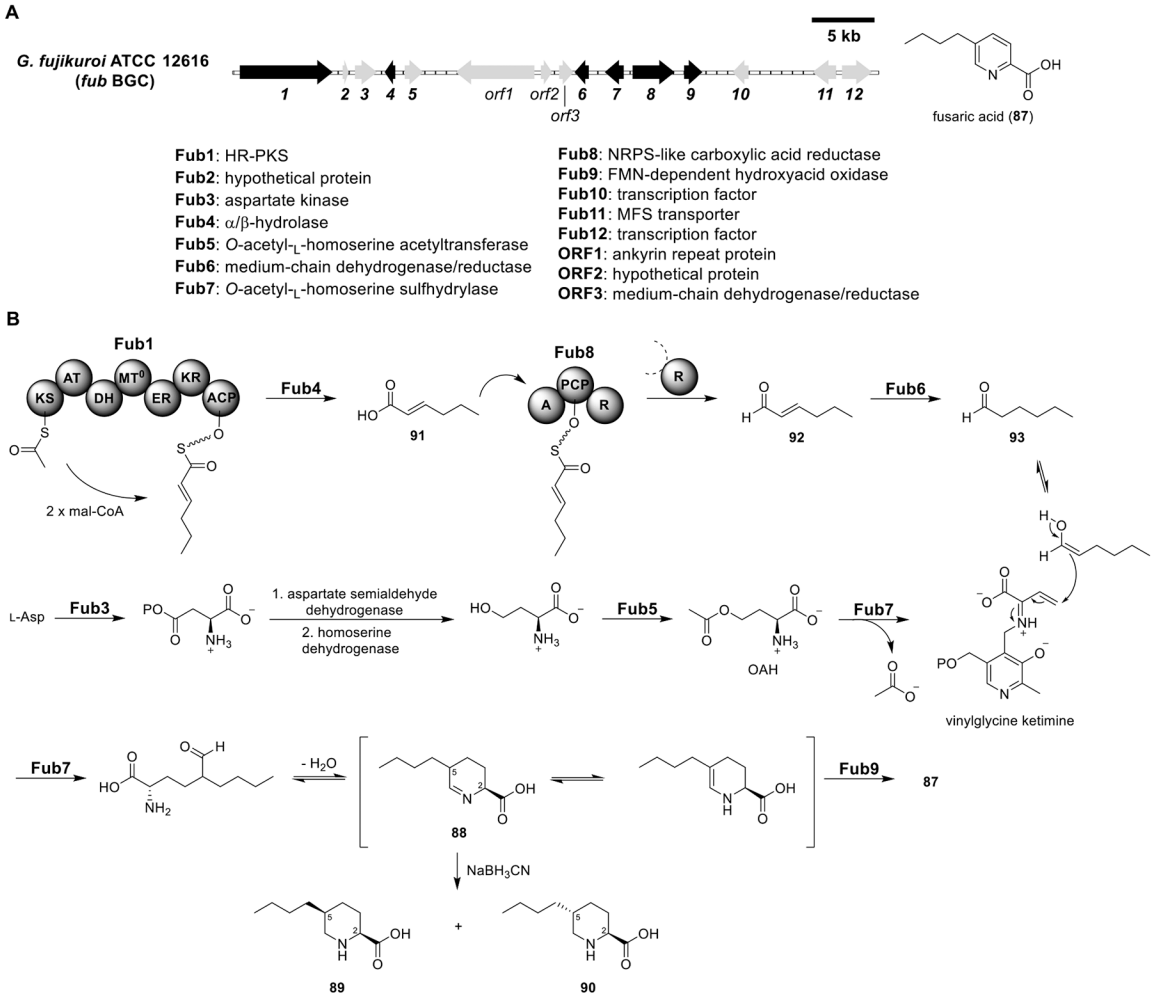

Figure 14.

Total biosynthesis of fusaric acid (**87**). (A) Organization and predicted gene functions of the *fub* BGC. Black ORFs encode for enzymes involved in the biosynthesis of **87**. (B) Proposed biosynthesis of **87**.

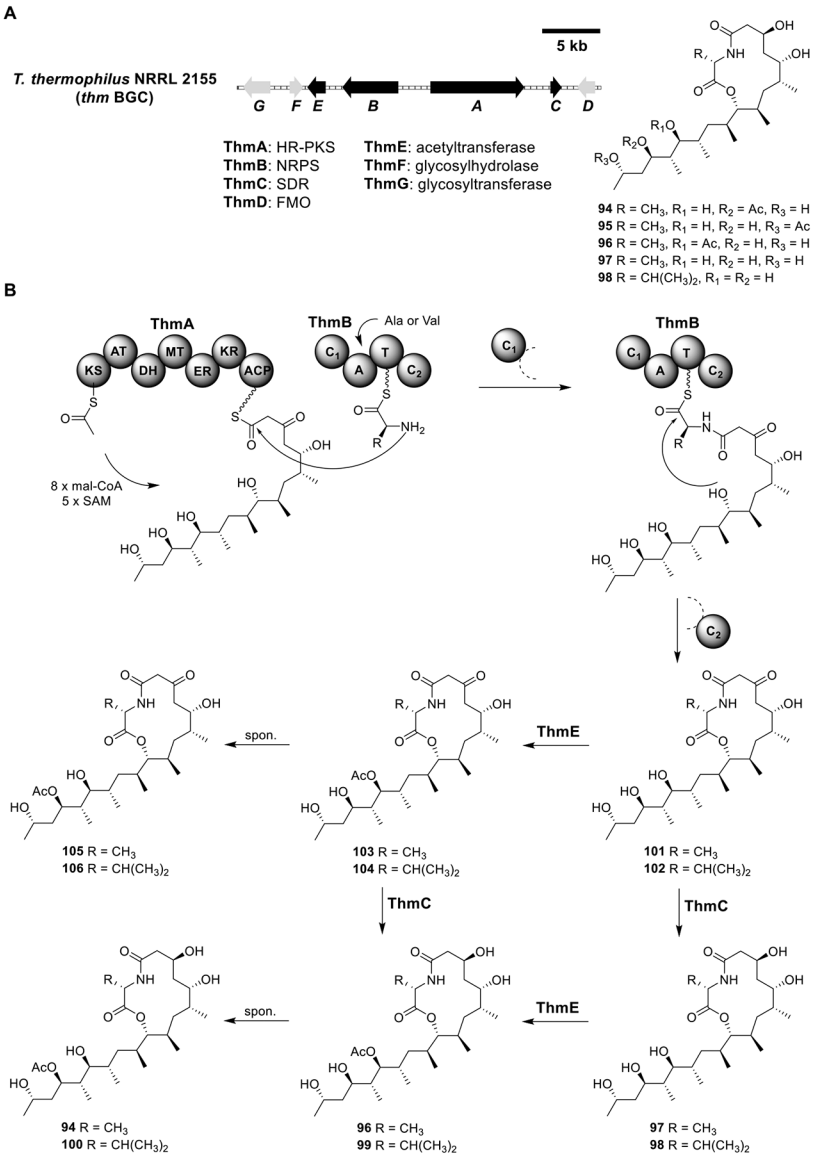

Figure 15.

Total biosynthesis of thermolides A–E (**94–98**). (A) Organization and predicted gene functions of the *thm* BGC. Black ORFs encode for enzymes involved in the biosynthesis of thermolides. (B) Proposed biosynthesis of thermolides.

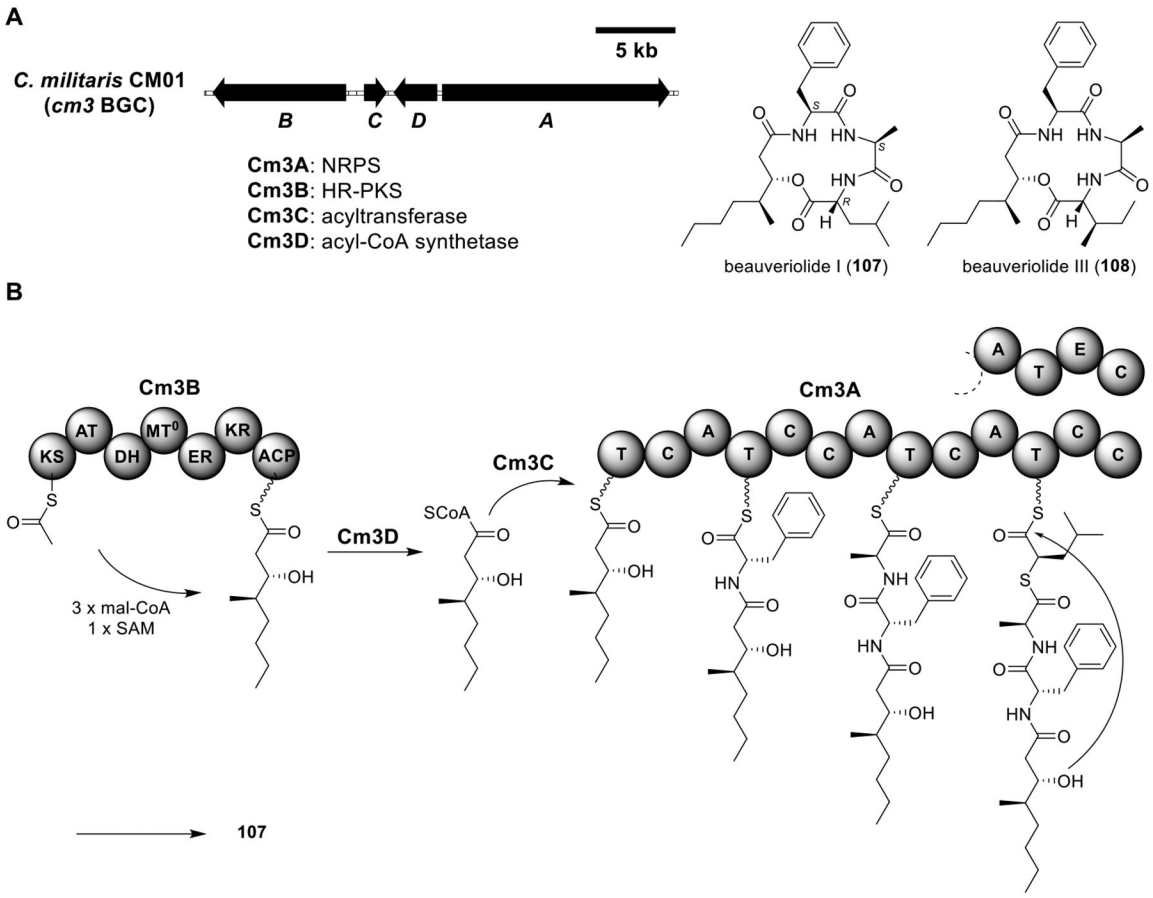

Figure 16.

Total biosynthesis of beauveriolides I (**107**) and III (**108**). (A) Organization and predicted gene functions of the *cm3* BGC. Black ORFs encode for enzymes involved in the biosynthesis of **107** and **108**. (B) Proposed biosynthesis of **107**.

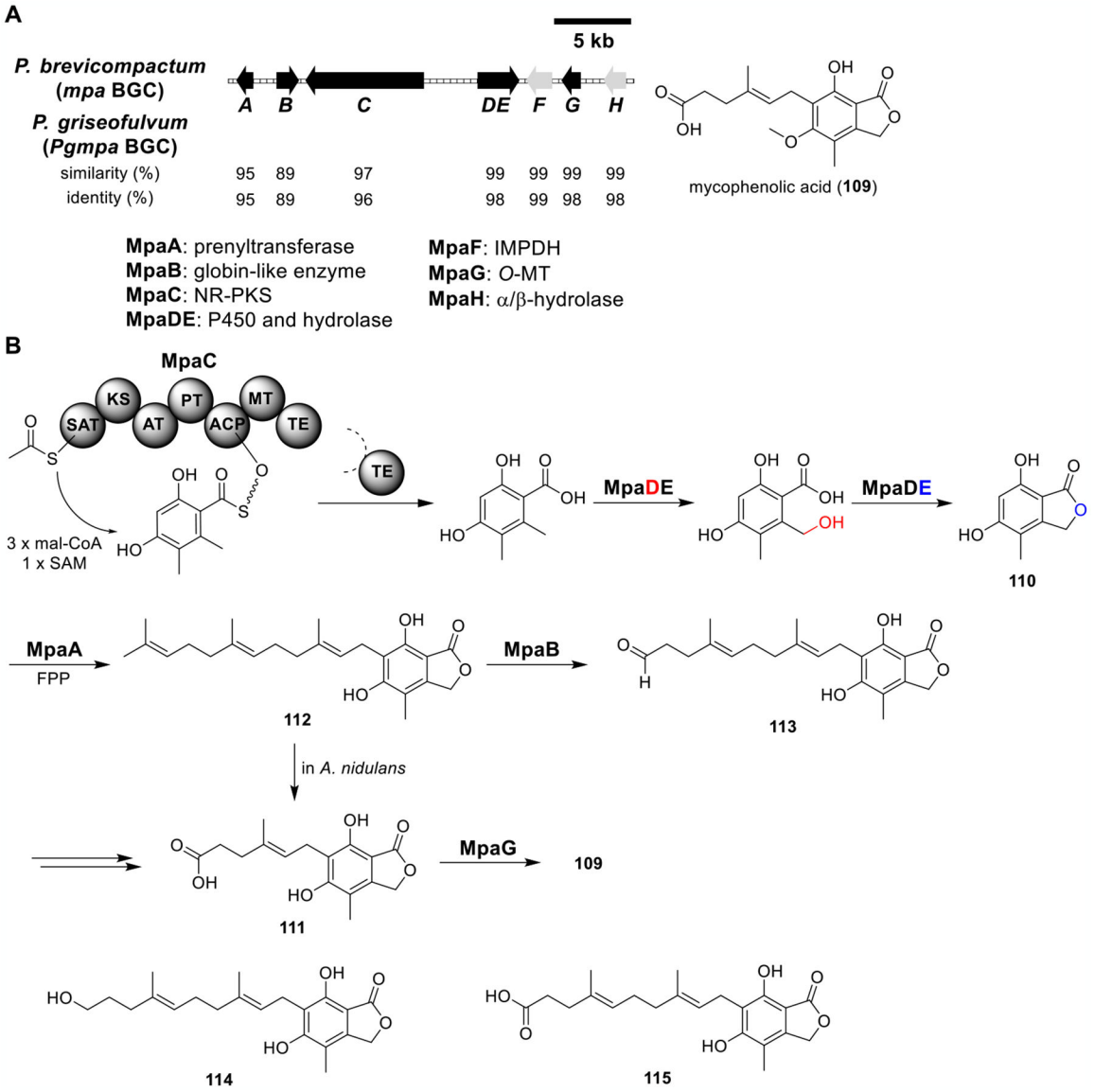

Figure 17.

Total biosynthesis of mycophenolic acid (**109**). (A) Organization and predicted gene functions of the *mpa and Pgmpa* BGCs. Black ORFs encode for enzymes involved in the biosynthesis of **109**. (B) Proposed biosynthesis of **109**.

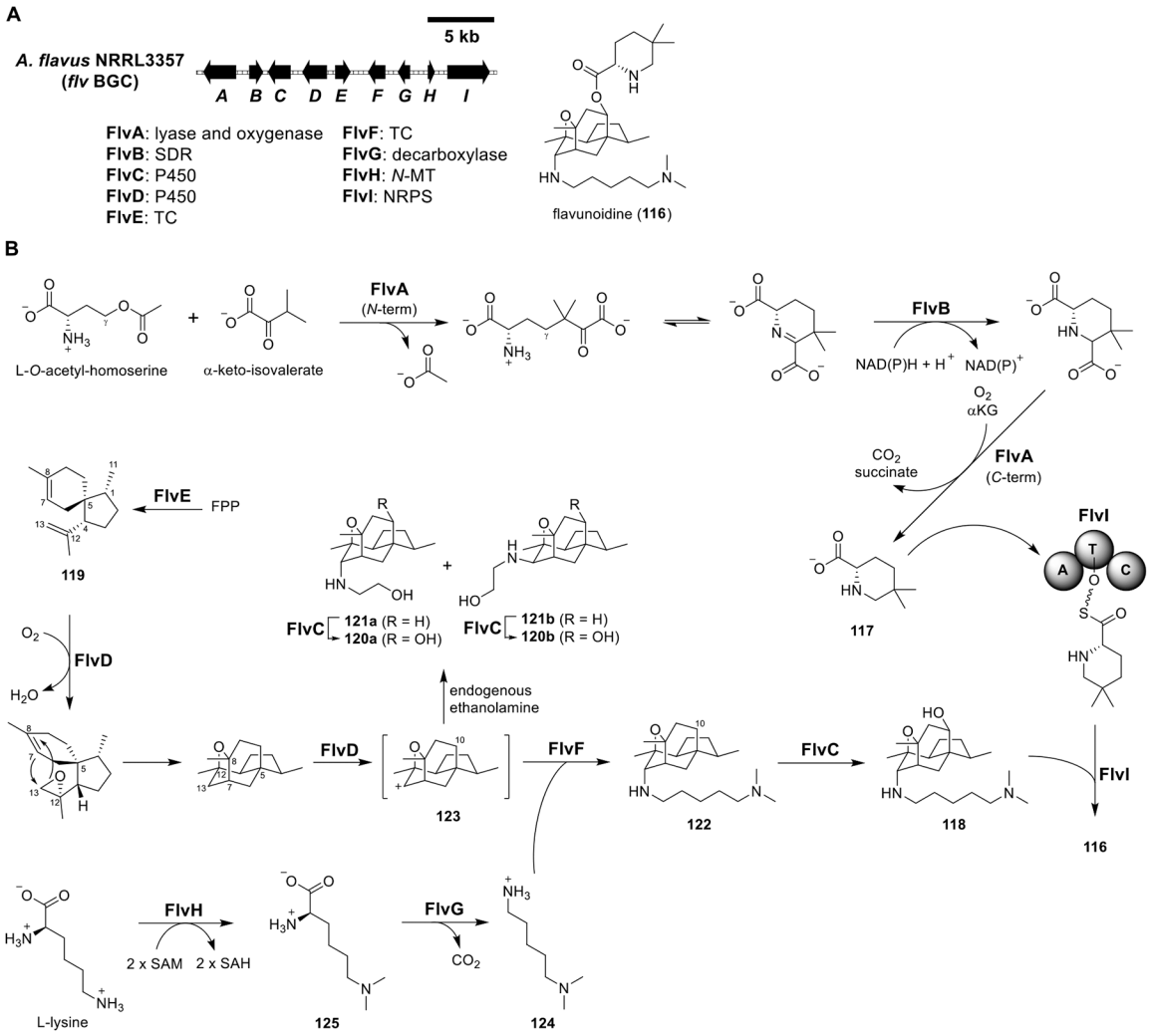

Figure 18.

Total biosynthesis of flavunoidine (**116**). (A) Organization and predicted gene functions of the *flv* BGC. Black ORFs encode for enzymes involved in the biosynthesis of **116**. (B) Proposed biosynthesis of **116**.

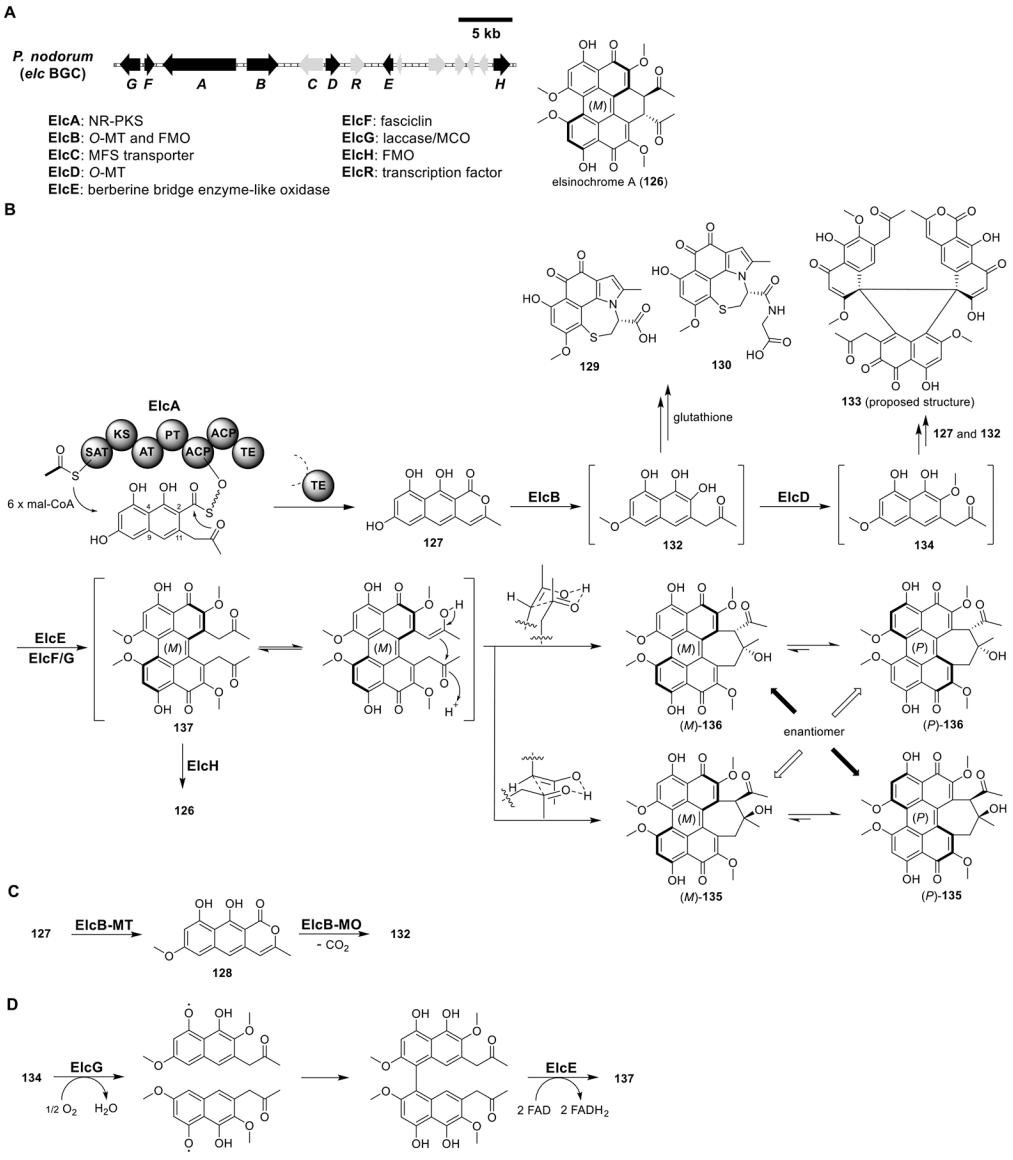

Figure 19.

Total biosynthesis of elsinochrome A (**126**). (A) Organization and predicted gene functions of the *elc* BGC. Black ORFs encode for enzymes involved in the biosynthesis of **126**. (B) Proposed biosynthesis of **126**. (C) Function of the didomain enzyme ElcB. (D) Proposed biosynthesis of **137** from **134**.

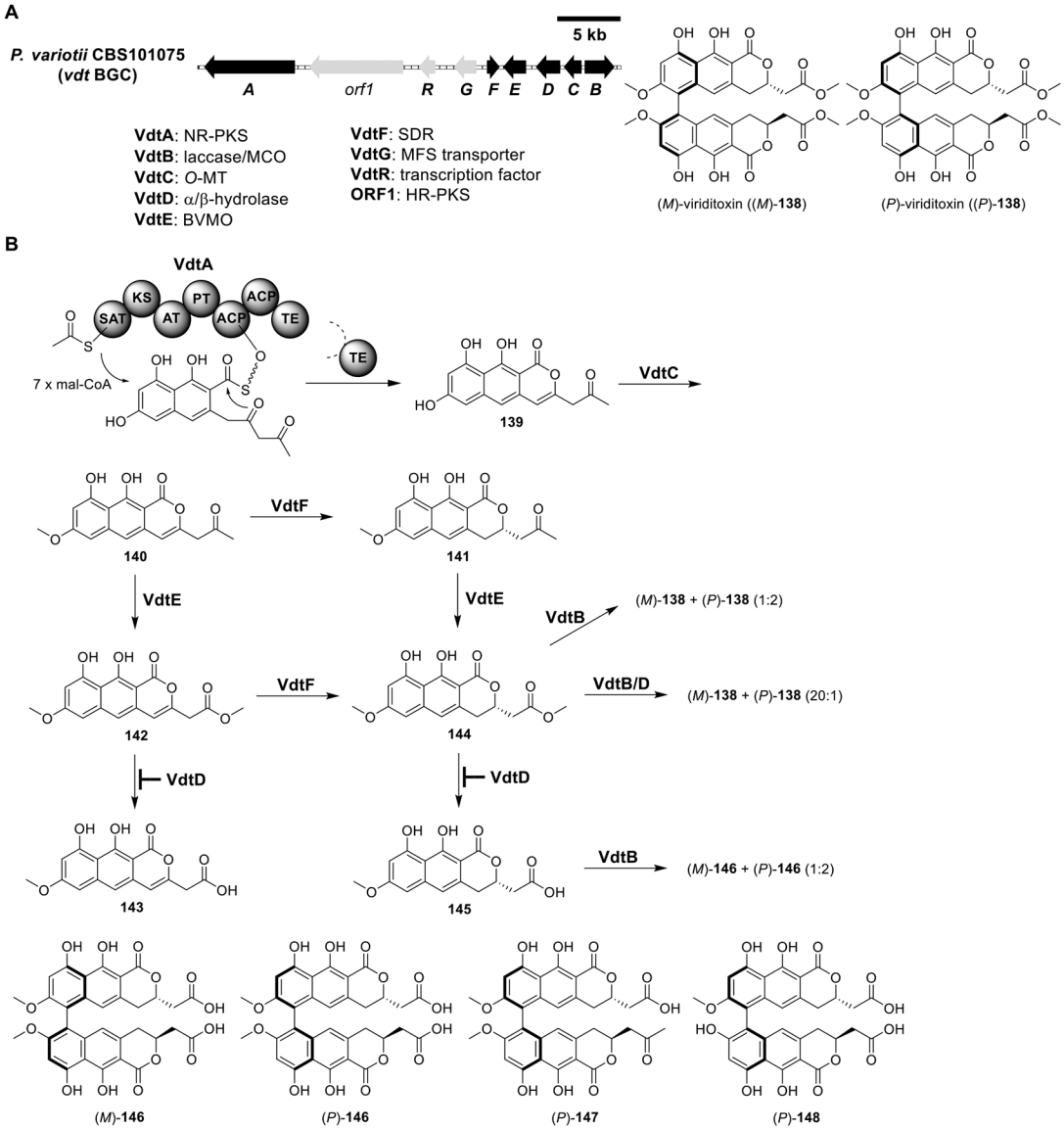

Figure 20.

Total biosynthesis of (*M*)-viriditoxin ((*M*)-**138**). (A) Organization and predicted gene functions of the *vdt* BGC. Black ORFs encode for enzymes involved in the biosynthesis of (*M*)-**138**. (B) The proposed biosynthesis of (*M*)-**138**.

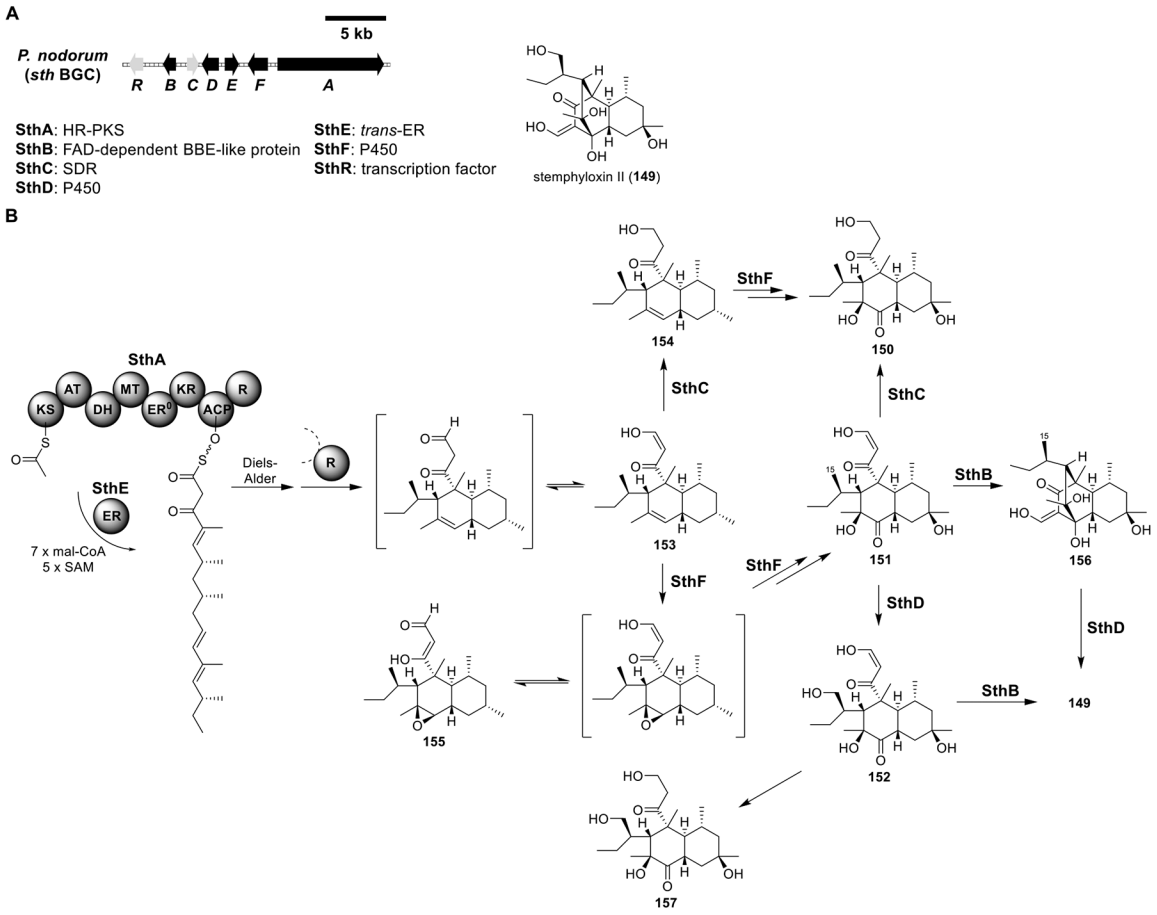

Figure 21.

Total biosynthesis of stemphyloxin II (**149**). (A) Organization and predicted gene functions of the *sth* BGC. Black ORFs encode for enzymes involved in the biosynthesis of **149**. (B) Proposed biosynthesis of **149**.

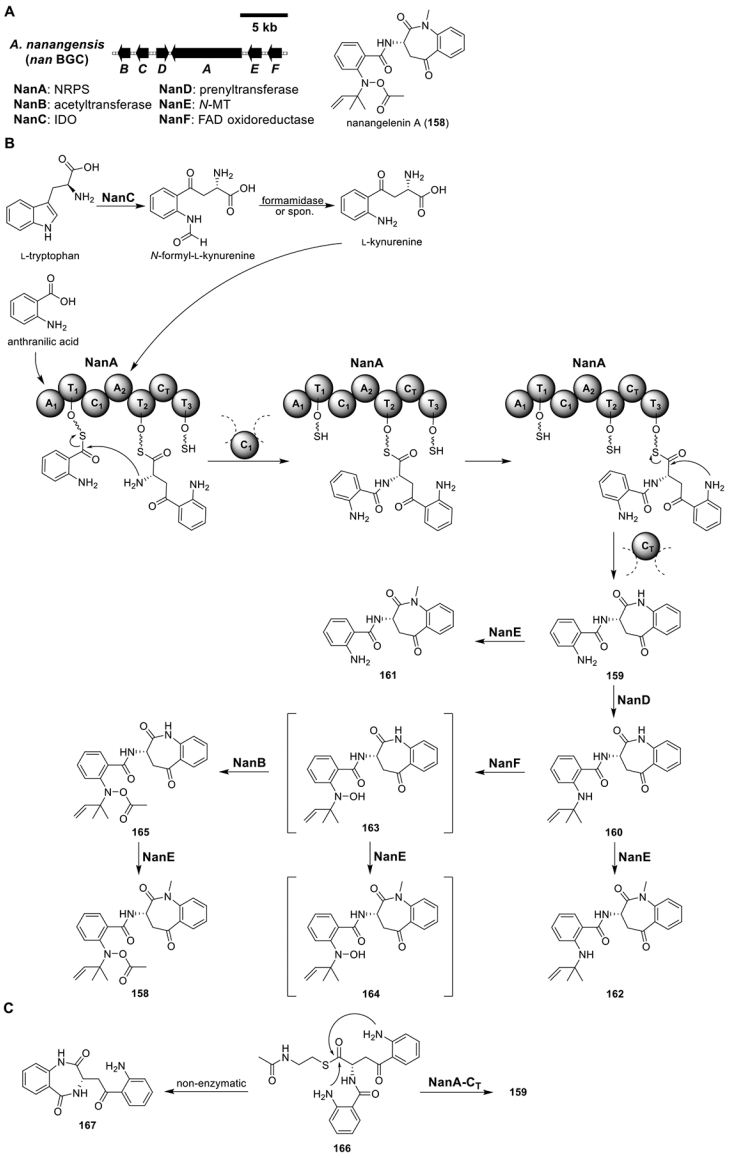

Figure 22.

Total biosynthesis of nanangelenin A (**158**). (A) Organization and predicted gene functions of the *nan* BGC. Black ORFs encode for enzymes involved in the biosynthesis of **158**. (B) Proposed biosynthesis of **158**. (C) Enzymatic and nonenzymatic cyclization of **166**.

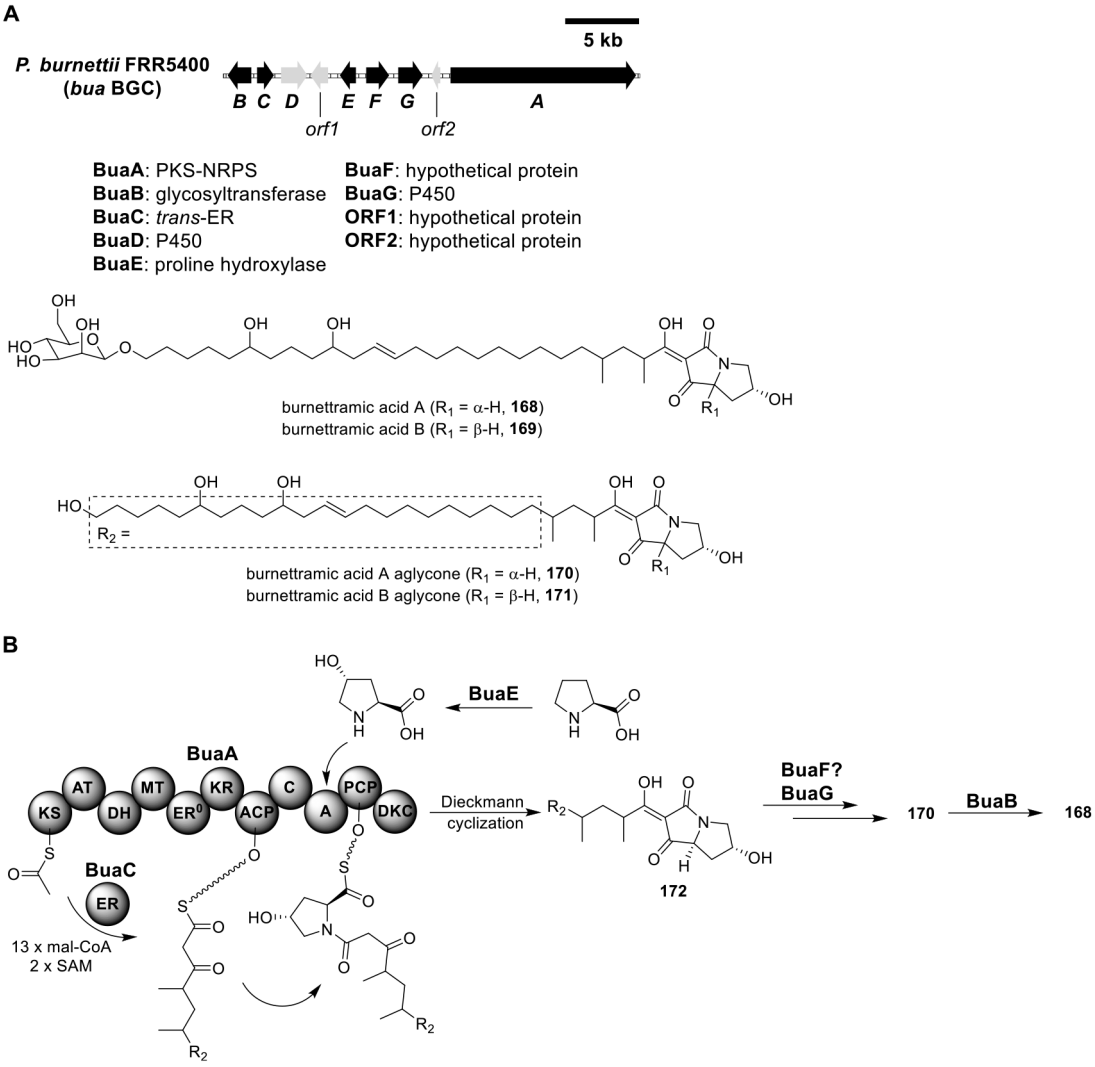

Figure 23.

Total biosynthesis of burnettramic acid A (**168**). (A) Organization and predicted gene functions in the *bua* BGC. Black ORFs encode for enzymes involved in the biosynthesis of **168**. (B) Proposed biosynthesis of **168**.

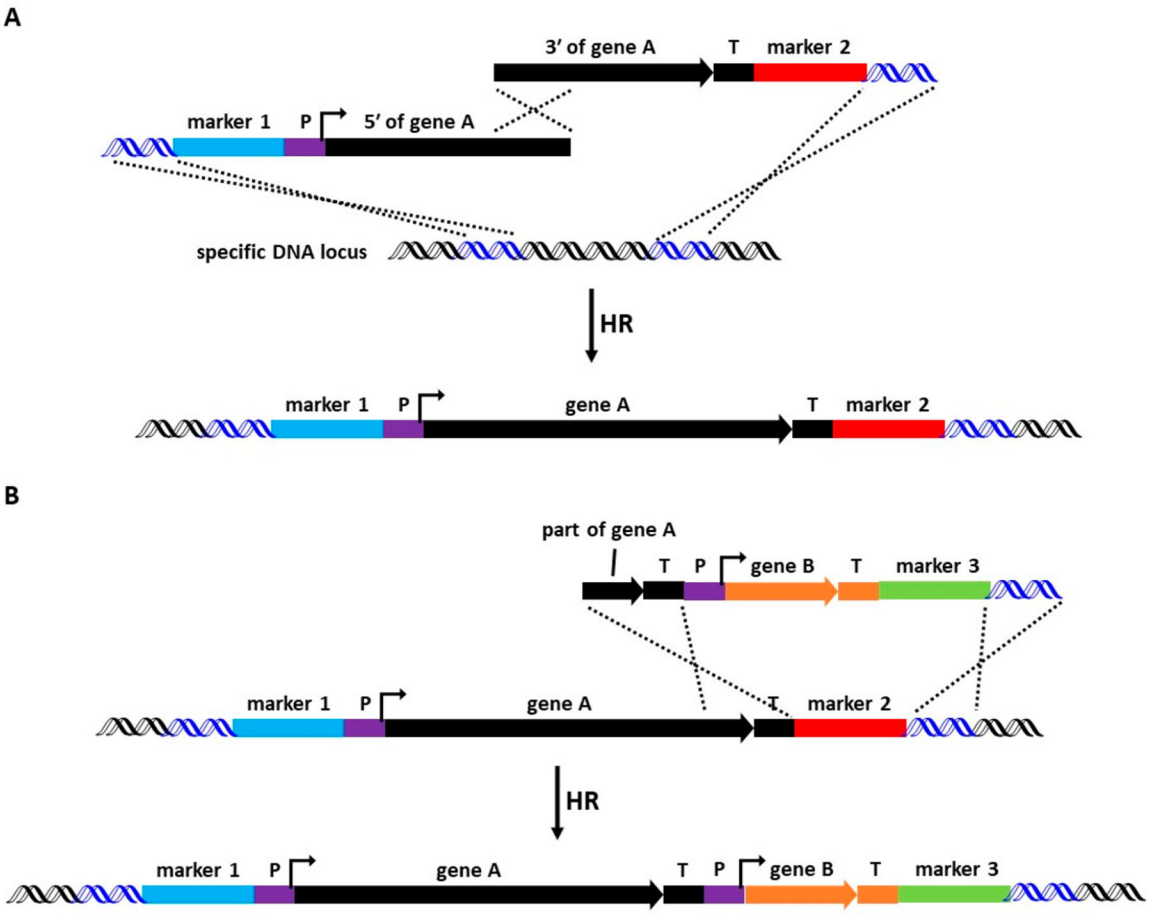

Figure 24.

Site-specific chromosomal integration with iterative recombination and maker recycling. (A) Two transforming DNA fragments can be obtained by fusion PCR. The first DNA fragment contains a ~1 kb sequence (blue) homologous to the integration site of the host genome, a selectable marker (maker 1), an inducible P*alcA* (P), and the 5′ portion of gene A. The second DNA fragment contains the 3′ portion of gene A overlapping by ~1 kb with the 5′ portion and extending ~100 bp downstream of the stop codon (T), marker 2, and another ~1 kb sequence (blue) homologous to the host genome. HR of the two transforming DNA fragments (cotransfomation) results in the integration of the complete expression cassette into the host genome. (B) HR of transforming DNA containing ~900 bp of the 3′ portion of gene A plus ~100 bp of T, a P, a smaller gene (gene B) plus ~100 bp of T, marker 3, and a ~1 kb homologous sequence (blue) results in the integration of the expression cassette of gene B and recycling of marker 2.

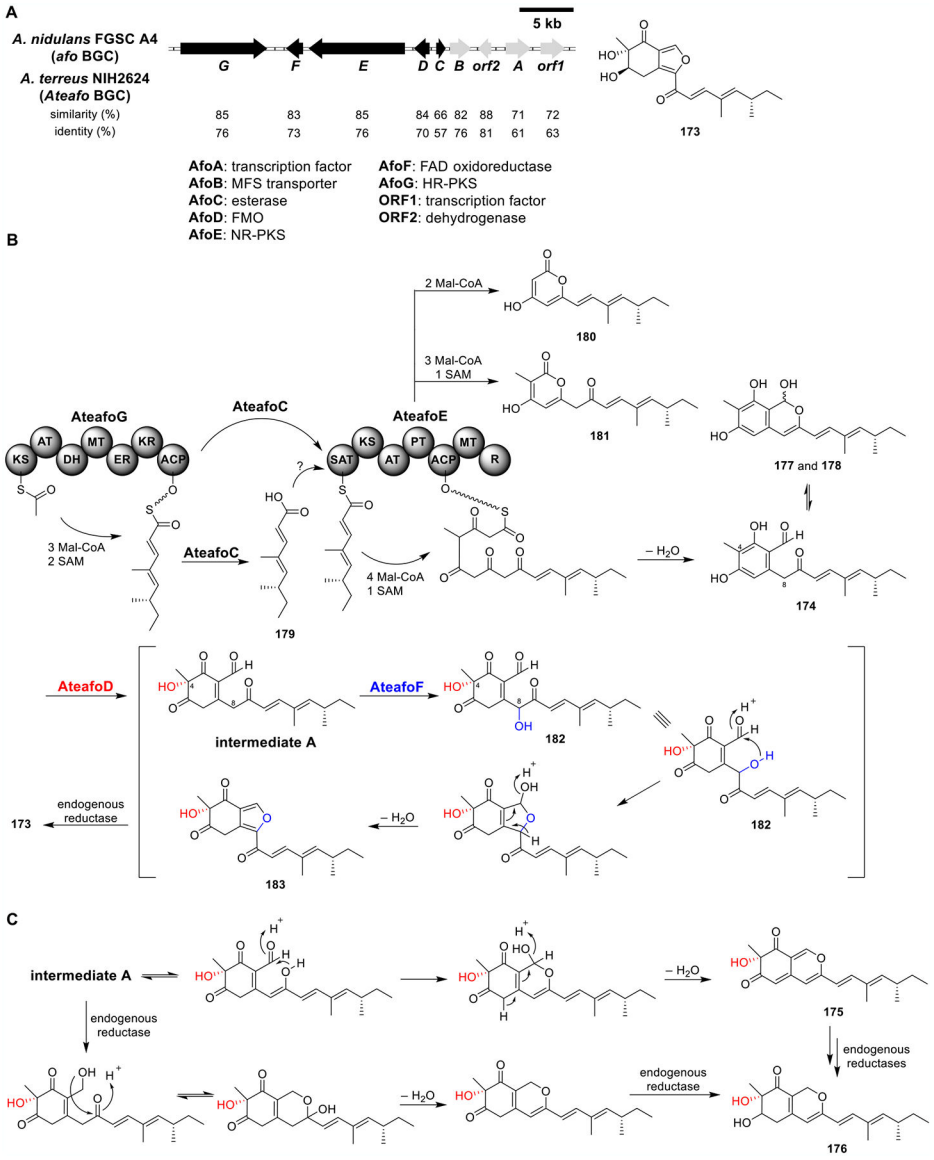

Figure 25.

Total biosynthesis of asperfuranone (**173**). (A) Organization and predicted gene functions of the *afo* and *Ateafo* BGCs. Black ORFs encode for enzymes involved in the biosynthesis of **173**. (B) Proposed biosynthesis of **173**.

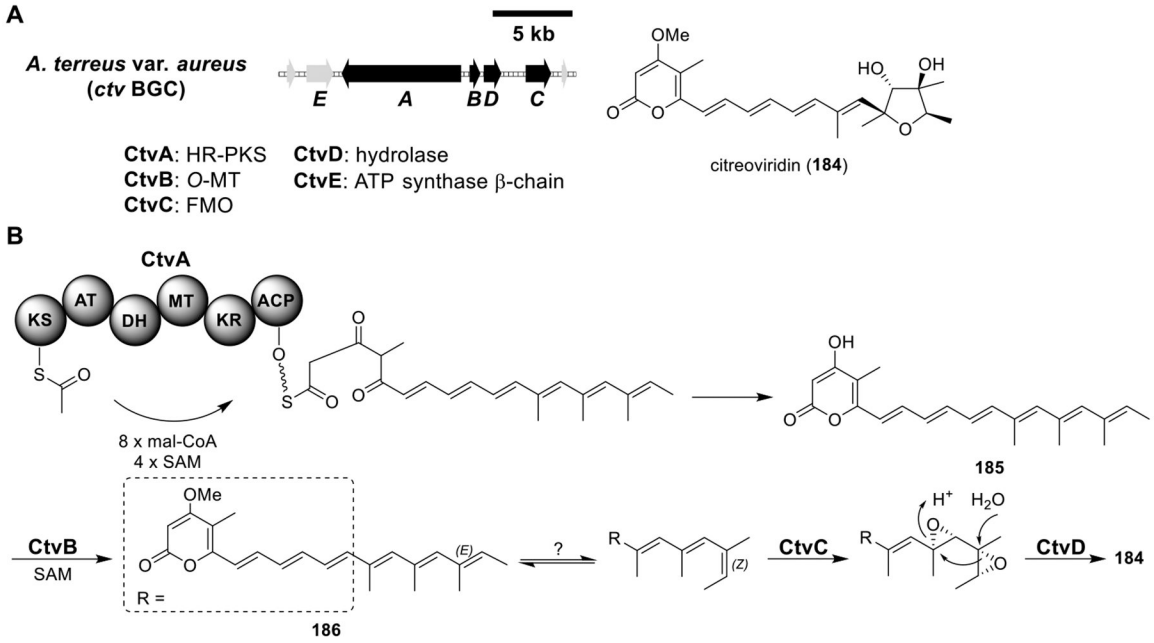

Figure 26.

Total biosynthesis of citreoviridin (**184**). (A) Organization and predicted gene functions of the *ctv* BGC. Black ORFs encode for enzymes involved in the biosynthesis of **184**. (B) Proposed biosynthesis of **184**.

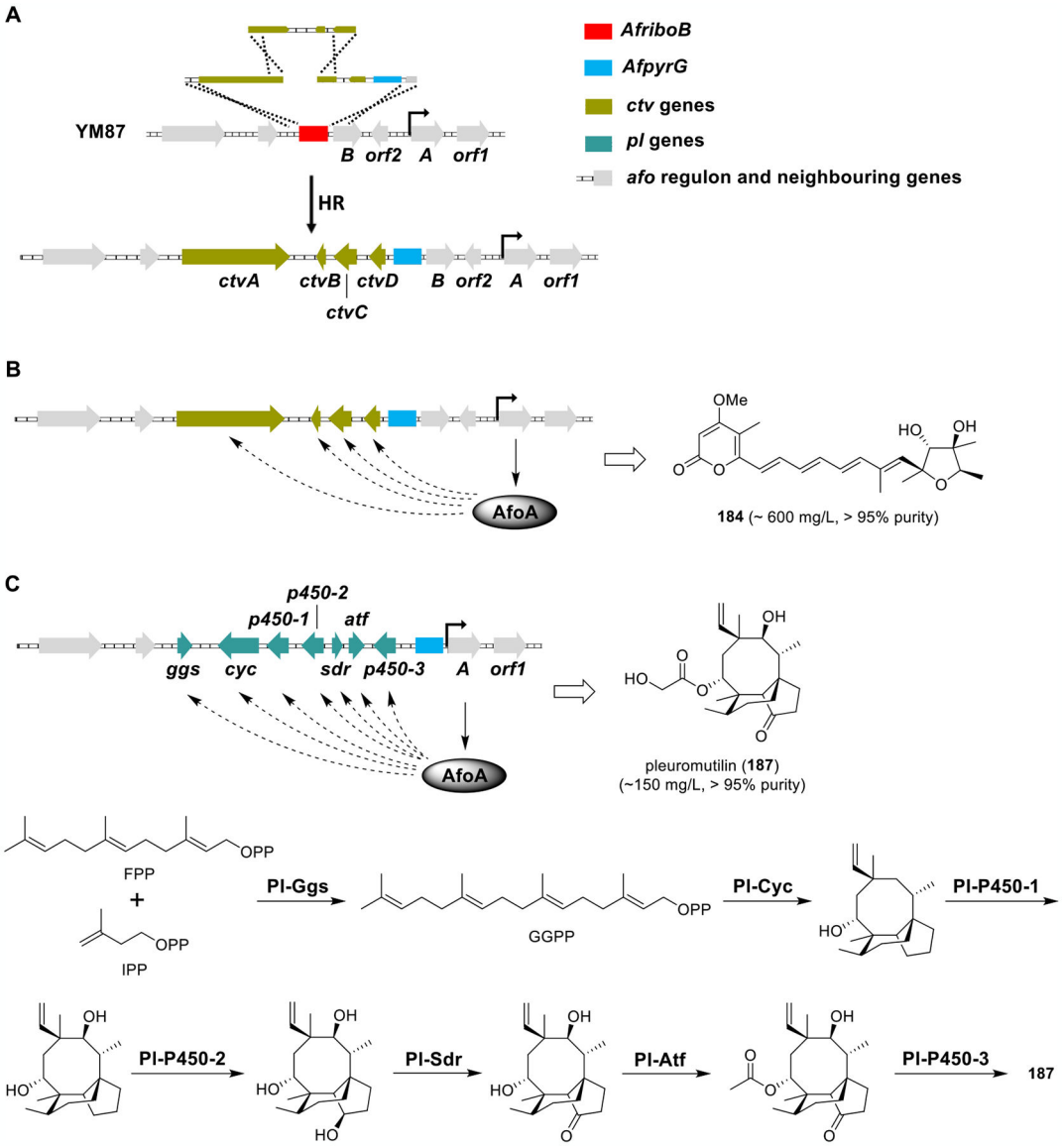

Figure 27.

Cluster refactoring with the *afo* regulon. (A) Reconstitution of *ctv* biosynthesis in the *afo* regulon. HR of the three transforming fragments with the *afo* locus of the recipient strain (YM87) replaced the coding sequences of *afo* with *ctv* genes (yellow). Transforming fragments were obtained by PCR amplification of the Gibson assembly products (see text for details). (B) Induction of the positive regulator *afoA* resulted in the activation of *ctvA–D* and the production of citreoviridin (**184**). (C) Using a similar approach, seven *afo* coding sequences (*afoB–G* and *orf 2*, see Figure 25A) were replaced by the seven *pl* genes (teal). Induction of *afoA* resulted in the production of pleuromutilin (**187**).

Table 1.

A. nidulans Hosts and Their Genotypes Used for Total Heterologous Biosynthesis

host strain	genotypes	refs
A1145 (TN02A7)	*argB::nkuA*Δ; *pyrG*89; *pyroA*4; *riboB*2	48
A1145ΔST	*argB::nkuA*Δ; *stcA*Δ; *pyrG*89; *pyroA*4; *riboB2*	53
A1145ΔEM	*argB::nkuA*Δ; *easA*Δ; *pyrG*89; *pyro0A*4; *riboB2*	53
A1145ΔSTΔEM	*argB::nkuA*Δ; *stcA*Δ; *easA*Δ; *pyrG*89; *pyroA*4; *riboB*2	53
LO4389	*argB::nkuA*Δ; *stc*Δ; *pyrG*89; *pyroA*4; *riboB*2	54
LO7890	*argB::nkuA*Δ; *stc*Δ; *eas*Δ; *afo*Δ; *mdp*Δ; *tdi*Δ; *aus*Δ; *ors*Δ; *pyrG*89; *pyroA*4; *riboB*2	55
LO8030	*argB::nkuA*Δ; *stc*Δ; *eas*Δ; *afo*Δ; *mdp*Δ; *tdi*Δ; *aus*Δ; *ors*Δ; *apt*Δ; *pyrG*89; *pyroA*4; *riboB*2	55

Table 2.

Comparison between Episomal Expression and Site-Specific Chromosomal Integration Expression in *A. nidulans*

expression system	transforming DNA	advantages	disadvantages
Episomal	• *E. coli*-yeast-fungal shuttle vectors containing expression cassettes • Assembled in yeast	• High yield of transforming DNA easily obtained by propagation in *E. coli* • Efficient assembly of large clusters in yeast • No disruption to the host chromosome • Multiple copies of the vectors in the nucleus might increase expression of heterologous genes • With 4 heterologous genes per vector and 3 selection markers available, theoretically insertion of 12 genes in one transformation is possible	• Possible loss of vector if selection pressure is not maintained • Only markers that allow for counter-selection can be recycled (*pyrG*) • Longer time of transforming DNA preparation
Site-specific chromosomal integration	• PCR products of expression cassettes flanked by homologous regions • Assembled by fusion PCR or Gibson assembly	• Genetic stability of expression cassettes for long-term bioproduction • Ease of rational engineering • Unlimited selection marker recycling • Rapid generation of integration DNA by fusion PCR and Gibson assembly • Visual selection of correct transformants (yellow or white colonies)	• Yield of transforming DNA dependent on PCR • Assembly of BGCs limited by fusion PCR (this limitation is circumvented by Gibson assembly) • Unknown effects of chromosomal disruption (albeit in a defined locus)